5-24-2012

A Specialized Citric Acid Cycle Requiring Succinyl-Coenzyme A (CoA):Acetate CoA-Transferase (AarC) Confers Acetic Acid Resistance on the Acidophile Acetobacter aceti

Elwood Mullins
Washington University in St. Louis

WASHINGTON UNIVERSITY IN ST. LOUIS

Department of Chemistry

Dissertation Examination Committee:
T. Joseph Kappock, Co-chair
Robert E. Blankenship, Co-chair
Dewey Holten
Joseph M. Jez
Kevin D. Moeller
Jacob Schaefer

A Specialized Citric Acid Cycle Requiring Succinyl-Coenzyme A (CoA):Acetate CoA-Transferase (AarC) Confers Acetic Acid Resistance on the Acidophile *Acetobacter aceti*

by

Elwood Arthur Mullins

A dissertation presented to the
Graduate School of Arts and Sciences
of Washington University in
partial fulfillment of the
requirements for the degree
of Doctor of Philosophy

May 2012

Saint Louis, Missouri

ABSTRACT

The characteristic ability of acetic acid bacteria to aerobically oxidize ethanol to acetic acid has been harnessed for millennia to produce vinegar. Acetic acid permeates cell membranes at low pH and generally inhibits bacterial growth at low millimolar concentrations. The strains used for vinegar production, however, thrive in near-molar concentrations. This remarkable resistance results from the combined contributions of several molecular mechanisms. This study examines the inherent acid stability of proteins from the industrial vinegar-production strain *Acetobacter aceti* 1023 and the process by which cytoplasmic acetic acid is "overoxidized" to carbon dioxide.

Acetate overoxidation in *A. aceti* strain 1023 is catalyzed by a variant citric acid cycle (CAC) that lacks succinyl-coenzyme A (CoA) synthetase. The acetic-acid-resistance protein succinyl-CoA:acetate CoA-transferase (SCACT, AarC) circumvents this deficiency and bypasses substrate-level phosphorylation and/or adenylation of acetate. Moreover, continuous acetate dissimilation by this specialized CAC is dependent upon only favorable oxidation of reduced cofactors.

Biphasic growth of *A. aceti* strain 1023 in yeast extract-peptone-dextrose-ethanol medium is accompanied by distinct stages of acetate production, conservation, and depletion. Acetate is initially accumulated as ethanol is oxidized in the first log phase, transiently maintained in the first stationary phase, and ultimately consumed in the second log phase. The high levels of AarC and SCACT activity present prior to the acetate depletion phase suggest that regulation of CAC enzyme levels is not the only mechanism by which premature acetate overoxidation is avoided. Acetate catabolism

may be further minimized during ethanol oxidation by the maintenance of a low cytoplasmic acetate concentration. *A. aceti* employs multiple means of active acetic acid efflux which may be driven by the energetically favorable oxidation of ethanol.

Selective pressure to function in a primary metabolic role increased the specificity and catalytic rapidity of AarC relative to other class I CoA-transferases. Catalysis relies upon a novel oxyanion hole configuration composed partly of the distal amide nitrogen of CoA to stabilize tetrahedral oxyanion intermediates. Structural alignments suggest this mechanism is employed by all class I enzymes. Favorable hydrogen-bonding and electrostatic interactions between the protein and the diphosphate moiety of CoA induce a protein conformational change that was previously predicted to accelerate CoA transfer. This motion is influenced by an auxiliary binding site that preconcentrates carboxylate substrates.

ACKNOWLEDGMENTS

I would like to thank my research advisor Prof. T. Joseph Kappock, the members of my research advisory committee Profs. Robert E. Blankenship and Dewey Holten, and the members of my dissertation examination committee Profs. Joseph M. Jez, Kevin D. Moeller, and Jacob Schaefer.

I would also like to thank the many people who contributed to this study. T. Joseph Kappock annotated the *A. aceti* strain 1023 genome and created the plasmids encoding the AarCH6 mutants. Julie A. Francois cloned *uctB* and *uctD* and assayed CAC enzyme activities and acetyl-CoA:carboxylate CoA-transferase activities in *A. aceti* lysates. Hong Jiang synthesized dethiaacetyl-CoA. Charles Z. Constantine purified *Aa*CSH6. Courtney M. Starks and Kelly L. Sullivan provided analytical gel-filtration analysis. Kayleigh E. Nyffeler isolated AarCH6-S71A, repeated the purification of untagged AarC, and performed previously omitted PCR-control reactions. Phillip A. Cole and Koichi Kondo generously furnished pREP4-*groELS* and *A. aceti* strains, respectively. Barbara L. Golden, Spencer M. Anderson, and the staff of LS-CAT and GM/CA-CAT provided assistance with crystallographic data collection and refinement. The Washington University Mass Spectrometry Resource and the Purdue Proteomics Facility performed mass analysis of intact proteins and small molecules. The Washington University Protein and Nucleic Acid Chemistry Laboratory and the Purdue University Genomics Core Facility sequenced PCR products and plasmids.

Funding was provided by the National Science Foundation and Purdue University Agricultural Research Programs.

TABLE OF CONTENTS

LIST OF FIGURES

LIST OF SCHEMES

LIST OF TABLES

Chapter 1.

Background and introduction

PERSPECTIVE

Vinegar production. Acetic acid bacteria (AAB) are Gram-negative, acidophilic α-proteobacteria that oxidize ethanol to acetic acid (*1*) using membrane-bound alcohol (*2*) and aldehyde (*3*) dehydrogenases (Scheme 1.1). This characteristic ability has been harnessed for millennia to produce vinegar (*4*). Cultures often progress through multiple growth phases (*5-7*), accumulating acetate through the oxidation of ethanol in the first log phase, conserving acetate during the first stationary phase, and then ultimately consuming acetate in the second log phase. Ideal strains for vinegar production exhibit little acetic acid consumption during the first log phase and an ability to tolerate high concentrations of acetic acid during a prolonged conservation phase (*7*).

Acetic acid resistance. Acetic acid permeates the cell membrane at low pH and generally inhibits bacterial growth at low-millimolar concentrations. Dissociation in the relatively alkaline cytoplasm diffusively traps acetate while decreasing the intracellular pH and poisoning the proton gradient (*8, 9*). Many AAB are nonetheless resistant to near-molar concentrations of acetic acid (*10, 11*). Molecular mechanisms of resistance in the AAB *Acetobacter aceti* include adaptation of cytoplasmic components (*12-14*) to internal acidification (Figure 1.1) (*15*), active acetic acid efflux via the putative ABC transporter AatA (*16*) and an unnamed acetic acid:proton antiporter (*17*), and production of acetic-

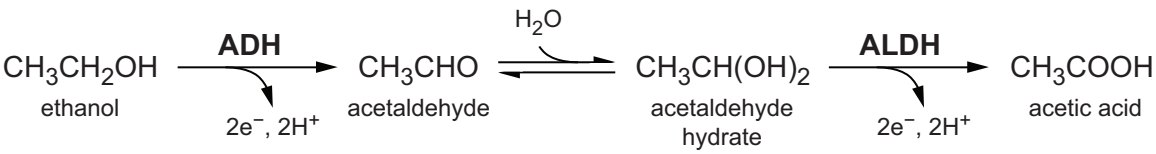

Scheme 1.1. Ethanol oxidation in the *A. aceti* periplasm. Membrane-bound alcohol (ADH) and aldehyde (ALDH) dehydrogenases convert ethanol to acetic acid.

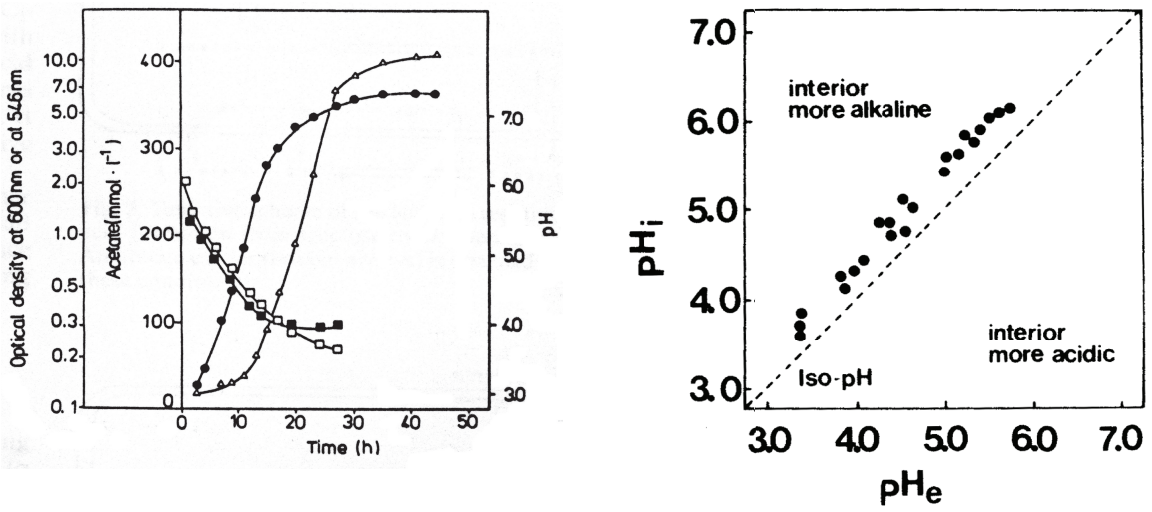

Figure 1.1. Intracellular and extracellular pH in growing *A. aceti* cultures. **(Left)** Both intracellular and extracellular pH decrease as ethanol is oxidized to acetic acid. Intracellular pH (closed squares), extracellular pH (open squares), acetic acid (open triangles), and optical density (closed circles). Intracellular pH was measured using [^{14}C]-acetylsalicylic acid. **(Right)** *A. aceti* maintains a relatively alkaline intracellular pH (pH_i) as both the intracellular and extracellular pH (pH_e) drop. Intracellular pH was measured using [^{14}C]-acetic acid. A similar plot was obtained using [^{14}C]-benzoic acid. Reprinted with permission from (*15*).

acid-inducible proteins, many with undefined biochemical roles, identified by proteomic screens (*9, 18*).

Members of the AAB genus *Acetobacter* were historically differentiated from those of *Gluconobacter* by a metabolic preference for ethanol and the ability to "overoxidize" acetate to CO_2, usually when ethanol was unavailable (*19*). Acetate overoxidation implicates the oxidative decarboxylations performed by citric acid cycle (CAC) dehydrogenases and suggests the presence of a complete CAC.

A. aceti strain 1023, an especially acetic-acid-resistant and comparatively thermotolerant vinegar factory isolate (*20, 21*), requires acetic-acid-resistance genes *aarABC* for growth on > 50 mM acetic acid at low pH (*22*). AarA is an NADH-insensitive hexameric form of citrate synthase (*23*). AarB is predicted to be a basic protein of 154 amino acids with no homologues or known function (*22*). AarC is required

for acetate overoxidation but is not acetyl-CoA synthetase and resembles several acyl-coenzyme A (CoA):carboxylate CoA-transferases (*24*).

CoA-transferases. CoA-transferases catalyze the reversible transfer of CoA from acyl-CoA thioesters to free acids and play diverse metabolic roles in organisms from all lines of descent. All three classes of CoA-transferase share mechanistic features, but only class I and II enzymes appear to have a common ancestor (*25*).

Class I CoA-transferases are frequently involved in fatty acid metabolism and often use acetyl-CoA and/or succinyl-CoA as a CoA donor (*26, 27*). Class I enzymes usually possess heterotetrameric or homodimeric structures. The larger, identical subunits in the homodimeric structures are composed of distinct N- and C-terminal domains that are orthologous to the smaller, unique subunits in the heterotetrameric structures (*27*). CoA transfer proceeds by a substituted-enzyme mechanism (*28, 29*) in which a catalytic glutamate forms covalent mixed anhydride (*30-32*) and thioester (*33*) intermediates. The carboxylate product characteristically dissociates before the carboxylate substrate binds (Scheme 1.2).

Class III CoA-transferases are commonly involved in specialized anaerobic pathways or activation of organic acids for subsequent decarboxylation (*25*). Class III enzymes possess unique interlocked homodimeric structures (*34*). CoA transfer proceeds by a ordered ternary mechanism in which a catalytic aspartate forms covalent mixed anhydride and thioester intermediates analogous to those formed by class I CoA-transferases (*35*). The carboxylate product, however, characteristically dissociates after the carboxylate substrate binds (Scheme 1.2).

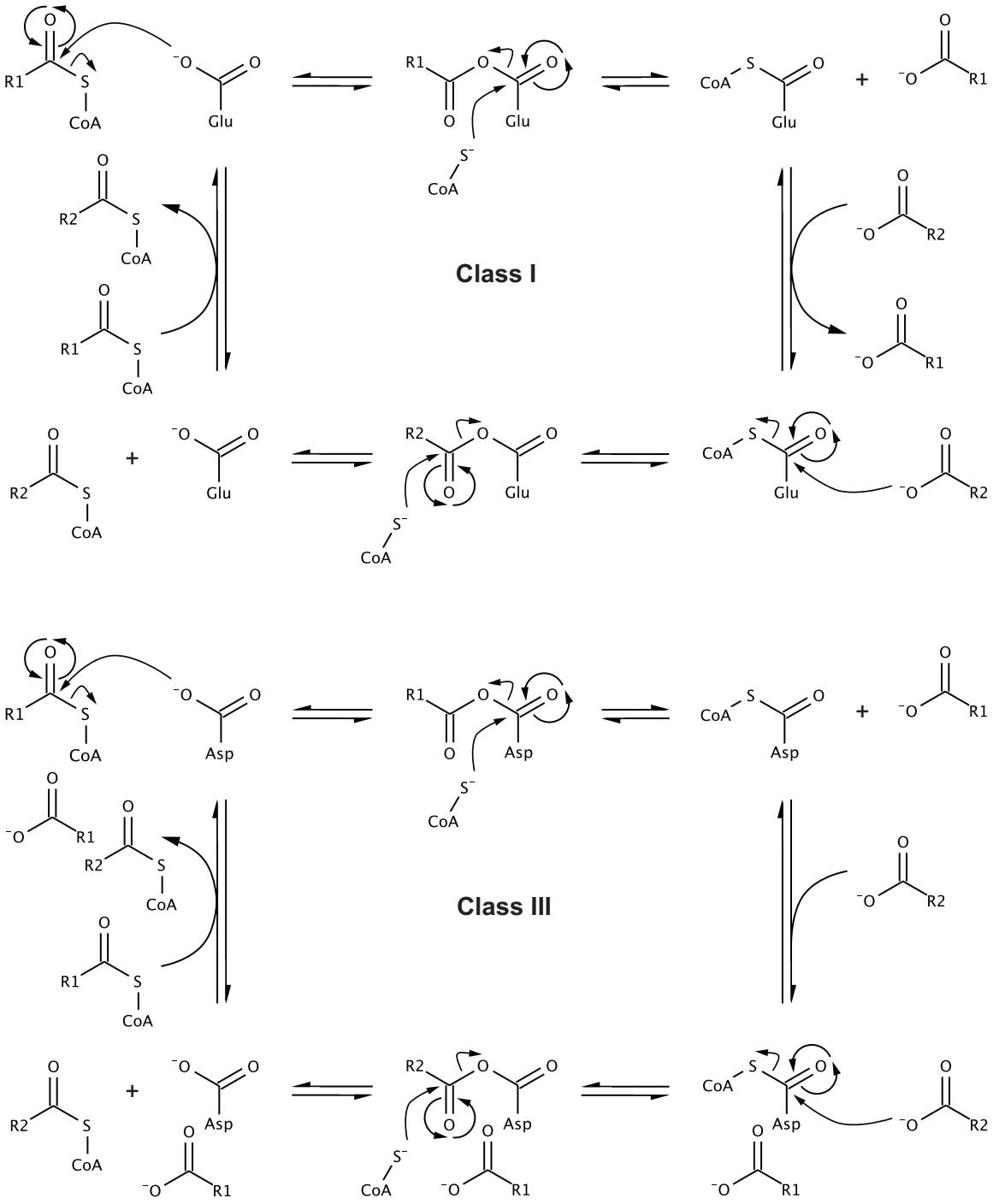

Scheme 1.2. Abbreviated class I and III CoA-transferase mechanisms. CoA-transferase reactions are catalyzed by three classes of enzymes with distinct but related mechanisms. **(Top)** Class I CoA-transferase mechanism. **(Bottom)** Class III CoA-transferase mechanism. Both class I and III reactions proceed through a series of mixed anhydride, tetrahedral oxyanion (not shown), and thioester intermediates. The classes differ in the identity of the nucleophilic carboxylate (class I, glutamate; class III, aspartate) and the order of substrate association and product dissociation (class I, ping-pong Bi-Bi mechanism; class III, ordered Bi-Bi mechanism).

Class II CoA-transferases function in the multiprotein complexes citrate lyase and citramalate lyase, converting citrate (or citramalate) to oxaloacetate (or pyruvate) and acetate. Citrate lyase and citramalate lyase possess heterooctadecameric structures composed of unique transferase, lyase, and acyl-carrier-protein (ACP) subunits (*36, 37*). An acetyl-dephosphoCoA prosthetic group is covalently attached to the ACP subunit (*25*). Class II enzymes lack both a nucleophilic glutamate (class I) and a nucleophilic aspartate (class III). Alternatively, the carboxylate substrate directly attacks the acetyl-dephosphoCoA-ACP thioester forming a free mixed anhydride intermediate and the dephosphoCoA-ACP thiolate. Subsequent attack by dephosphoCoA-ACP thiolate at the

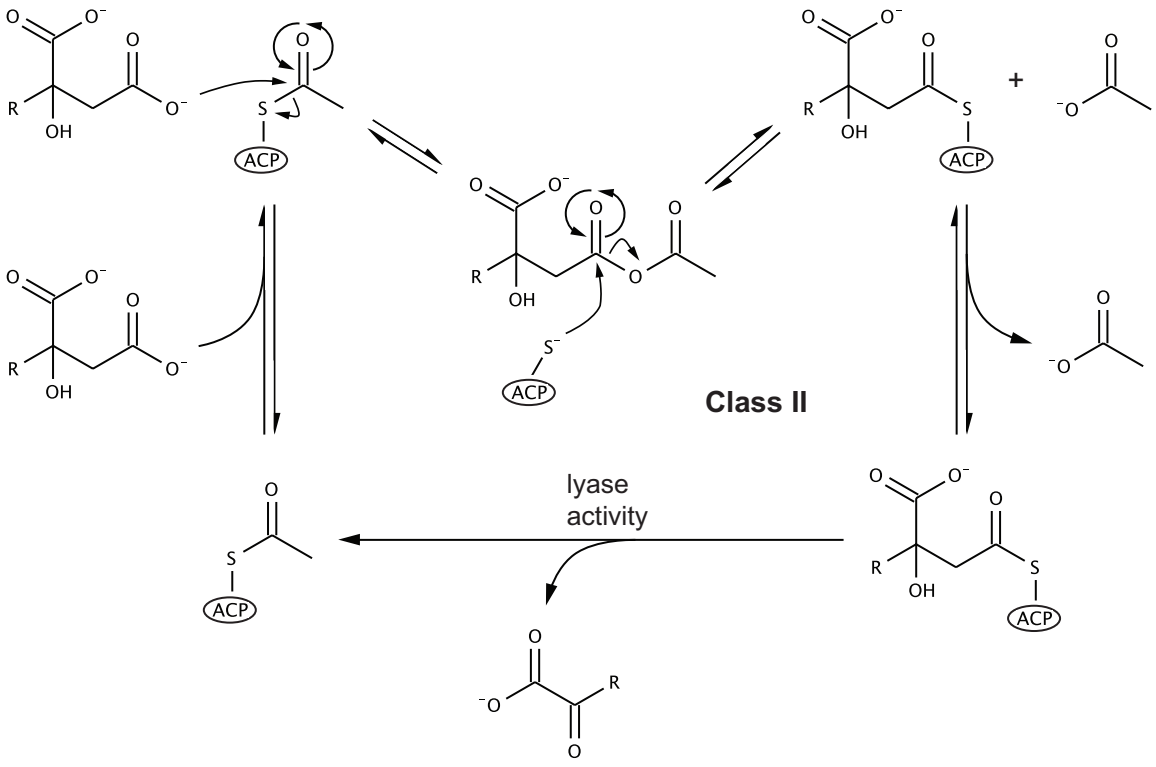

Scheme 1.3. Abbreviated class II CoA-transferase mechanism. Class II CoA-transferases function in the multiprotein complexes citrate lyase [R = $-CH_2COO^-$ (citrate → oxaloacetate + acetate)] and citramalate lyase [R = $-CH_3$ (citramalate → pyruvate + acetate)]. Reactions proceed through a series of mixed anhydride, tetrahedral oxyanion (not shown), and thioester intermediates. A retro-aldol reaction completes the catalytic cycle. The recycled thioester is shuttled between lyase and transferase active sites by a dephosphoCoA prosthetic group covalently anchored to acyl-carrier-protein (ACP).

citryl (or citramalyl) carbonyl of the mixed anhydride produces the acyl-dephosphoCoA-ACP intermediate and acetate. A retro-aldol reaction catalyzed by the lyase subunit forms the second carboxylate product (oxaloacetate or pyruvate) and regenerates the acetyl-dephosphoCoA prosthetic group (Scheme 1.3) (*36*).

PURPOSE

Chapter 2 defines the link between the CAC and acetic acid resistance in *A. aceti*. The acetic-acid-resistance gene *aarC* encodes succinyl-CoA:acetate CoA-transferase (AarC, SCACT). AarC reversibly catalyzes CoA transfer from succinyl-CoA to acetate forming acetyl-CoA and succinate. Acetyl-CoA is then readily converted to carbon dioxide by the specialized *A. aceti* CAC. Reannotation of the *aarABC* gene cluster revealed the presence of a gene in the *aarA-aarC* intergenic region encoding the phosphoprotein phosphatase SixA. SixA regulates the ArcA/ArcB two-component anoxic-redox-control system (*38*), permitting high levels of CAC enzyme synthesis in the presence of high concentrations of extracellular acetate. [The contents of Chapter 2 were published in E. A. Mullins et al. (*39*).]

Chapter 3 examines the molecular mechanism(s) by which acetate overoxidation is regulated in *A. aceti*. In yeast extract-peptone-dextrose-ethanol medium, *A. aceti* cultures accumulate acetate in the first log phase, conserve acetate in the intervening stationary phase, and ultimately deplete acetate in the second log phase. Despite moderately high levels of AarA and AarC and correspondingly high levels of CS and SCACT activities, little acetic acid is consumed prior to the second log phase. Premature acetate

overoxidation may be minimized through the maintenance of a low cytoplasmic acetate concentration.

Chapter 4 analyzes structure-function and structure-activity relationships in AarC. Crystallography, molecular modeling, and molecular mechanics calculations were combined to produce the first complete structural description of the ground-state complexes and intermediates in a class I CoA-transferase reaction. AarC utilizes a novel oxyanion hole configuration composed partly of the distal amide nitrogen of CoA to stabilize tetrahedral intermediates. Structural alignments suggest this mechanism is employed by all class I enzymes. Protein conformational dynamics, influenced by a previously unidentified auxiliary carboxylate binding site, are integral to the acceleration of CoA transfer.

REFERENCES

1. Asai, T. (1968) *Acetic acid bacteria: classification and biochemical activities*, University of Tokyo Press, Tokyo.

2. Ameyama, M., and Adachi, O. (1982) Alcohol dehydrogenase from acetic acid bacteria, membrane bound, *Methods Enzymol. 89*, 450-457.

3. Ameyama, M., and Adachi, O. (1982) Aldehyde dehydrogenase from acetic acid bacteria, membrane bound, *Methods Enzymol. 89*, 491-497.

4. Bourgeois, J. F., and Barja, F. (2009) The history of vinegar and of its acetification systems, *Arch. Sci. 62*, 147-160.

5. Saeki, A., Matsushita, K., Takeno, S., Taniguchi, M., Toyama, H., Theeragool, G., Lotong, N., and Adachi, O. (1999) Enzymes responsible for acetate oxidation by acetic acid bacteria, *Biosci. Biotechnol. Biochem. 63*, 2102-2109.

6. Sakurai, K., Arai, H., Ishii, M., and Igarashi, Y. (2011) Transcriptome response to different carbon sources in *Acetobacter aceti*, *Microbiology 157*, 899-910.

7. Saeki, A., Taniguchi, M., Matsushita, K., Toyama, H., Theeragool, G., Lotong, N., and Adachi, O. (1997) Microbiological aspects of acetate oxidation by acetic acid bacteria, unfavorable phenomena in vinegar fermentation, *Biosci. Biotechnol. Biochem. 61*, 317-323.

8. Russell, J. B. (1992) Another explanation for the toxicity of fermentation acids at low pH: anion accumulation versus uncoupling, *J. Appl. Bacteriol. 73*, 363-370.

9. Steiner, P., and Sauer, U. (2001) Proteins induced during adaptation of *Acetobacter aceti* to high acetate concentrations, *Appl. Environ. Microbiol. 67*, 5474-5481.

10. Nakano, S., Fukaya, M., and Horinouchi, S. (2004) Enhanced expression of aconitase raises acetic acid resistance in *Acetobacter aceti*, *FEMS Microbiol. Lett. 235*, 315-322.

11. Nakano, S., and Fukaya, M. (2008) Analysis of proteins responsive to acetic acid in *Acetobacter*: molecular mechanisms conferring acetic acid resistance in acetic acid bacteria, *Int. J. Food Microbiol. 125*, 54-59.

12. Constantine, C. Z., Starks, C. M., Mill, C. P., Ransome, A. E., Karpowicz, S. J., Francois, J. A., Goodman, R. A., and Kappock, T. J. (2006) Biochemical and structural studies of N^5-carboxyaminoimidazole ribonucleotide mutase from the acidophilic bacterium *Acetobacter aceti*, *Biochemistry 45*, 8193-8208.

13. Francois, J. A., and Kappock, T. J. (2007) Alanine racemase from the acidophile *Acetobacter aceti*, *Protein Expr. Purif. 51*, 39-48.

14. Mullins, E. A., Starks, C. M., Francois, J. A., Sael, L., Kihara, D., and Kappock, T. J. (2012) Formyl-coenzyme A (CoA):oxalate CoA-transferase from the acidophile *Acetobacter aceti* has a distinctive electrostatic surface and inherent acid stability, *Protein Sci. 21*, 686-696.

15. Menzel, U., and Gottschalk, G. (1985) The internal pH of *Acetobacterium wieringae* and *Acetobacter aceti* during growth and production of acetic acid, *Arch. Microbiol. 143*, 47-51.

16. Nakano, S., Fukaya, M., and Horinouchi, S. (2006) Putative ABC transporter responsible for acetic acid resistance in *Acetobacter aceti*, *Appl. Environ. Microbiol. 72*, 497-505.

17. Matsushita, K., Inoue, T., Adachi, O., and Toyama, H. (2005) *Acetobacter aceti* possesses a proton motive force-dependent efflux system for acetic acid, *J. Bacteriol. 187*, 4346-4352.

18. Lasko, D. R., Schwerdel, C., Bailey, J. E., and Sauer, U. (1997) Acetate-specific stress response in acetate-resistant bacteria: an analysis of protein patterns, *Biotechnol. Prog. 13*, 519-523.

19. Bergey, D. H., Krieg, N. R., and Holt, J. G. (1984) *Bergey's manual of systematic bacteriology*, Williams & Wilkins, Baltimore, MD.

20. Ohmori, S., Arima, K., Beppu, T., and Masai, H. (1980) Isolation and identification of acetic acid bacteria for submerged acetic acid fermentation at high temperature, *Agric. Biol. Chem. 44*, 2901-2906.

21. Ohmori, S., Uozumi, T., and Beppu, T. (1982) Loss of acetic acid resistance and ethanol oxidizing ability in an *Acetobacter* strain, *Agric. Biol. Chem. 46*, 381-389.

22. Fukaya, M., Takemura, H., Okumura, H., Kawamura, Y., Horinouchi, S., and Beppu, T. (1990) Cloning of genes responsible for acetic acid resistance in *Acetobacter aceti*, *J. Bacteriol. 172*, 2096-2104.

23. Francois, J. A., Starks, C. M., Sivanuntakorn, S., Jiang, H., Ransome, A. E., Nam, J. W., Constantine, C. Z., and Kappock, T. J. (2006) Structure of a NADH-insensitive hexameric citrate synthase that resists acid inactivation, *Biochemistry 45*, 13487-13499.

24. Fukaya, M., Takemura, H., Tayama, K., Okumura, H., Kawamura, Y., Horinouchi, S., and Beppu, T. (1993) The *aarC* gene responsible for acetic acid assimilation confers acetic acid resistance on *Acetobacter aceti*, *J. Ferment. Bioeng. 76*, 270-275.

25. Heider, J. (2001) A new family of CoA-transferases, *FEBS Lett. 509*, 345-349.

26. Rangarajan, E. S., Li, Y., Ajamian, E., Iannuzzi, P., Kernaghan, S. D., Fraser, M. E., Cygler, M., and Matte, A. (2005) Crystallographic trapping of the glutamyl-CoA thioester intermediate of family I CoA transferases, *J. Biol. Chem. 280*, 42919-42928.

27. Macieira, S., Zhang, J., Velarde, M., Buckel, W., and Messerschmidt, A. (2009) Crystal structure of 4-hydroxybutyrate CoA-transferase from *Clostridium aminobutyricum*, *Biol. Chem. 390*, 1251-1263.

28. Hersh, L. B., and Jencks, W. P. (1967) Coenzyme A transferase. Kinetics and exchange reactions, *J. Biol. Chem. 242*, 3468-3480.

29. Hersh, L. B., and Jencks, W. P. (1967) Coenzyme A transferase. Isolation and properties of an enzyme-coenzyme A intermediate, *J. Biol. Chem. 242*, 3481-3486.

30. White, H., and Jencks, W. P. (1976) Mechanism and specificity of succinyl-CoA:3-ketoacid coenzyme A transferase, *J. Biol. Chem. 251*, 1688-1699.

31. White, H., Solomon, F., and Jencks, W. P. (1976) Utilization of the inactivation rate of coenzyme A transferase by thiol reagents to determine properties of the enzyme-CoA intermediate, *J. Biol. Chem. 251*, 1700-1707.

32. Pickart, C. M., and Jencks, W. P. (1979) Formation of stable anhydrides from CoA transferases and hydroxamic acids, *J. Biol. Chem. 254*, 9120-9129.

33. Solomon, F., and Jencks, W. P. (1969) Identification of an enzyme-γ-glutamyl coenzyme A intermediate from coenzyme A transferase, *J. Biol. Chem. 244*, 1079-1081.

34. Ricagno, S., Jonsson, S., Richards, N., and Lindqvist, Y. (2003) Formyl-CoA transferase encloses the CoA binding site at the interface of an interlocked dimer, *EMBO J. 22*, 3210-3219.

35. Berthold, C. L., Toyota, C. G., Richards, N. G., and Lindqvist, Y. (2008) Reinvestigation of the catalytic mechanism of formyl-CoA transferase, a class III CoA-transferase, *J. Biol. Chem. 283*, 6519-6529.

36. Dimroth, P., and Eggerer, H. (1975) Isolation of subunits of citrate lyase and characterization of their function in the enzyme complex, *Proc. Natl. Acad. Sci. USA 72*, 3458-3462.

37. Buckel, W., and Bobi, A. (1976) The enzyme complex citramalate lyase from *Clostridium tetanomorphum*, *Eur. J. Biochem. 64*, 255-262.

38. Matsubara, M., and Mizuno, T. (2000) The SixA phospho-histidine phosphatase modulates the ArcB phosphorelay signal transduction in *Escherichia coli*, *FEBS Lett. 470*, 118-124.

39. Mullins, E. A., Francois, J. A., and Kappock, T. J. (2008) A specialized citric acid cycle requiring succinyl-coenzyme A (CoA):acetate CoA-transferase (AarC) confers acetic acid resistance on the acidophile *Acetobacter aceti*, *J. Bacteriol. 190*, 4933-4940.

Chapter 2.

Explication of the specialized citric acid cycle of *Acetobacter aceti*

INTRODUCTION

Acetic acid bacteria (AAB) are Gram-negative, acidophilic α-proteobacteria that oxidize ethanol to acetic acid using membrane-bound alcohol dehydrogenase (ADH) and aldehyde dehydrogenase (ALDH) enzymes. AAB are remarkably resistant to the membrane-permeable toxins ethanol and acetic acid at low pH. Members of the AAB genus *Acetobacter* were historically differentiated from those of *Gluconobacter* by a metabolic preference for ethanol and the ability to "overoxidize" acetate to carbon dioxide, usually when ethanol was unavailable (*1*). Acetate overoxidation implicates the oxidative decarboxylations performed by citric acid cycle (CAC) dehydrogenases and suggests the presence of a complete CAC.

Molecular mechanisms of acetic acid resistance in *Acetobacter aceti* include adaptation of cytoplasmic components (*2, 3*) to internal acidification (*4*), active acetic acid efflux via the putative ABC transporter AatA (*5*) and an unnamed acetic acid:proton antiporter (*6*), and production of acetic-acid-inducible proteins, many with undefined biochemical roles, identified by proteomic screens (*7, 8*).

A. aceti strain 1023, an especially acetic-acid-resistant and comparatively thermotolerant vinegar factory isolate (*9, 10*), requires acetic-acid-resistance genes *aarABC* for growth on > 50 mM acetic acid at low pH (*11*). AarA is an NADH-insensitive hexameric form of citrate synthase (*12*). AarB is predicted to be a basic protein of 154 amino acids with no homologues or known function (*11*). AarC is required for acetate oxidation but is not acetyl-CoA synthetase and resembles several acyl-coenzyme A (CoA):carboxylate CoA-transferases (*13*).

The apparent requirement of the *A. aceti* CAC for acetic acid resistance may indicate a direct role in depleting cytoplasmic acetate by way of acetyl-CoA oxidation to carbon dioxide or a general contribution to energy production. *A. aceti* requires vigorous oxygenation at high acetate levels and low pH (*14*), consistent with either CAC role. A draft genome sequence of *A. aceti* strain 1023 (*3*), however, lacks malate dehydrogenase (Mdh) and succinyl-CoA synthetase (SCS) genes.

This study shows that *A. aceti* possesses a complete but modified CAC, enabling direct acetate incorporation by an internal shunt. Mdh and SCS are functionally replaced by malate:quinone oxidoreductase (Mqo) and succinyl-CoA:acetate CoA-transferase (SCACT), respectively. SCACT is encoded by *aarC*. This biochemical function explains genetic evidence for essential roles in acetic acid resistance and acetic acid metabolism (*11, 13*).

MATERIALS AND METHODS

Reagents and general analytical methods. Chemicals were purchased from Sigma-Aldrich or Fisher in the highest purity available unless otherwise noted. Dethiaacetyl-CoA was synthesized by H. Jiang as described previously (*12*). Oligodeoxynucleotide (ODN) primers were obtained from Integrated DNA Technologies and used without further purification. *A. aceti* citrate synthase with a C-terminal hexahistidine affinity tag (*Aa*CSH6) was purified by C. Z. Constantine as described previously (*12*). Restriction enzymes, DNA modifying enzymes, and DNA size standards were purchased from New England Biolabs. Protein quantitation by the method of Bradford and analytical gel-

filtration were performed as described previously (*3*). Absorbance measurements were recorded on a Cary Bio 100 UV-visible spectrophotometer (Varian) or an 8453 UV-visible spectrophotometer (Agilent Technologies). Polymerase chain reaction (PCR) products and plasmids were sequenced by the Washington University in St. Louis Protein and Nucleic Acid Chemistry Laboratory. Protein mass was determined by electrospray-ionization time-of-flight mass spectrometry (ESI-TOF-MS) by the Washington University Mass Spectrometry Resource.

Sequence Analysis. A draft genome sequence for *A. aceti* strain 1023 (Table 2.1) was assembled into several hundred contigs by T. J. Kappock using PCAP (*15*). Open reading frames were identified using CRITICA, RBSFINDER, and GLIMMER 2.3.1 (*16, 17*). The combined set of open reading frames was analyzed using LipoP 1.0 (*18*) and SigP 3.0 (*19*) to predict subcellular location and then annotated automatically with InterProScan (*20*) and the KEGG (*21*) annotation server.

Propagation of *A. aceti* strains. Yeast extract-peptone-dextrose (YPD) plates supplemented with 2% (v/v) ethanol (YPDE) were streaked from frozen glycerol stocks (Table 2.1). After three days at 30 °C, single colonies were picked and transferred to 500-mL YPDE (2%) solutions in 2.8-L Fernbach flasks. Cultures were propagated at 30 °C with vigorous shaking (200 rpm) for 2 days, and cells were harvested by centrifugation and stored at –80 °C for subsequent analysis.

Cloning and mutagenesis. DNA manipulations were performed using standard molecular biology techniques (*22*). PCRs were performed using *A. aceti* strain 1023 gDNA isolated with 20/G genomic tips (Qiagen), appropriate ODN primers (Table 2.2),

Table 2.1. Bacterial strains and plasmids used in this study

Strain or plasmid	Description[a]	Source
Strains		
A. aceti 1023	Acetic-acid-tolerant factory strain	K. Kondo[b]
A. aceti 2002	*A. aceti* type strain, DSM 2002	DSMZ
E. coli C41(DE3)	F′ *ompT hsdS*$_B$(r_B^- m_B^-) *gal dcm* (DE3)	Avidis[c]
E. coli DH5α	F′ φ80*lacZ*ΔM15 Δ(*lacZYA-argF*)U169 *deoR recA1 endA1 hsdR17*(r_K^- m_K^+) *phoA supE44 thi-1 gyrA96 relA1*	Invitrogen[d]
Plasmids		
pET23a	T7 promoter expression vector, Ap^r	Novagen
pET23d	T7 promoter expression vector, Ap^r	Novagen
pET28a	T7 promoter expression vector, Km^r	Novagen
pJK286	Derivative of pET23a, encodes UctB	This study
pJK357	Derivative of pET23a, encodes AarC	This study
pJK358	Derivative of pET23a, encodes UctD	This study
pJK359	Derivative of pET23a, encodes UctA	This study
pJK360	Derivative of pET23d, encodes UctC[e]	This study
pJK361	Derivative of pET28a, encodes H6AarC[f]	This study
pJK385	Derivative of pJK357, encodes AarCH6[g]	This study

[a] Ampicillin resistant (Ap^r) and kanamycin resistant (Km^r). [b] Described in reference (*9*). [c] Described in reference (*60*). [d] Described in reference (*61*). [e] Encodes a Thr2→Ala mutation as part of a unique NcoI restriction site. [f] An upstream start codon adds MGSSHHHHHHSSGLVPRGSH to the N-terminus of AarC. [g] QuickChange mutagenesis was performed to introduce a Ter506→Ser mutation, adding SLEHHHHHH to the C-terminus of AarC.

and Vent DNA polymerase. Mutagenesis reactions were performed using the QuikChange II Site-Directed Mutagenesis kit (Stratagene), the indicated template plasmids (Table 2.1), and appropriate ODN primers (Table 2.2).

Expression of candidate SCACT genes. *E. coli* C41(DE3) cells transformed with pJK286, pJK357, pJK358, pJK359, or pJK360 were propagated on Luria-Bertani (LB) medium containing 0.1 g/L ampicillin (LB/Amp). Production cultures (50 mL LB/Amp)

Table 2.2. ODN primers used in this study

ODN	Sequence (5′ → 3′)[a]	Product(s)
1022	CTG GTA AGC TTA GTC TCT CAA GAT GCA GTC	pJK286
1168	AGG TAG ACA TAT GGG CAC GAC	pJK286
1221	CAG GAA GCC CTC ATA TGA CAG AGC G	pJK357/pJK361
1223	TGG ACC AGA ACA TAT GAC AAA AGT TAA AAC	pJK358
1224	CTT GTT TGA ATT CGG CGG TAA TGT GTT AA	pJK358
1225	CCA AAG GAT CAC ATA TGT CAG ACA AAT TAC	pJK359
1226	AAA ATA AAT GAA TTC TAT AAT TAG GAG AGT AAT TCA CG	pJK359
1228	GAA TGT ATG AAT TCA GGC GTC ATT TTG CC	pJK360
1279	GGA CCC ATG GCT GAA ACC ACG C	pJK360
1280	GCA ATA CTC GAG TTA TGA TGG GAG C	pJK357/pJK361
1290	TGC TCC CAT CAT CAC TCG AGC ACC AC	pJK385
1291	GTG GTG CTC GAG TGA TGA TGG GAG CA	pJK385

[a] Changes in the coding region relative to the genomic sequence are underlined.

were inoculated with overnight cultures at a 1:50 dilution and grown at 37 °C to an OD_{600} = 0.6. Production of recombinant protein was then induced by addition of isopropyl-β-D-1-thiogalactopyranoside (IPTG) to 0.4 mM. Cells were grown at 15 °C an additional 16 h, harvested by centrifugation, and either used immediately or stored at –80 °C.

Purification of AarCH6. *E. coli* C41(DE3) cells transformed with pJK385 were propagated on LB medium containing 0.1 g/L ampicillin (LB/Amp). Production cultures (1 L LB/Amp) were inoculated with overnight cultures at a 1:500 dilution and grown at 37 °C to an OD_{600} = 0.6. Production of recombinant AarCH6 was then induced by addition of IPTG to 0.4 mM. Cells were grown at 15 °C an additional 16 h, harvested by centrifugation, and either used immediately or stored at –80 °C. All subsequent steps were performed at 4 °C. Cells (typically 5 g/L culture) were resuspended in 5 mL/g TK

buffer (50 mM Tris•HCl, pH 8.0, and 100 mM potassium chloride) and disrupted by three cycles of sonication. Lysate was cleared by centrifugation at 30,000*g* for 30 min, addition of streptomycin to 1% (w/v) from a 10% (w/v) stock, incubation for 15 min, and additional centrifugation at 30,000*g* for 30 min. Solid ammonium sulfate was then added to the cleared lysate to 35% saturation (208 g/L) over 30 min. After equilibrating an additional 30 min, solids were removed by centrifugation at 30,000*g* for 10 min. Solid ammonium sulfate was then added to the supernatant to 75% saturation (275 g/L) over 30 min. After equilibrating an additional 30 min, solids were collected by centrifugation at 30,000*g* for 10 min, dissolved in a minimal volume of TK buffer, and applied to a Ni^{2+}-charged nitrilotriacetic acid (Ni-NTA) agarose column (1.0 cm × 2.6 cm, 2.0 mL) equilibrated in buffer A (50 mM Tris•HCl, pH 8.0, and 300 mM sodium chloride). The column was washed with 10 column volumes of buffer A containing 10 mM imidazole and then developed in a linear gradient of imidazole (10 → 500 mM, 30 mL × 30 mL). Fractions containing AarCH6 were identified by sodium dodecyl sulfate polyacrylamide gel electrophoresis (SDS-PAGE), pooled, and concentrated to > 5 mg/mL by ultrafiltration (Amicon Ultra-15, 30,000 MWCO). Concentrated AarCH6 was exchanged into TK buffer by several cycles of dilution and reconcentration. Single-use aliquots were stored at –80 °C.

CAC enzyme activity assays. *A. aceti* cell pellets were resuspended in 5 mL/g 25 mM HEPES, pH 8.0, and 100 mM sodium chloride and then disrupted by five cycles of sonication. Half of the lysate was centrifuged at 16,100*g* for 20 min (fast-spin lysate), while the other half of the lysate was centrifuged at 2,700*g* for 10 min (slow-spin lysate).

Enzyme activity assays were performed by J. A. Francois at 25 °C (0.5-mL final volume). In all cases, a unit (U) is defined as the amount of enzyme that forms 1 μmole of product per minute.

Citrate synthase assays were performed as described previously (*23*) except that reactions were initiated by the addition of fast-spin lysate (0.75 – 7.5 μg). Aconitase, α-ketoglutarate dehydrogenase, fumarase, and Mdh assays were performed using fast-spin lysate as described previously (*23*). SCS assays, detecting thioester formation at 230 nm, were performed using slow-spin lysate as described previously (*24*). Assays for the opposite direction, coupling succinyl-CoA cleavage to consumption of 5,5'-dithiobis-(2-nitrobenzoic acid) (DTNB) (*23*), gave unacceptably high background rates in cell-free lysates. Succinate dehydrogenase assays were performed as described previously (*25*) except that the reactions contained 50 mM potassium phosphate, pH 8.0, 100 mM potassium chloride, 20 mM succinate, 50 μM phenazine methosulfate, 50 μM 2,6-dichlorophenolindophenol, and 19 – 56 μg total cell lysate. Succinate-dependent dye reduction was initiated by the addition of lysate ($\Delta\varepsilon_{578}$ = 18 mM^{-1} cm^{-1}). Cell membranes used for Mqo assays were obtained by J. A. Francois as described previously (*26*). Assay mixtures contained 50 mM HEPES, pH 7.5, 10 mM potassium acetate, 10 mM calcium chloride, 5 mM magnesium chloride, 5 mM (*S*)-L-malate, 50 μM 2,6-dichlorophenolindophenol, and resupended *A. aceti* cell membranes (3 – 19 μg protein). Malate-dependent dye reduction was initiated by the addition of membranes ($\Delta\varepsilon_{600}$ = 22 mM^{-1} cm^{-1}).

Citrate synthase-dependent SCACT assays. SCACT assays were performed at 25 °C in 50 mM potassium phosphate, pH 8.0, 100 mM potassium chloride, the indicated substrates, and enzyme to initiate the reaction (0.5-mL final volume). The source of enzyme was 60 – 250 μg *A. aceti* fast-spin lysate, 1 – 250 μg recombinant *E. coli* lysate, or 5 – 50 ng pure AarCH6. Forward-direction reaction mixtures (VisF assays) contained 350 mM potassium acetate, 0.5 mM succinyl-CoA, or varied amounts of one substrate. Reverse-direction reaction mixtures (VisR assays) contained 20 mM succinate, 0.5 mM acetyl-CoA, or varied amounts of one substrate. After 0.5 and 5 min, aliquots (50 μL) were removed from the VisF/VisR reaction mixture and added to citrate synthase assays (0.5-mL final volume) containing 0.4 mM DTNB, 0.3 mM oxaloacetate, and 2 U *Aa*CSH6, but lacking acetyl-CoA. The resulting burst of thionitrobenzene formation due to CoA thiol formation was used to quantitate acetyl-CoA ($\Delta\varepsilon_{412}$ = 14.1 mM^{-1} cm^{-1}) (*27*).

Fifteen carboxylates (oxalate, formate, malate, aspartate, ascorbate, alanine, citrate, nicotinate, pyruvate, lactate, glycine, oxaloacetate, succinate, tartrate, and fumarate) were screened as possible CoA-acceptors by J. A. Francois using a variant of the VisR assay. The primary reaction (0.5-mL final volume) contained 50 mM Tris•HCl, pH 8.0, 20 mM potassium chloride, 50 mM carboxylate, pH 8.0, 50 μM acetyl-CoA, and 100 μg fast-spin lysate (passed through a prepacked PD-10 column containing Sephadex G-25M) added to initiate the reaction. After fixed times (0.5 – 30 min), aliquots (50 μL) from the primary reaction were added to citrate synthase assays (0.5-mL final volume) containing 0.4 mM DTNB, 0.3 mM oxaloacetate, and 0.01 U *Aa*CSH6, but lacking acetyl-CoA.

High performance liquid chromatography (HPLC)-coupled SCACT assays. SCACT assays were performed at 25 °C in 50 mM potassium phosphate, pH 8.0, 100 mM potassium chloride, the indicated substrates, and 5 – 50 ng pure AarCH6 used to initiate the reaction (0.5-mL final volume). Forward-direction reaction mixtures (LCF assays) contained 350 mM potassium acetate, 0.2 mM succinyl-CoA, or varied amounts of one substrate. Reverse-direction reaction mixtures (LCR assays) contained 20 mM succinic acid, 1 mM acetyl-CoA, or varied amounts of one substrate. After 0 and 5 min, aliquots (0.1 mL) of the reaction mixture were transferred into 6.25% trichloroacetic acid (0.4 mL), vortexed briefly, and centrifuged at 16,100*g* for 3 min. The soluble portion was then transferred to an autosampler vial and analyzed by HPLC.

Velocities were determined by referencing the product acyl-CoA peak area to an acetyl-CoA calibration curve (ε_{260} = 16.4 mM^{-1} cm^{-1}) (*28*). Velocities are averages of three or four determinations unless otherwise noted. Kinetic constants were determined using Prism (GraphPad) to fit equations for Michaelis-Menten kinetics, competitive inhibition, or substrate inhibition (*29*). A sum-of-squares F test was used to discriminate between alternative kinetic models.

HPLC analysis. CoA and CoA thioesters were resolved on a Breeze HPLC system (Waters) equipped with a Symmetry C18 column (4.6 mm × 75 mm, 3.5 μm; Waters) by a modified literature method (*30*). Elution was performed at ambient temperature and a flow rate of 0.8 mL/min with detection at 260 nm. A mixture of 100 mM sodium phosphate and 75 mM sodium acetate, pH 4.6, was used in a water/methanol solvent system. The gradient program was 0 – 5 min, 9% methanol (isocratic); 5 – 15 min, 9 →

15% methanol (linear gradient); 15 – 17 min, 15% methanol (isocratic); 17 – 22 min, 15 → 9% methanol (linear gradient); and 22 – 27 min, 9% methanol (isocratic). Injections (25 – 100 μL) were performed by a 717plus autosampler (Waters).

Under these conditions, peaks corresponding to CoA (8.0 min), succinyl-CoA (15.2 min), and acetyl-CoA (16.7 min) were well resolved from each other in mixtures. All peaks, including those of dethiaacetyl-CoA (10.2 min) and acetoacetyl-CoA (16.4 min), were identified by comparison to pure standards. In all cases, (acyl-)CoA peak areas were computed as the sum of the major peak and a trailing (acyl-)isoCoA peak. The latter are 2'-phosphoryl isomers that are common contaminants in commercial (acyl-)CoA preparations (*31*).

Covalent inactivation of AarCH6. AarCH6 (0.5 μg) was incubated for 10 min at 25 °C in a 0.5-mL mixture containing 50 mM potassium phosphate, pH 8.0, 100 mM potassium chloride, and 100 μM acetyl-CoA. Sodium borohydride was added to 10 mM from a 500 mM stock solution and incubated an additional 10 min. An aliquot (5 μL) of the enzyme solution was then immediately added to an otherwise complete LCR assay to measure residual enzymatic activity. Control reactions lacked sodium borohydride, acetyl-CoA, or both. The remainder of the protein solutions were flash-frozen, stored at – 80 °C, and subsequently analyzed by ESI-TOF-MS.

Fluorescence titrations. Fluorescence emission spectra were recorded by T. J. Kappock at 20 °C using a Cary Eclipse fluorescence spectrophotometer (Varian) with excitation at 285 nm (1.5 nm slit width) and detection at 300 – 420 nm (5 nm slit width). Intrinsic protein fluorescence emission spectra of a stirred solution of 1 μM AarCH6 in

50 mM potassium phosphate, pH 8.0, and 100 mM potassium chloride were acquired 1 min after the addition of each aliquot of dethiaacetyl-CoA. Succinate was then added to the AarCH6•dethiaacetyl-CoA complex. The effect of dethiaacetyl-CoA addition on *N*-acetyltryptophanamide fluorescence emission spectra was used to assess inner filter effects.

Nucleotide sequence accession numbers. The sequences reported herein have the following GenBank accession numbers: *uctA*, DQ668371; *uctB-oxc-uctC-duf1275*, DQ668372; *uctD*, DQ668373; *aarA-sixA-tyrA-orf1-aarC*, DQ631551; and *mqo*, DQ674275.

RESULTS

Reannotation of genes in the *aarABC* gene cluster. Conditionally essential acetic-acid-resistance (*aar*) genes were identified in mutant *A. aceti* strain 1023 derivatives that could not survive exposure to 50 mM acetic acid at low pH but were able to grow at an equivalent pH generated by the membrane-impermeant mineral acid HCl (*11*). Insertional inactivation experiments were used to define the *aarABC* genes and an apparently essential gene *X* (Figure 2.1) (*32*).

New gene annotations predicted three ORFs on the opposite strand: *orf1*, encoding a putative metallophosphoesterase; *tyrA*, encoding chorismate mutase; and *sixA*, encoding a transcriptional regulator involved in a phosphohistidine relay system. Gene synteny in other AAB genomes supports the new assignments (*3, 33, 34*) (http://genome.jgi-psf.org/finished_microbes/acicr/acicr.home.html). AAB have a collinear *orf1-sixA-gltA*

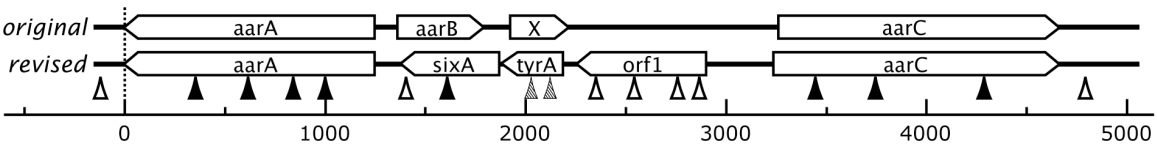

Figure 2.1. Revised annotation of the *aar* region in *A. aceti* strain 1023. The ORFs from the original gene assignment were determined using kanamycin cassette insertional inactivation at restriction sites indicated with vertical arrows (*11*). Insertion points were characterized as resistant to 50 mM acetic acid (open triangles), sensitive (filled triangles), or apparently essential (shaded triangles). Original assigned functions were *aarA*, citrate synthase; *aarB*, unknown; *X*, unknown; and *aarC*, possible CoA-transferase or acyl-CoA-hydrolase. Neither *aarB* nor *X* has significant similarity to other inferred protein sequences. The new assigned functions are *orf1*, putative metallophosphoesterase; *tyrA*, chorismate mutase; and *sixA*, phosphoprotein phosphatase affecting the ArcA/ArcB two-component regulator. The revised assignment includes a single-base insertion in the *aarC* region that lengthens the ORF slightly. The scale bar is in units of bp.

arrangement (*gltA*, citrate synthase, is the equivalent of *A. aceti aarA*), except in *Acidiphilium cryptum*, which has the putative phosphatase *orf1* located elsewhere. In *A. aceti* strain 1023 and *Gluconobacter oxydans*, *tyrA* is inserted between *orf1* and *sixA*, while *Granulibacter bethesdensis* has two genes inserted between *sixA* and *gltA*. In the revised assignment, *aarC* is divergently transcribed from all other genes in the *aar* gene region.

Annotation of genes involved in acetate metabolism. A draft 3-Mb *A. aceti* strain 1023 genome (*3*) contains all genes needed for six of the eight canonical CAC enzymes. Genes for SCS, Mdh, and glyoxylate shunt enzymes were not identified. A gene encoding membrane-bound Mqo, a functional replacement for Mdh found in diverse bacteria (*26, 35*), is present. Genes encoding enzymes needed to convert acetate to acetyl-CoA, allowing for acetate dissimilation by the CAC, are also present: acetyl-CoA synthetase (Acs) or acetate kinase (AckA) and phosphotransacetylase (Pta).

Five CoA-transferase genes, four with unassigned functions (*uctA − D*) and *aarC*, were annotated in the draft genome sequence. The originally reported *aarC* gene (GenBank accession number D13291) encodes a protein with 496 residues. The revised *aarC* gene

encodes a protein with 505 residues. The only coding region sequence difference is an insertion of a G after nucleotide 178 in the original sequence report (G210 in the revised sequence). The revised AarC has a different sequence in residues 1 − 54 (residues 1 − 40 in the original AarC).

Expression and screening of candidate SCACT genes. All five CoA-transferase genes (*uctA* − *D* and *aarC*) were cloned into pET vectors and overexpressed in *E. coli* C41(DE3) (Figure 2.2). Only UctD and AarC possessed detectable SCACT activity in VisR assays. Despite the dramatically lower solubility of AarC, the specific activity of the AarC-containing lysate was 333-fold higher than that of the UctD-containing lysate.

N- and C-terminally hexahistidine-tagged AarC (H6AarC and AarCH6, respectively) were examined in parallel overproduction experiments. While AarCH6 exhibited slightly lower solubility than AarC, H6AarC was completely insoluble. AarCH6 was purified and characterized as described below.

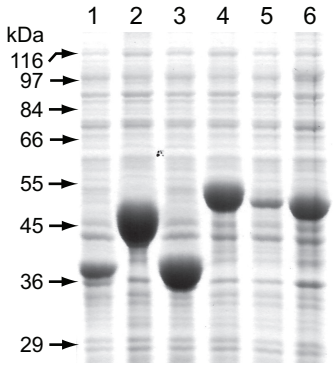

Figure 2.2. Overproduction of candidate SCACTs in *E. coli* C41(DE3). Lysates were cleared by centrifugation (16,100*g* for 10 min), analyzed by SDS-PAGE, and screened for SCACT activity using the VisR assay. The relative activity of each protein in the same culture volume is expressed as a percentage of AarC activity (a vector-only control had 0.008% relative activity). Lane 1: UctA (41.5 kDa expected, 0.007%); lane 2: UctB (47.6 kDa expected, 0.01%); lane 3: UctC (41.8 kDa expected, 0.01%); lane 4: UctD (55.5 kDa expected, 0.3%); lane 5: AarC (54.8 kDa expected, 100%); and lane 6: AarC, total lysate (insoluble protein and cellular debris were not removed by centrifugation). All lanes contain comparable amounts of lysate. Size standard positions are indicated.

Detection and quantitation of enzyme activities. Congruent with genome sequence data, six of eight canonical CAC enzyme activities were found in *A. aceti* cell lysates (Table 2.3). No activity was detected for SCS, Mdh, or the glyoxylate shunt enzymes isocitrate lyase and malate synthase [J. A. Francois]. SCACT and Mqo activities, however, were detected [J. A. Francois]. SCACT activity was initially identified using a variant of the VisR assay, measuring succinate-dependent decomposition of acetyl-CoA. Of the 15 carboxylic acids screened, only succinate supported activity.

Previously published "single-pot" CoA-transferase assays using citrate synthase to quantitate acetyl-CoA would allow kinetic characterization in only the biosynthetic direction (succinyl-CoA + acetate → acetyl-CoA + succinate) and were deemed inadequate for use in this study. Discontinuous VisF/VisR methods, which allow SCACT activity to be assayed in both the biosynthetic direction and the nonbiosynthetic direction, were developed for use with complex cell lysates. HPLC-based LCF/LCR assays were created to quantitate individual (acyl-)CoAs and allow for discrimination between acyl-CoA-hydrolase and CoA-transferase activities (Figure 2.3A). Reaction quenching conditions that minimized but did not eliminate acyl-CoA decomposition over a timescale of hours were identified (Figure 2.3B/C). Replicate experiments were performed such that the mean velocity at each concentration was determined with the same average delay. Velocity corrections based on the observed rates of acyl-CoA decomposition would increase the reported k_{cat} values by less than 10%.

Purification of AarCH6. AarCH6 was purified by ammonium sulfate fractionation and immobilized metal affinity chromatography. Purity was assessed after each stage of

Table 2.3. CAC enzyme activities in *A. aceti* strains[a]

Step	Enzyme	Sp. activity (nmol product formed/min/mg protein) in *A. aceti* strain:		Assay direction[b]	pH
		1023	2002		
1	citrate synthase	1200 ± 60	1050 ± 80	F	8.0
2	aconitase	2200 ± 200	5460 ± 4	H	8.0
3	isocitrate dehydrogenase	1280 ± 10 (NAD^+) 590 ± 20 ($NADP^+$)	530 ± 80 (NAD^+) 520 ± 50 ($NADP^+$)	F	8.0
4	α-ketoglutarate dehydrogenase	28 ± 4	98 ± 2	F	7.0
5	succinyl-CoA synthetase	ND[c]	ND	R	7.2
5′	succinyl-CoA:acetate CoA-transferase	170 ± 4 80 ± 20	114 ± 2 53 ± 5	F R	8.0
6	succinate dehydrogenase	22 ± 3	21 ± 2	F	8.0
7	fumarase	600 ± 100	700 ± 100	R	7.0
8	malate dehydrogenase	ND	ND	R	8.0
8′	malate:quinone oxidoreductase	46 ± 2	69 ± 3	F	7.5

[a] Succinyl-CoA:acetate CoA-transferase activity was measured using VisF/VisR assays. All other enzyme activities were assayed as described in the Materials and Methods. J. A. Francois assayed the canonical CAC enzymes and Mqo. [b] F, biosynthetic; R, nonbiosynthetic; H, half-reaction (citrate→aconitate). [c] Not detected.

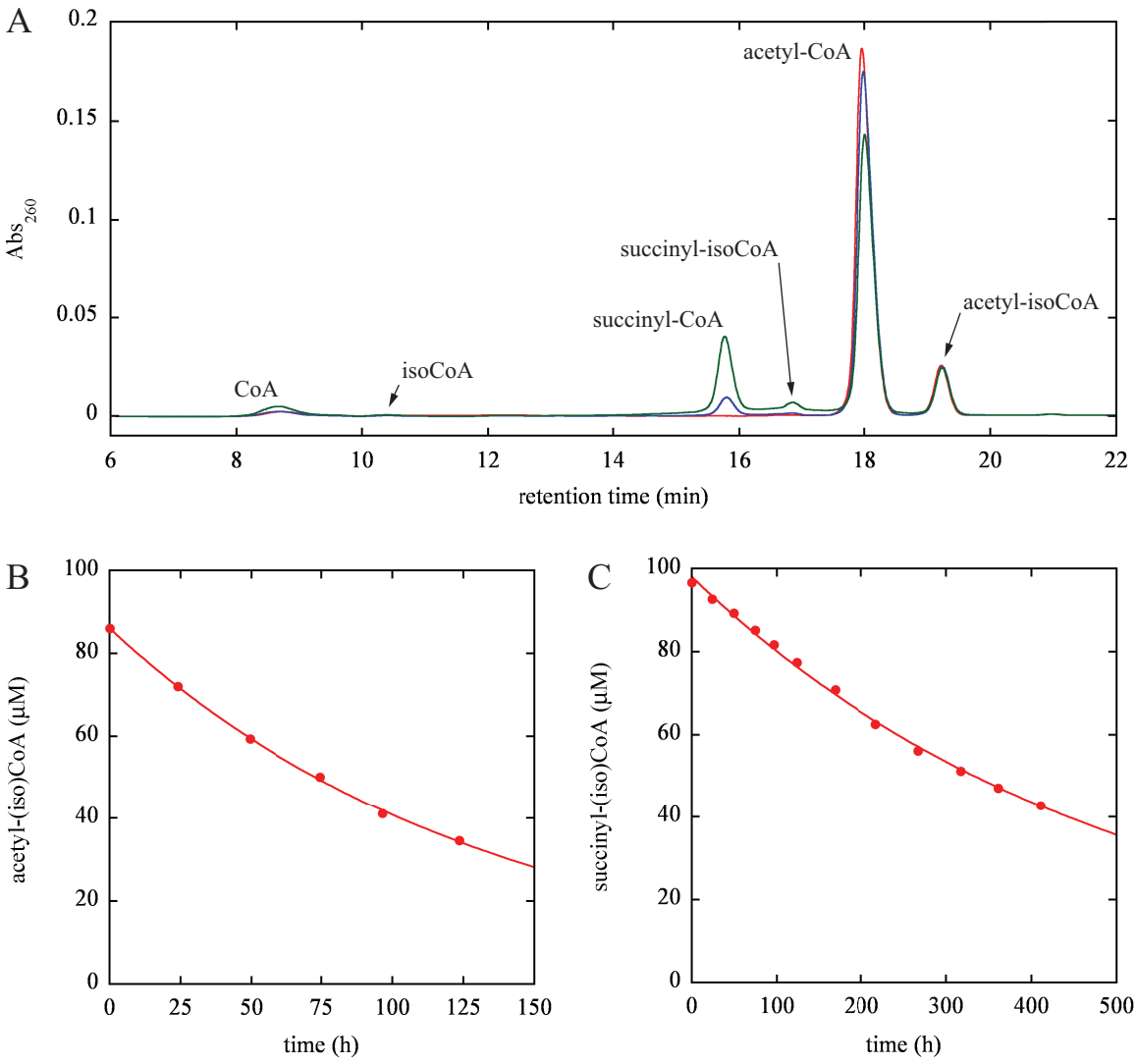

Figure 2.3. HPLC analysis of CoA, acetyl-CoA, and succinyl-CoA. **(A)** Conversion of acetyl-CoA to succinyl-CoA using pure AarCH6. Aliquots were removed from an LCR assay and quenched at t = 0 (red), 5 (blue), and 40 min (green). A small increase in the CoA peak area is evident. **(B/C)** Decomposition of acyl-(iso)CoAs in quenched reaction mixtures incubated at 22 °C. The solid lines represent fits of each dataset to the single-exponential decay function $[A]_t = [A]_0 \exp(-kt)$. **(B)** Acetyl-CoA half-life determination. The fitted parameters are $[A]_0 = 86$ μM and $k = 0.0075 \pm 0.0001$ h^{-1} (92 h half-life). **(C)** Succinyl-CoA half-life determination. The fitted parameters are $[A]_0 = 98$ μM and $k = 0.00202 \pm 0.00003$ h^{-1} (343 h half-life). At pH 8, both acetyl-CoA and succinyl-CoA have ~10 h half-lives.

the isolation by SDS-PAGE (Figure 2.4) and specific activity (Table 2.4). ESI-TOF-MS analysis of AarCH6 was consistent with a 513-residue protein lacking Met1 (55,846 ± 2 Da observed; 55,847 Da expected; Figure A.1). Analytical gel-filtration produced a single

Table 2.4. AarCH6 purification chart[a]

Stage	Protein (mg)	Activity (U)[b]	Sp. activity (U/mg)	Fold purification	Yield (%)
Clarified lystate	570	3500	6.1	1.0	100
35 − 75% $(NH_4)_2SO_4$	460	2900	6.3	1.0	83
Ni-NTA	9.5	710	75	12	20

[a] AarCH6 was purified from 8 1-L production cultures (~40 g cell paste). [b] SCACT activity was measured using the VisR assay.

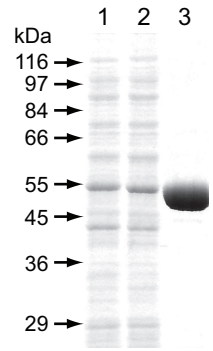

Figure 2.4. Purification of AarCH6. Purity was assessed throughout the purification by SDS-PAGE and specific activity (Table 2.4). Lane 1: clarified lysate, lane 2: 35 − 75% ammonium sulfate, and lane 3: Ni-NTA. Each lane contains 5 µg protein. Size standard positions are indicated.

peak with a molecular mass of 160 kDa, congruent with a dimeric or trimeric solution state [C. M. Starks].

Kinetic characterization of AarCH6. The determination of accurate kinetic parameters for AarCH6 was complicated by apparent acetate substrate inhibition (Figure 2.5A) and the presence of CoA, a common contaminant in commercial acyl-CoAs (~5% in acetyl-CoA, ~10% in succinyl-CoA) that hinders substrate saturation. Accurate acid substrate kinetic constants for class I CoA-transferases require saturation of the enzyme with the acyl-CoA substrate. LCF/LCR assays allowed simultaneous determination of CoA levels and enzyme activity. Similar kinetic parameters were obtained using both LCF/VisF and LCR/VisR assays (Figure 2.5A/C).

Steady-state kinetic analysis was performed for each substrate at a single, saturating, but minimally inhibitory concentration of the second substrate (Table 2.5). LCR assays spiked with CoA showed that CoA is an effective competitive inhibitor versus acetyl-CoA (Figure 2.6B). A plot of velocity versus [acetyl-CoA] is only satisfactorily fit if inhibition due to residual CoA is taken into account (Figure 2.5D). The increased scatter in velocities determined with succinyl-CoA (LCF assay) gave fits that were not improved

by correcting for CoA inhibition (Figure 2.5B). If CoA is an equally potent competitor for each acyl-CoA substrate, the values given underestimate the succinyl-CoA K_m and k_{cat} values by ~15% but have a negligible effect on K_{eq}.

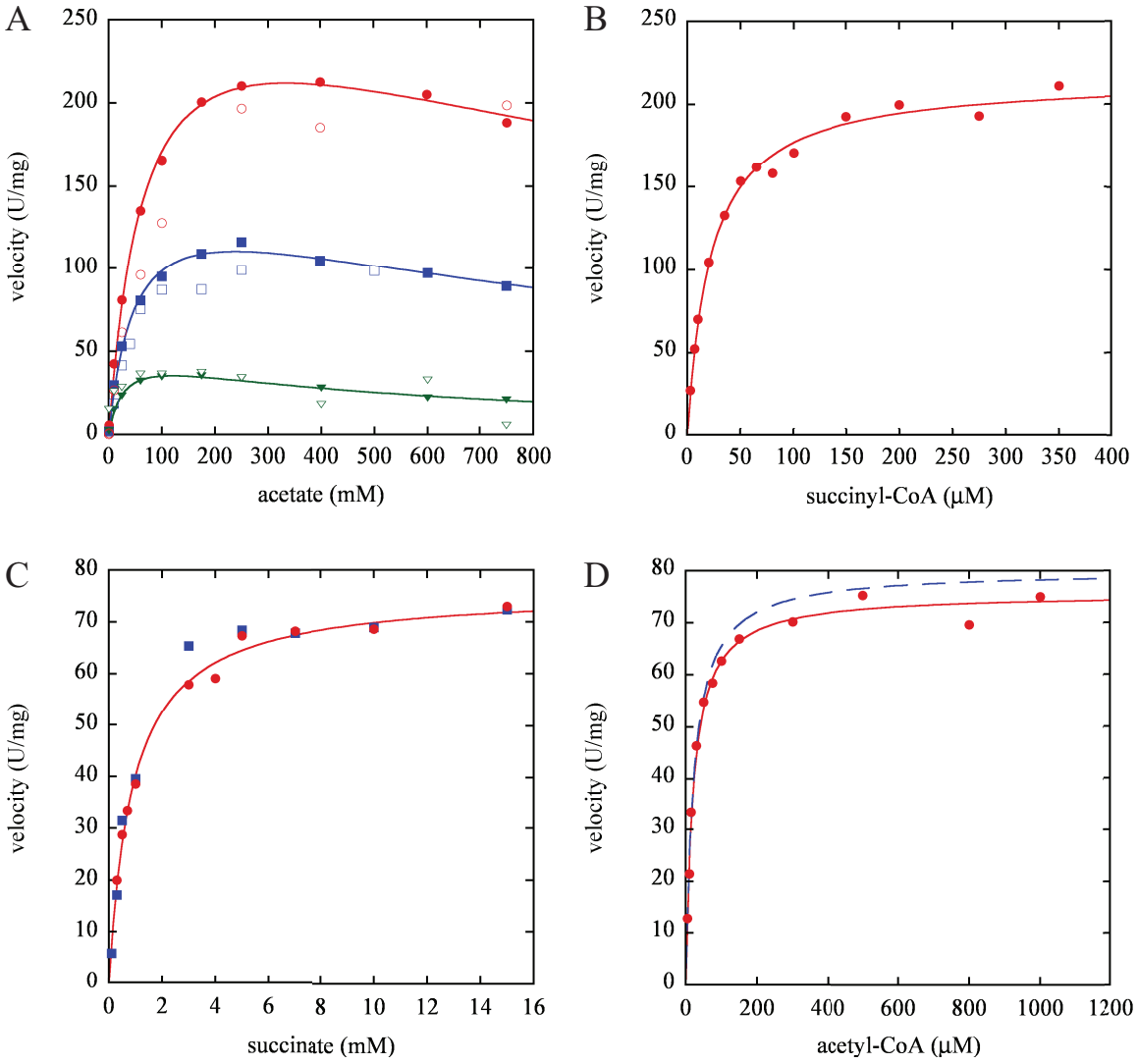

Figure 2.5. Kinetic characterization of AarCH6. **(A)** Acetate saturation data at pH 8.0 (red circles), pH 6.0 (blue squares), and pH 5.0 (green triangles) obtained with the LCF (solid symbols) and the VisF (open symbols) assays using a fixed concentration of succinyl-CoA (0.2 mM). Substrate inhibition was observed under all pH conditions examined. **(B)** Succinyl-CoA saturation data at pH 8.0 obtained with the LCF assay using a fixed concentration of acetate (350 mM). **(C)** Succinate saturation data at pH 8.0 obtained with the LCR (red circles) and VisR (blue squares) assays using a fixed concentration of acetyl-CoA (1.0 or 0.5 mM, respectively). **(D)** Acetyl-CoA saturation data at pH 8.0 obtained with the LCR assay using a fixed concentration of succinate (20 mM). The red solid line is a fit of the data accounting for competitive inhibition due to CoA contamination (determined using LCR assays spiked with additional CoA). The blue dashed line is a simulation using the fitted parameters, representing the expected acetyl-CoA saturation curve without the influence of CoA contamination ([CoA] = 0).

Table 2.5. AarCH6 kinetic constants[a]

Substrate or inhibitor	Parameter	Value
acetate (pH 8.0)[b]	k_{cat} (s^{-1})	280 ± 40
	K_m (mM)	70 ± 20
	k_{cat}/K_m (M^{-1} s^{-1})	(4 ± 1) × 10^3
	$K_{i,acetate}$ (mM)	1600 ± 800
acetate (pH 6.0)[b]	k_{cat} (s^{-1})	147 ± 9
	K_m (mM)	50 ± 10
	k_{cat}/K_m (M^{-1} s^{-1})	(2.9 ± 0.6) × 10^3
	$K_{i,acetate}$ (mM)	1100 ± 300
acetate (pH 5.0)[b]	k_{cat} (s^{-1})	49 ± 6
	K_m (mM)	29 ± 8
	k_{cat}/K_m (M^{-1} s^{-1})	(1.7 ± 0.5) × 10^3
	$K_{i,acetate}$ (mM)	500 ± 100
succinyl-CoA[b]	k_{cat} (s^{-1})	201 ± 8
	K_m (μM)	22 ± 4
	k_{cat}/K_m (M^{-1} s^{-1})	(9 ± 2) × 10^6
succinate[c]	k_{cat} (s^{-1})	71 ± 2
	K_m (mM)	0.9 ± 0.1
	k_{cat}/K_m (M^{-1} s^{-1})	(7.9 ± 0.9) × 10^4
acetyl-CoA[c]	k_{cat} (s^{-1})	75 ± 2
	K_m (μM)	22 ± 2
	k_{cat}/K_m (M^{-1} s^{-1})	(3.4 ± 0.3) × 10^6
	$K_{i,CoA}$ (μM)[e]	16 ± 2
---	K_{eq}[f]	0.14 ± 0.05
acetoacetate[d]	k_{cat} (s^{-1})	37 ± 3
	K_m (mM)	130 ± 10
	k_{cat}/K_m (M^{-1} s^{-1})	(2.8 ± 0.4) × 10^2
dethiaacetyl-CoA	K_i (μM)[g]	17 ± 3
	K_d (μM)	0.8 ± 0.2

[a] Assays were performed at 25 °C and pH 8.0 unless otherwise noted. Turnover numbers were **(cont.)**

calculated assuming one active site per 55.8 kDa subunit (1 s^{-1} = 1.07 U/mg). [b] LCF assays were performed using a fixed concentration of either succinyl-CoA (0.2 mM) or acetate (350 mM) and a variable concentration of the other substrate. [c] LCR assays were performed using a fixed concentration of either acetyl-CoA (1.0 mM) or succinate (20 mM) and a variable concentration of the other substrate. [d] Modified LCF assays were performed using a fixed concentration of succinyl-CoA (0.2 mM) and a variable concentration of acetoacetate (1 − 100 mM). [e] Modified LCR assays were performed using a variable concentration of acetyl-CoA (5 − 1,200 μM) and fixed concentrations of succinate (20 mM) and CoA (unadjusted or adjusted to a final concentration of 40, 70, or 100 μM). [f] The equilibrium constant was calculated using the Haldane relationship [$K_{eq} = (k_{cat}/K_{m,succinyl\text{-}CoA} \times k_{cat}/K_{m,acetate})/(k_{cat}/K_{m,acetyl\text{-}CoA} \times k_{cat}/K_{m,succinate})$] (*62*). [g] Modified LCR assays were performed using a variable concentration of acetyl-CoA (10 − 300 μM) and fixed concentrations of succinate (20 mM) and dethiaacetyl-CoA (0, 5, 25, or 50 μM).

Acetoacetate is a cosubstrate for several CoA-transferases that convert succinyl-CoA to succinate (*36, 37*). LCF assays containing acetoacetate instead of acetate showed that AarCH6 is also able to use acetoacetate as a CoA-acceptor. [The product peak had the same HPLC retention time as an authentic acetoacetyl-CoA standard.] The acetoacetate k_{cat}/K_m, however, is only 7% of that of acetate assayed under the same conditions (Table 2.5).

Preliminary mechanistic analysis of AarCH6. A previously published sequence alignment of active-site residues from several class I CoA-transferases (*38*) suggests that AarC(H6) is a class I enzyme. Class I CoA-transferases first bind the acyl-CoA substrate forming a glutamyl-CoA thioester intermediate and a carboxylate product (*39, 40*). The carboxylate product is then released before the carboxylate substrate is bound, accounting for the observed ping-pong kinetics (*41*) and susceptibility to borohydride inactivation (*40, 42, 43*). Sodium borohydride treatment of AarCH6 that had been incubated with acetyl-CoA caused near-complete loss of enzyme activity (0.7% relative activity) with respect to a control lacking both acetyl-CoA and sodium borohydride (100% relative activity, 79 U/mg), consistent with reduction of the glutamyl-CoA thioester intermediate to 5-hydroxynorvaline. ESI-TOF-MS analysis of the borohydride-treated enzyme

complex was also consistent with the anticipated –14 Da change (55,832 ± 2 Da observed; 55,833 Da expected; Figure A.2). Sodium borohydride treatment of AarCH6 in

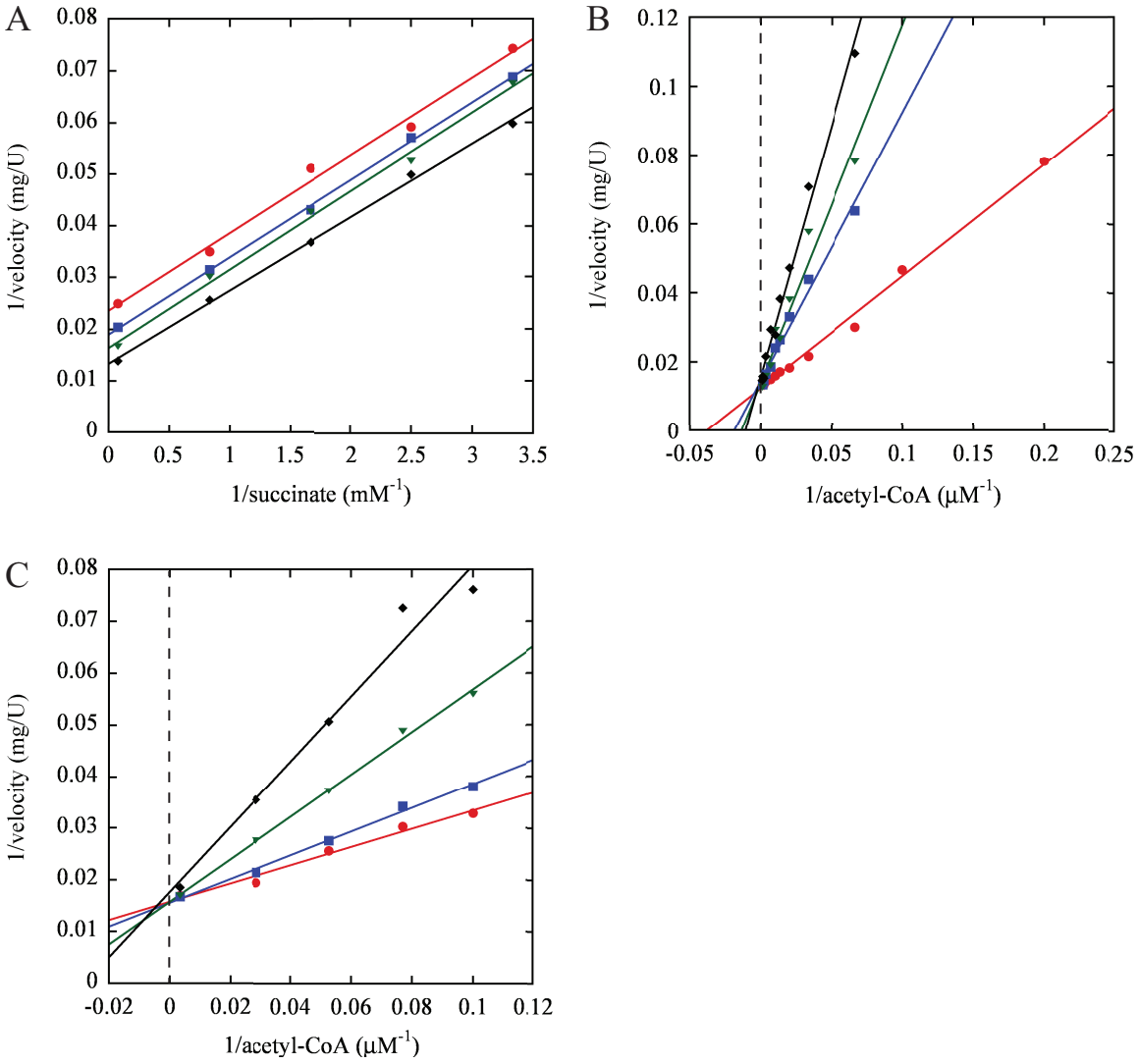

Figure 2.6. Further kinetic characterization of AarCH6. **(A)** Parallel lines indicative of ping-pong kinetics were observed in a modified LCR assays containing a variable concentration of succinate (0.3 – 13 mM) and a fixed concentration of acetyl-CoA [10 (red circles), 19 (blue squares), 60 (green triangles), or 300 µM (black diamonds)]. **(B)** CoA was determined to be a competitive inhibitor in modified LCR assays containing a variable concentration of acetyl-CoA (5 – 1200 µM) and fixed concentrations of succinate (20 mM) and CoA [unadjusted (red circles) or adjusted to a final concentration of 40 (blue squares), 70 (green triangles), or 100 µM (black diamonds)]. **(C)** Dethiaacetyl-CoA was determined to be a competitive inhibitor in modified LCR assays containing a variable concentration of acetyl-CoA (10 – 300 µM) and fixed concentrations of succinate (20 mM) and dethiaacetyl-CoA [0 (red circles), 5 (blue squares), 25 (green triangles), or 50 µM (black diamonds)]. In all panels, the solid lines illustrate linear regressions to datasets of the same color and were not used in the determination of enzyme kinetic parameters. Kinetic parameters and error estimates (Table 2.5) were determined by global nonlinear fitting as described in the Materials and Methods. Velocities in panels A and C are averages of two determinations.

the absence of acetyl-CoA caused partial inactivation (71% relative activity), which may indicate that a portion of the enzyme was isolated as the covalent AarCH6-CoA adduct. Steady-state kinetic experiments produced nonintersecting lines in double-reciprocal plots (Figure 2.6A), congruent with ping-pong kinetics and a modified-enzyme mechanism.

DISCUSSION

Genetic screens identified two categories of *Acetobacter* genes affecting acetic acid resistance: (i) those that improve the acetic acid resistance of *A. aceti* strains when introduced or overexpressed, including the *aarABC* gene cluster (*11*) and the aconitase gene (*44*), and (ii) those that improve the acetic acid resistance of *E. coli*, including the RecG (*45*) and AatA genes (*5*). This study further defines the mechanism by which the *aarABC* gene cluster confers acetic acid resistance and assesses the potential role of the CAC and related pathways in acetic acid dissimilation.

The *A. aceti* CAC converts acetate to carbon dioxide, a characteristic ability of members of the genus *Acetobacter*. A prerequisite is efficient conversion of acetate to acetyl-CoA, which can be performed by AckA/Pta or Acs. Pta and Acs activities increase in *A. aceti* during acetate oxidation (*46*). Sustained acetyl-CoA oxidation requires a complete CAC. SCS genes, however, are not present in a draft *A. aceti* strain 1023 genome sequence, and SCS activity was not detected in *A. aceti* strain 1023 lysate.

When grown in the presence of glucose, *A. aceti* is able to assimilate carbon from acetate (*5*) or ethanol (*47*). [Ethanol is presumably oxidized to acetate in the course of

assimilation.] Isocitrate lyase and malate synthase activities have been reported in *A. aceti* cells grown on acetate as the sole carbon source (*48*), which would be consistent with acetate assimilation by the glyoxylate shunt. However, genes for the glyoxylate shunt enzymes are not present in a draft *A. aceti* strain 1023 genome sequence (*3*). *A. aceti* may assimilate acetate by a different route. Alternative pathways are present in several other α-proteobacteria that lack isocitrate lyase (*49*).

The findings described herein show that *A. aceti* contains a complete but unorthodox CAC in which the acetic-acid-resistance protein AarC (SCACT) converts succinyl-CoA and acetate to succinate and acetyl-CoA. This bypass facilitates the metabolic activation and oxidation of acetate and constitutes part of a conditionally essential detoxification pathway required for survival at high acetic acid concentrations.

Potential advantages of SCACT. The use of SCACT bypasses a nucleotide requirement in the CAC and the need for initial acetate phosphorylation or adenylation (Figure 2.7), decreasing the sensitivity of flux through the CAC to the energy state of the cell. The metabolic demand for free CoA is similarly reduced. Moreover, sustained acetic acid detoxification by irreversible oxidation would require only the favorable regeneration of reduced pathway cofactors.

AarC homologues in other AAB. Southern hybridization experiments indicated that sequences homologous to *aarC* are widely present in AAB of the genus *Acetobacter* (*13*). Examination of three genome sequences from more diverse AAB revealed a close match to AarC in only *A. cryptum* (YP_001234564, $E = 1 \times 10^{-132}$), which also contains SCS genes (http://genome.jgi-psf.org/finished_microbes/acicr/acicr.home.html). Genes

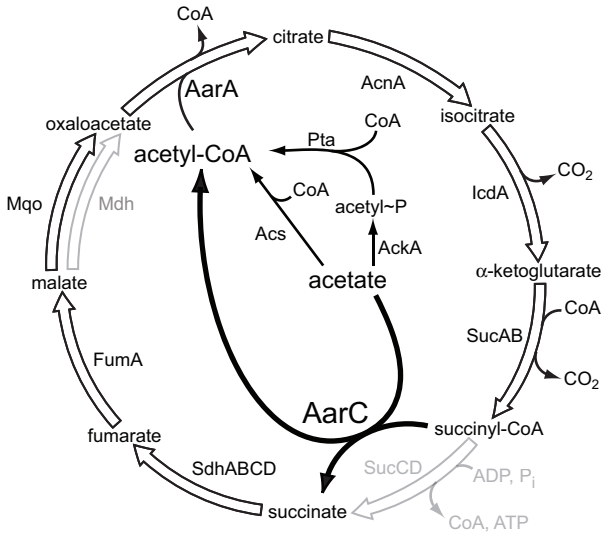

Figure 2.7. Acetate oxidation by an unorthodox *A. aceti* CAC. Gray lines indicate CAC genes that are not found in a draft *A. aceti* strain 1023 genome sequence (*3*). Each has a functional replacement. Using periplasmic dehydrogenases, *A. aceti* produces large quantities of acetic acid from ethanol and must contend with a constant influx of the former. Together with a complete oxidative phosphorylation pathway, this variant CAC functions in the eight-electron oxidation of acetic acid: $CH_3COOH + 2\ O_2 \rightarrow 2\ CO_2 + 2\ H_2O$. This pathway skips AckA, Acs, and SCS (*sucCD*), the only steps that would be directly influenced by cytoplasmic nucleotide pools, and reduces the number of enzymes that have free CoA substrates from two to one. The initial electron acceptors, two NAD^+, one FAD, and one ubiquinone (presumed to be Q9 in *A. aceti*), would give a lower energy yield than the canonical CAC but have an additional irreversible step, the Mqo-mediated quinone reduction. Genes for the glyoxylate shunt enzymes isocitrate lyase and malate synthase are not found in *A. aceti* strain 1023.

homologous to *aarC* were not found in the complete genome sequences of the AAB *G. bethesdensis CGDNIH1* (*33*) or *G. oxydans* (*34*). *G. bethesdensis CGDNIH1*, however, does possess SCS genes. Only *G. oxydans* lacks the genes necessary for a complete CAC.

Comparison with other CAC bypasses. *Helicobacter pylori* lacks several typical CAC components (*26, 50*), including Mdh, which is replaced by Mqo, and SCS, which is replaced by succinyl-CoA:acetoacetate CoA-transferase (*36*). AarC is also able to support succinyl-CoA:acetoacetate CoA-transferase activity, albeit with a substantially lower k_{cat}/K_m than that of either acetate or succinate (Table 2.5). Given the likelihood that the concentration of acetate is much greater than the concentration of acetoacetate in the *A.*

aceti cytoplasm and that genetic experiments associate *aarC* with acetate metabolism (*11, 13*), AarC is likely to function principally as SCACT.

Mycobacterium tuberculosis lacks both α-ketoglutarate dehydrogenase and SCS, which are replaced by α-ketoglutarate decarboxylase and succinic semialdehyde dehydrogenase (*23*). [Neither of these activities was detected in *A. aceti* lysates (J. A. Francois).] Like the *A. aceti* SCACT bypass, the succinic semialdehyde bypass avoids CoA- and nucleotide-dependent steps in the CAC.

All three bypasses preserve the typical cyclic course of the CAC and thereby differ from the "branched" CAC variants in facultative and obligate anaerobes (*51*).

Metabolic flux. The kinetic and mechanistic parameters of SCACT delineate potential effect(s) on metabolic flux. *A. aceti* strain 1023 tolerates > 0.5 M acetic acid, but *aar*-disrupted strains are unable to survive 50 mM acetic acid (*11*). Since there is likely no difference in acetate permeation, removal of cytoplasmic acetate appears to become critical at ~10^{-2} M. The observed acetate K_m values are in this range (Table 2.5), consistent with a conditionally essential detoxification role for AarC. At lower pH, the acetate K_m decreases, possibly increasing the rate of acetate oxidation during intense acetic acid stress.

The thiotransesterification reactions performed by CoA-transferases tend to have small $|\Delta G|$ values. The slightly unfavorable SCACT reaction (K_{eq} = 0.14; ΔG = +1.2 kcal/mol) would be mitigated at high acetate levels or when acetyl-CoA is rapidly consumed by the CAC, i.e., during vigorous aeration. Additionally, the near-thermoneutrality of the SCACT reaction is likely to be maintained in *A. aceti* as the cytoplasmic pH drops (*4*).

Acetate dissimilation. Reliance on a complete CAC for acetate removal might explain the vigorous oxygenation requirements of *A. aceti* cultures, which become critical at high acetic acid levels (*14, 52*). Together with ADH-mediated ethanol oxidation, the CAC supplies energy for many cellular processes, including the maintenance of a proton gradient. Transient oxygen deprivation sharply decreases cell viability within minutes (*14*), which is not consistent with energy loss due to a slow collapse of the transmembrane pH gradient. Instead, evidence presented here indicates that a complete CAC, including AarC, supports the overoxidation of acetate to carbon dioxide (Figure 2.7). Cytoplasmic acetate would rapidly accumulate if cofactor reoxidation slows, which is consistent with the observed rapid loss of cell viability during inadequate culture aeration.

In many Gram-negative bacteria, NADH limits CAC flux under anaerobic conditions. Citrate synthase (*53*) and Mdh (*54*) are susceptible to allosteric and product inhibition, respectively. However, both the acid-tolerant *H. pylori* and the acidophilic *A. aceti* contain citrate synthase forms that are insensitive to NADH (*12, 50*). Additionally, Mdh is replaced by Mqo in both organisms. Ubiquinone reduction by Mqo is more favorable than NAD^+ reduction by Mdh and is largely independent of the [NADH]/[NAD^+] ratio. Both properties would tend to favor the production of oxaloacetate. In *A. aceti*, these adaptations may avoid suppression of acetate dissimilation during periods of acetic acid stress.

Acetate secretion by bacteria is often due to activation of the carbon overflow pathway during anaerobiosis or when the central metabolic pathways are overtaxed (*55*). NAD^+

and CoA are recovered as acetyl-CoA is converted to CoA and acetate, a diffusible compound that leaves the cytoplasm but can be recovered in the stationary phase. In AAB, vigorous periplasmic ethanol oxidation ensures that the acetate concentration gradient is always directed inward, precluding the diffusive loss of excess cytoplasmic acetate. Oxidation of acetate to carbon dioxide by the AarC-modified *A. aceti* CAC allows diffusive carbon loss, since carbon dioxide is favored over bicarbonate at low pH and can traverse bacterial cell membranes (*56*).

A CAC regulator in the *aarA-aarC* intergenic region. New assignments in the *A. aceti aarA-aarC* intergenic region explain several previously confusing observations, including the singular gene *X* and *aarB* sequences that are apparently unique to *A. aceti*. The gene *X* region was reannotated as *tyrA* (chorismate mutase). Chorismate mutase performs a key step in aromatic amino acid biosynthesis, suggesting that the inviability of strains disrupted in the *X*/*tyrA* region (*11*) may have resulted from a nutritional deficiency. Additionally, the *aarB* region was reannotated as *sixA* (phosphoprotein phosphatase). SixA regulates the ArcA/ArcB anoxic-redox-control system, one of a small number of global regulatory systems in *E. coli* that represses the synthesis of aerobic metabolic enzymes during anaerobic conditions (*57, 58*). The observed increase in CAC enzyme activities in an ArcA-knockout (*59*) suggests that SixA-dependent suppression of the ArcA/ArcB anoxic-redox-control system would stimulate flux through the CAC. Reassignment of the conditionally essential *aarB* region to *sixA* is congruent with known AarA and AarC functions.

Conclusion. The functional assignment of AarC (SCACT) reconciles the apparent need for a complete CAC for acetic acid resistance and the absence of SCS genes in a draft *A. aceti* strain 1023 genome sequence. AarC forms an internal shunt that enables direct incorporation of acetate into the CAC and facilitates the dissimilation of diffusively trapped cytoplasmic acetate.

FUTURE DIRECTIONS

The specialized CAC described herein has obvious significance for acetic acid resistance and dissimilation but somewhat ambiguous implications for acetate assimilation. Unlike the glyoxylate shunt enzymes isocitrate lyase and malate synthase, AarC does not bypass the two oxidative decarboxylations performed by CAC dehydrogenases. The ability of *A. aceti* to utilize acetate as a sole carbon source is contentious (*13, 48*). This phenotypic discrepancy may be indicative of genotypic variance among members of a genetically unstable genus (*32*). Sequencing of the *A. aceti* strain 2002 genome would allow for comparison of the type strain and a vinegar-production strain. Two such strains should be representative of the significant genetic diversity found within *A. aceti*.

Suppression of acetate catabolism during ethanol oxidation is critical for efficient vinegar production and requires that the dissimilatory nature of the *A. aceti* CAC be curtailed. The molecular manner in which acetate overoxidation is regulated is unknown. Measuring levels of *aarC* (mRNA), AarC, and SCACT activity as a function of medium composition (ethanol, acetate, and glucose concentrations) and pH could provide

information that would ultimately allow the design of more effective industrial vinegar-production strains. Initial findings are presented in Chapter 3.

REFERENCES

1. Bergey, D. H., Krieg, N. R., and Holt, J. G. (1984) *Bergey's manual of systematic bacteriology*, Williams & Wilkins, Baltimore, MD.

2. Constantine, C. Z., Starks, C. M., Mill, C. P., Ransome, A. E., Karpowicz, S. J., Francois, J. A., Goodman, R. A., and Kappock, T. J. (2006) Biochemical and structural studies of N^5-carboxyaminoimidazole ribonucleotide mutase from the acidophilic bacterium *Acetobacter aceti*, *Biochemistry 45*, 8193-8208.

3. Francois, J. A., and Kappock, T. J. (2007) Alanine racemase from the acidophile *Acetobacter aceti*, *Protein Expr. Purif. 51*, 39-48.

4. Menzel, U., and Gottschalk, G. (1985) The internal pH of *Acetobacterium wieringae* and *Acetobacter aceti* during growth and production of acetic acid, *Arch. Microbiol. 143*, 47-51.

5. Nakano, S., Fukaya, M., and Horinouchi, S. (2006) Putative ABC transporter responsible for acetic acid resistance in *Acetobacter aceti*, *Appl. Environ. Microbiol. 72*, 497-505.

6. Matsushita, K., Inoue, T., Adachi, O., and Toyama, H. (2005) *Acetobacter aceti* possesses a proton motive force-dependent efflux system for acetic acid, *J. Bacteriol. 187*, 4346-4352.

7. Lasko, D. R., Schwerdel, C., Bailey, J. E., and Sauer, U. (1997) Acetate-specific stress response in acetate-resistant bacteria: an analysis of protein patterns, *Biotechnol. Prog. 13*, 519-523.

8. Steiner, P., and Sauer, U. (2001) Proteins induced during adaptation of *Acetobacter aceti* to high acetate concentrations, *Appl. Environ. Microbiol. 67*, 5474-5481.

9. Ohmori, S., Arima, K., Beppu, T., and Masai, H. (1980) Isolation and identification of acetic acid bacteria for submerged acetic acid fermentation at high temperature, *Agric. Biol. Chem. 44*, 2901-2906.

10. Ohmori, S., Uozumi, T., and Beppu, T. (1982) Loss of acetic acid resistance and ethanol oxidizing ability in an *Acetobacter* strain, *Agric. Biol. Chem. 46*, 381-389.

11. Fukaya, M., Takemura, H., Okumura, H., Kawamura, Y., Horinouchi, S., and Beppu, T. (1990) Cloning of genes responsible for acetic acid resistance in *Acetobacter aceti*, *J. Bacteriol. 172*, 2096-2104.

12. Francois, J. A., Starks, C. M., Sivanuntakorn, S., Jiang, H., Ransome, A. E., Nam, J. W., Constantine, C. Z., and Kappock, T. J. (2006) Structure of a NADH-insensitive hexameric citrate synthase that resists acid inactivation, *Biochemistry 45*, 13487-13499.

13. Fukaya, M., Takemura, H., Tayama, K., Okumura, H., Kawamura, Y., Horinouchi, S., and Beppu, T. (1993) The *aarC* gene responsible for acetic acid assimilation confers acetic acid resistance on *Acetobacter aceti*, *J. Ferment. Bioeng. 76*, 270-275.

14. Muraoka, H., Watabe, Y., and Ogasawara, N. (1982) Effect of oxygen deficiency on acid production and morphology of bacterial cells in submerged acetic fermentation by *Acetobacter aceti*, *J. Ferment. Technol. 60*, 171-180.

15. Huang, X., Wang, J., Aluru, S., Yang, S. P., and Hillier, L. (2003) PCAP: a whole-genome assembly program, *Genome Res. 13*, 2164-2170.

16. Badger, J. H., and Olsen, G. J. (1999) CRITICA: coding region identification tool invoking comparative analysis, *Mol. Biol. Evol. 16*, 512-524.

17. Delcher, A. L., Harmon, D., Kasif, S., White, O., and Salzberg, S. L. (1999) Improved microbial gene identification with GLIMMER, *Nucleic Acids Res. 27*, 4636-4641.

18. Juncker, A. S., Willenbrock, H., Von Heijne, G., Brunak, S., Nielsen, H., and Krogh, A. (2003) Prediction of lipoprotein signal peptides in Gram-negative bacteria, *Protein Sci. 12*, 1652-1662.

19. Bendtsen, J. D., Nielsen, H., von Heijne, G., and Brunak, S. (2004) Improved prediction of signal peptides: SignalP 3.0, *J. Mol. Biol. 340*, 783-795.

20. Mulder, N. J., Apweiler, R., Attwood, T. K., Bairoch, A., Bateman, A., Binns, D., Bradley, P., Bork, P., Bucher, P., Cerutti, L., Copley, R., Courcelle, E., Das, U., Durbin, R., Fleischmann, W., Gough, J., Haft, D., Harte, N., Hulo, N., Kahn, D., Kanapin, A., Krestyaninova, M., Lonsdale, D., Lopez, R., Letunic, I., Madera, M., Maslen, J., McDowall, J., Mitchell, A., Nikolskaya, A. N., Orchard, S., Pagni, M., Ponting, C. P., Quevillon, E., Selengut, J., Sigrist, C. J., Silventoinen, V., Studholme, D. J., Vaughan, R., and Wu, C. H. (2005) InterPro, progress and status in 2005, *Nucleic Acids Res. 33*, D201-D205.

21. Kanehisa, M., Goto, S., Hattori, M., Aoki-Kinoshita, K. F., Itoh, M., Kawashima, S., Katayama, T., Araki, M., and Hirakawa, M. (2006) From genomics to chemical genomics: new developments in KEGG, *Nucleic Acids Res. 34*, D354-D357.

22. Ausubel, F. M., Brent, R., Kingston, E., Moore, D. D., Siedman, J. D., Smith, J. A., and Struhl, K. (2000) *Current protocols in molecular biology*, John Wiley & Sons, New York, NY.

23. Tian, J., Bryk, R., Itoh, M., Suematsu, M., and Nathan, C. (2005) Variant tricarboxylic acid cycle in *Mycobacterium tuberculosis*: identification of α-ketoglutarate decarboxylase, *Proc. Natl. Acad. Sci. USA 102*, 10670-10675.

24. Ramaley, R. F., Bridger, W. A., Moyer, R. W., and Boyer, P. D. (1967) The preparation, properties, and reactions of succinyl-coenzyme A synthetase and its phosphorylated form, *J. Biol. Chem. 242*, 4287-4298.

25. Fernandes, A. S., Pereira, M. M., and Teixeira, M. (2001) The succinate dehydrogenase from the thermohalophilic bacterium *Rhodothermus marinus*: Redox-Bohr effect on heme b_L, *J. Bioenerg. Biomembr. 33*, 343-352.

26. Kather, B., Stingl, K., van der Rest, M. E., Altendorf, K., and Molenaar, D. (2000) Another unusual type of citric acid cycle enzyme in *Helicobacter pylori*: the malate:quinone oxidoreductase, *J. Bacteriol. 182*, 3204-3209.

27. Riddles, P. W., Blakeley, R. L., and Zerner, B. (1979) Ellman's reagent: 5,5'-dithiobis(2-nitrobenzoic acid)--a reexamination, *Anal. Biochem. 94*, 75-81.

28. Dawson, R. M. C. (1986) *Data for biochemical research*, 3rd ed., Clarendon Press, Oxford, United Kingdom.

29. Cleland, W. W. (1979) Statistical analysis of enzyme kinetic data, *Methods Enzymol. 63*, 103-138.

30. Demoz, A., Garras, A., Asiedu, D. K., Netteland, B., and Berge, R. K. (1995) Rapid method for the separation and detection of tissue short-chain coenzyme A esters by reversed-phase high-performance liquid chromatography, *J. Chromatogr. B Biomed. Appl. 667*, 148-152.

31. Burns, K. L., Gelbaum, L. T., Sullards, M. C., Bostwick, D. E., and May, S. W. (2005) Iso-coenzyme A, *J. Biol. Chem. 280*, 16550-16558.

32. Beppu, T. (1993) Genetic organization of *Acetobacter* for acetic acid fermentation, *Antonie Van Leeuwenhoek 64*, 121-135.

33. Greenberg, D. E., Porcella, S. F., Zelazny, A. M., Virtaneva, K., Sturdevant, D. E., Kupko, J. J., 3rd, Barbian, K. D., Babar, A., Dorward, D. W., and Holland, S. M. (2007) Genome sequence analysis of the emerging human pathogenic acetic acid bacterium *Granulibacter bethesdensis*, *J. Bacteriol. 189*, 8727-8736.

34. Prust, C., Hoffmeister, M., Liesegang, H., Wiezer, A., Fricke, W. F., Ehrenreich, A., Gottschalk, G., and Deppenmeier, U. (2005) Complete genome sequence of the acetic acid bacterium *Gluconobacter oxydans*, *Nat. Biotechnol. 23*, 195-200.

35. Goldie, A. H., Narindrasorasak, S., and Sanwal, B. D. (1978) An unusual type of regulation of malate oxidase synthesis in *Escherichia coli*, *Biochem. Biophys. Res. Commun. 83*, 421-426.

36. Corthesy-Theulaz, I. E., Bergonzelli, G. E., Henry, H., Bachmann, D., Schorderet, D. F., Blum, A. L., and Ornston, L. N. (1997) Cloning and characterization of *Helicobacter pylori* succinyl CoA:acetoacetate CoA-transferase, a novel prokaryotic member of the CoA-transferase family, *J. Biol. Chem. 272*, 25659-25667.

37. Hersh, L. B., and Jencks, W. P. (1967) Coenzyme A transferase. Kinetics and exchange reactions, *J. Biol. Chem. 242*, 3468-3480.

38. Mack, M., and Buckel, W. (1997) Conversion of glutaconate CoA-transferase from *Acidaminococcus fermentans* into an acyl-CoA hydrolase by site-directed mutagenesis, *FEBS Lett. 405*, 209-212.

39. Rochet, J. C., and Bridger, W. A. (1994) Identification of glutamate 344 as the catalytic residue in the active site of pig heart CoA transferase, *Protein. Sci. 3*, 975-981.

40. Solomon, F., and Jencks, W. P. (1969) Identification of an enzyme-γ-glutamyl coenzyme A intermediate from coenzyme A transferase, *J. Biol. Chem. 244*, 1079-1081.

41. Heider, J. (2001) A new family of CoA-transferases, *FEBS Lett. 509*, 345-349.

42. Hersh, L. B., and Jencks, W. P. (1967) Coenzyme A transferase. Isolation and properties of an enzyme-coenzyme A intermediate, *J. Biol. Chem. 242*, 3481-3486.

43. Hersh, L. B., and Jencks, W. P. (1967) Isolation of an enzyme-coenzyme A intermediate from succinyl coenzyme A-acetoacetate coenzyme A transferase, *J. Biol. Chem. 242*, 339-340.

44. Nakano, S., Fukaya, M., and Horinouchi, S. (2004) Enhanced expression of aconitase raises acetic acid resistance in *Acetobacter aceti*, *FEMS Microbiol. Lett. 235*, 315-322.

45. Steiner, P., and Sauer, U. (2003) Overexpression of the ATP-dependent helicase RecG improves resistance to weak organic acids in *Escherichia coli*, *Appl. Microbiol. Biotechnol. 63*, 293-299.

46. Saeki, A., Matsushita, K., Takeno, S., Taniguchi, M., Toyama, H., Theeragool, G., Lotong, N., and Adachi, O. (1999) Enzymes responsible for acetate oxidation by acetic acid bacteria, *Biosci. Biotechnol. Biochem. 63*, 2102-2109.

47. Rao, M. R., and Stokes, J. L. (1953) Utilization of ethanol by acetic acid bacteria, *J. Bacteriol. 66*, 634-638.

48. Stouthamer, A. H., van Boom, J. H., and Bastiaanse, A. J. (1963) Metabolism of C2 compounds in *Acetobacter aceti*, *Antonie van Leeuwenhoek 29*, 393-406.

49. Alber, B. E., Spanheimer, R., Ebenau-Jehle, C., and Fuchs, G. (2006) Study of an alternate glyoxylate cycle for acetate assimilation by *Rhodobacter sphaeroides*, *Mol. Microbiol. 61*, 297-309.

50. Pitson, S. M., Mendz, G. L., Srinivasan, S., and Hazell, S. L. (1999) The tricarboxylic acid cycle of *Helicobacter pylori*, *Eur. J. Biochem. 260*, 258-267.

51. Cronan, J. E., Jr., and Laporte, D. (1996) Tricarboxylic acid cycle and glyoxylate bypass, in *Escherichia coli and Salmonella: cellular and molecular biology* (Neidhardt, F. C., Curtiss III, R., Ingraham, J. L., Lin, E. C. C., Low, K. B., Magasanik, B., Reznikoff, M., Riley, M., Schaechter, M., and Umbarger, H. E., Eds.) 2nd ed., pp 202-216, American Society for Microbiology, Washington, DC.

52. Mesa, M. M., Caro, I., and Cantero, D. (1996) Viability reduction of *Acetobacter aceti* due to the absence of oxygen in submerged cultures, *Biotechnol. Prog. 12*, 709-712.

53. Nguyen, N. T., Maurus, R., Stokell, D. J., Ayed, A., Duckworth, H. W., and Brayer, G. D. (2001) Comparative analysis of folding and substrate binding sites between regulated hexameric type II citrate synthases and unregulated dimeric type I enzymes, *Biochemistry 40*, 13177-13187.

54. Wise, D. J., Anderson, C. D., and Anderson, B. M. (1997) Purification and kinetic characterization of *Haemophilus parasuis* malate dehydrogenase, *Arch. Biochem. Biophys. 344*, 176-183.

55. Wolfe, A. J. (2005) The acetate switch, *Microbiol. Mol. Biol. Rev. 69*, 12-50.

56. Merlin, C., Masters, M., McAteer, S., and Coulson, A. (2003) Why is carbonic anhydrase essential to *Escherichia coli*?, *J. Bacteriol. 185*, 6415-6424.

57. Bauer, C. E., Elsen, S., and Bird, T. H. (1999) Mechanisms for redox control of gene expression, *Annu. Rev. Microbiol. 53*, 495-523.

58. Iuchi, S., and Lin, E. C. (1988) *arcA* (*dye*), a global regulatory gene in *Escherichia coli* mediating repression of enzymes in aerobic pathways, *Proc. Natl. Acad. Sci. USA 85*, 1888-1892.

59. Perrenoud, A., and Sauer, U. (2005) Impact of global transcriptional regulation by ArcA, ArcB, Cra, Crp, Cya, Fnr, and Mlc on glucose catabolism in *Escherichia coli*, *J. Bacteriol. 187*, 3171-3179.

60. Miroux, B., and Walker, J. E. (1996) Over-production of proteins in *Escherichia coli*: mutant hosts that allow synthesis of some membrane proteins and globular proteins at high levels, *J. Mol. Biol. 260*, 289-298.

61. Laboratories, B. R. (1986) BRL pUC host: *E. coli* DH5α competent cells, *Focus 8*, 9.

62. Cleland, W. W. (1982) An analysis of Haldane relationships, *Methods Enzymol. 87*, 366-369.

Chapter 3.

Propagation of *Acetobacter aceti* and preliminary analysis of the *aar* gene cluster

INTRODUCTION

The characteristic ability of acetic acid bacteria (AAB) to aerobically oxidize ethanol to acetic acid has been harnessed for millennia to produce vinegar (*1*). This process is often accompanied by diauxic growth (*2-4*). Cultures accumulate acetate in the first log phase as ethanol is oxidized, maintain acetate during the first stationary phase, and then deplete acetate in the second log phase. Ideal strains for vinegar production exhibit little acetic acid consumption during the first log phase and an ability to tolerate high concentrations of acetic acid during a prolonged conservation phase (*4*).

A genetic screen of the industrial vinegar-production strain *Acetobacter aceti* 1023 identified a gene region that was essential for acetic acid resistance (*5*). The *aar* gene cluster contains five genes, of which three have roles in acetic acid resistance: *aarA* encodes citrate synthase (CS, AarA) (*5, 6*), *sixA* encodes a phosphoprotein phosphatase (SixA) that modulates synthesis of citric acid cycle (CAC) enzymes (*7*), and *aarC* encodes succinyl-CoA:acetate CoA-transferase (SCACT, AarC) (Chapter 2). AarA and AarC constitute part of a specialized CAC that provides acetic acid resistance by catalyzing the "overoxidation" of cytoplasmic acetic acid to carbon dioxide. AarC facilitates this process by circumventing substrate-level phosphorylation and/or adenylation of acetate.

The glyoxylate shunt enzymes isocitrate lyase and malate synthase, which bypass the oxidative decarboxylations performed by CAC dehydrogenases, are absent from *A. aceti* strain 1023 (Chapter 2). The lack of a glyoxylate shunt suggests that rapid acetate

depletion in the second log phase occurs primarily, if not exclusively, by dissimilatory (catabolic) means, and not by assimilatory (anabolic) means as suggested previously (*8*).

This study seeks to correlate transcriptional and translational levels of *aar* products with acetate levels during biphasic growth and to identify the molecular mechanism(s) by which acetate overoxidation is regulated.

MATERIALS AND METHODS

Reagents and general analytical methods. Chemicals were purchased from Sigma-Aldrich or Fisher in the highest purity available unless otherwise noted. Oligodeoxynucleotide (ODN) primers were obtained from Integrated DNA Technologies and used without further purification. *A. aceti* citrate synthase (*Aa*CS or AarA) and *Aa*CS with a C-terminal hexahistidine affinity tag (*Aa*CSH6) were isolated by C. M. Starks and C. Z. Constantine, respectively, as described previously (*6*). Restriction enzymes, DNA modifying enzymes, and DNA size standards were purchased from New England Biolabs. Protein quantitation by the method of Bradford was performed as described previously (*9*). Absorbance measurements were recorded on an 8453 UV-visible spectrophotometer (Agilent Technologies). Polymerase chain reaction (PCR) products and plasmids were sequenced by the Purdue University Genomics Core Facility. Protein mass was determined by matrix-assisted laser-desorption/ionization time-of-flight mass spectrometry (MALDI-TOF-MS) by the Purdue Proteomic Facility.

Cloning and mutagenesis. DNA manipulations were performed using standard molecular biology techniques (*10*). PCRs were performed using *A. aceti* strain 1023

(Table 3.1) gDNA isolated with 20/G genomic tips (Qiagen), appropriate ODN primers (Table 3.2), and Vent DNA polymerase. Mutagenesis reactions were performed using the QuikChange II Site-Directed Mutagenesis kit (Stratagene), the indicated template plasmids (Table 3.1), and appropriate ODN primers (Table 3.2).

Propagation of *A. aceti* strains. Yeast extract-peptone-dextrose (YPD, Sigma) plates supplemented with 2% (v/v) ethanol (YPDE) were streaked from frozen *A. aceti* glycerol stocks (Table 3.1). After three days at 30 °C, single colonies were picked and transferred to 500-mL YPDE (2%) solutions in 2.8-L Fernbach flasks. Cultures were propagated at 30 °C with vigorous shaking (200 rpm) for 12 days. Aliquots (10 mL) were periodically

Table 3.1. Bacterial strains and plasmids used in this study

Strain or plasmid	Description[a]	Source
Strains		
A. aceti 1023	Acetic-acid-tolerant factory strain	K. Kondo[b]
A. aceti 10-8	Derivative of strain 1023, *pro*	K. Kondo[c]
A. aceti 2002	*A. aceti* type strain, DSM 2002	DSMZ
A. aceti AS10	Derivative of strain 10-8, *pro,* acetic acid sensitive	K. Kondo[c]
E. coli C41(DE3)	F′ *ompT hsdS*$_B$(r_B^- m_B^-) *gal dcm* (DE3)	Avidis[d]
E. coli DH5α	F′ φ80*lacZ*ΔM15 Δ(*lacZYA-argF*)U169 *deoR recA1 endA1 hsdR17*(r_K^- m_K^+) *phoA supE44 thi-1 gyrA96 relA1*	Invitrogen[e]
Plasmids		
pET23a	T7 promoter expression vector, Ap^r	Novagen
pJK385	T7 promoter expression construct, encodes AarCH6, Ap^r	Chapter 2
pJK502	Derivative of pET23a, encodes SixAH6[f]	This study
pJK504	Derivative of pJK385, encodes AarCH6-C357Y[g]	This study

[a] Ampicillin resistant (Ap^r). [b] Described in reference (*23*). [c] Described in reference (*5*). [d] Described in reference (*24*). [e] Described in reference (*25*). [f] PCR was performed to introduce a Ter175→Ser mutation, adding SLEHHHHH to the C-terminus of SixA. [g] QuickChange mutagenesis was performed to introduce a Cys357→Tyr mutation.

Table 3.2. ODN primers used in this study

ODN	Sequence (5′ → 3′)[a]	Product
413	GAG CTC GAA TTC TTA GCG TTT GGC AAG CGG CAC ATA GTC AC	*aarA*
416	GAT ATA CAT ATG AGC GCG TCG CAG AAA GAA GGT AAG CTA TC	*aarA*
1221	CAG GAA GCC CTC ATA TGA CAG AGC G	*aarC*
1280	GCA ATA CTC GAG TTA TGA TGG GAG C	*aarC*
2004	GCC GCC ATA TGC GCC GCC TTG TTC TG	*sixA*
2005	GGC ATC TCG AGT GAG GGT CGC GCG AAT GT	*sixA*
2023	GCC GAT ACA ACC ACC AAT AAA AGC T	*aar*[b]
2028	GTT TAG GCT ACA TTG CCA TGA ACG GCA TGA	pJK504
2029	TCA TGC CGT TCA TGG CAA TGT AGC CTA AAC	pJK504
2037	GCC GGC ATA TGA CCG TGA CAG ACG ACC A	*tyrA*
2038	GCC GGC ATA TGC GAA ACG GAC TCC GCA	*orf1*
2053	GG TAG CGT TTA TTC GCT CTG CCG	*aar*[b]

[a] Changes in the coding region relative to the genomic sequence are underlined. [b] The PCR amplicon extends ~100 bp beyond both ends of the *aar* gene cluster.

removed and cells were harvested by centrifugation. Cell-free medium aliquots and cell pellets were stored at –80 °C for subsequent analyses. Additional aliquots (3 mL) were removed for RNA purification, mixed with 2 volumes of RNAprotect Bacteria reagent (Qiagen), and incubated at room temperature for 5 minutes. Cells were then harvested by centrifugation and cell pellets were stored at –80 °C. [Note: ethanol was added after the YPD medium was autoclaved.]

Titration of acetate in *A. aceti* cultures. Percent acidity in *A. aceti* cultures was determined by titration with 0.1 M sodium hydroxide (standardized with potassium hydrogen phthalate) as described previously (*2, 11*). Uninoculated broth was also titrated to determine the minimal background percent acidity present in YPD medium.

Enzyme activity assays. Frozen cell pellets were resuspended in 10 mL ice-cold water, repelleted by centrifugation, and then resuspended in 1 mL 50 mM potassium phosphate, pH 8.0, and 100 mM potassium chloride. Cells were lysed by three cycles of sonication, and debris was removed by centrifugation (16,100*g* and 4 °C for 15 min). SCACT and CS activities in soluble lysates were determined using DTNB-dependent VisR and CS assays as described previously (Chapter 2).

Isolation of RNA from *A. aceti* strain 1023. RNA was isolated using the RNeasy Mini kit (Qiagen) according to the instructions of the manufacturer (protocol 4: enzymatic lysis and proteinase K digestion of bacteria). Contaminating gDNA was removed by double on-column DNase treatment using the RNase-Free DNase set (Qiagen). RNA used for transcriptional mapping was also subjected to in-solution DNase treatment and then repurified using the RNeasy Mini kit.

Reverse transcription-PCR (RT-PCR) amplification of *aarA*, *sixA*, and *aarC*. One-step RT-PCR mixtures contained 1x Green GoTaq Flexi buffer, 4 mM dithioreitol (DTT), 1.25 mM magnesium chloride, 0.2 mM dNTPs, 1 μg DNase-treated total RNA, 0.3 μM ODN primers (Table 3.2), 200 U Superscript II RNase H^- reverse transcriptase (Invitrogen), and 2.5 U GoTaq DNA polymerase (Promega). Reverse transcriptase was omitted from PCR-control reactions. Amplification was performed in three stages: stage 1 (1 cycle), 30 min at 50 °C, 5 min at 94 °C; stage 2 (20 cycles, *aarA*; 25 cycles, *sixA* and *aarC*), 0.5 min at 94 °C, 1 min at 62.5 °C, 1.5 min at 72 °C; and stage 3 (1 cycle), 5 min at 72 °C.

Approximate mapping of *aar* transcripts by RT-PCR. One-step RT-PCR was performed as described above except that the annealing temperature (stage 2) was reduced to 57.5 °C and the number of cycles in stage 2 was increased to 30. Reverse transcriptase or reverse transcriptase and RNA were omitted from PCR-control reactions. Reactions lacking RNA were supplemented with 10 ng gDNA and performed by K. E. Nyffeler.

PCR amplification of the *aar* gene cluster. PCR mixtures contained 1x Phusion HF buffer, 0.2 mM dNTPs, 125 ng *A. aceti* gDNA isolated with 20/G genomic tips (Qiagen), 0.2 μM ODN primers (Table 3.2), and 1 U Phusion DNA polymerase (New England Biolabs). Amplification was performed in three stages: stage 1 (1 cycle), 2 min at 98 °C; stage 2 (30 cycles), 10 s at 98 °C, 0.5 min at 65 °C, 2.5 min at 72 °C; and stage 3 (1 cycle), 5 min at 72 °C.

Purification of SixAH6. *E. coli* C41(DE3) cells freshly transformed with pJK502 were propagated on Luria-Bertani (LB) medium containing 0.1 g/L ampicillin and 0.2% (w/v) glucose (LB/Amp/Glc). [Cultures inoculated from frozen glycerol stocks failed to overproduce SixAH6.] Production cultures (1 L LB/Amp/Glc) were inoculated with overnight cultures at a 1:100 dilution and grown at 37 °C to an OD_{600} = 0.6. Cells were then harvested by centrifugation and resuspended in 1 L LB/Amp containing 0.4 mM isopropylthio-β-D-1-galactopyranoside (IPTG). Cultures were grown at 37 °C an additional 3 h. Cells were then pelleted by centrifugation and stored at –80 °C. All subsequent steps were performed at 4 °C. Cells (typically 5 g/L culture) were resuspended in 5 mL/g 50 mM potassium phosphate, pH 6.0, and 100 mM potassium

chloride and disrupted by three cycles of sonication. Lysate was cleared by centrifugation at 30,000*g* for 30 min, addition of streptomycin to 1% (w/v) from a 10% (w/v) stock, incubation for 15 min, and additional centrifugation at 30,000*g* for 30 min. Solid ammonium sulfate was then added to the cleared lysate to 25% saturation (144 g/L) over 30 min. After equilibrating an additional 30 min, solids were removed by centrifugation at 30,000*g* for 10 min. Solid ammonium sulfate was then added to the supernatant to 45% saturation (123 g/L) over 30 min. After equilibrating an additional 30 min, solids were collected by centrifugation at 30,000*g* for 10 min, dissolved in a minimal volume of TK buffer (50 mM Tris•HCl, pH 8.0, and 100 mM potassium chloride), and applied to a Ni^{2+}-charged nitrilotriacetic acid (Ni-NTA) agarose column (1.5 cm × 4.5 cm, 8.0 mL). The column was washed with 5 column volumes of TK buffer containing 20 mM imidazole and then developed in a linear gradient of imidazole (20 → 500 mM, 80 mL × 80 mL). Fractions containing SixAH6 were identified by sodium dodecyl sulfate polyacrylamide gel electrophoresis (SDS-PAGE), pooled, and concentrated to > 5 mg/mL by ultrafiltration (Amicon Ultra-15; 3,000 MWCO). The concentration of imidazole was reduced by several cycles of dilution and reconcentration. Single-use aliquots were flash-frozen and stored at –80 °C.

Preliminary analysis of SixA levels by Western blotting. Soluble proteins in *A. aceti* strain 1023 lysate (previously prepared for enzyme activity assays) were separated by SDS-PAGE (12%) and subsequently transferred to a PVDF membrane (0.2 μm, BioRad). Transfer was performed for 1h at 100 V in Towbin buffer [25 mM Tris, 192 mM glycine, and 20% (v/v) methanol]. The membrane was then blocked for 1 h with TTBS solution

[100 mM Tris•HCl, pH 7.5, 150 mM sodium chloride, and 0.1% (v/v) Tween 20] and probed for 1 h with custom polyclonal rabbit α-SixAH6 primary antibody (diluted 1:50,000 in TTBS solution; Cocalico Biologicals). Excess antibody was removed by rinsing four times for 15 min with TTBS solution. The membrane was then probed for 1 h with goat α-rabbit IgG (H+L) HRP conjugate secondary antibody (diluted 1:250,000 in TTBS solution, Jackson ImmunoResearch). Excess antibody was again removed by rinsing four times for 15 min with TTBS solution. The membrane was then soaked for 5 min in a 1:1 mixture of stable peroxide and luminol/enhancer solutions (Thermo Scientific). Chemiluminescence was promptly measured using a ChemiImager 5500 imaging system (Alpha Innotech). The charge-coupled device (CCD) detector was exposed to the blots for 1 − 5 min.

Preliminary analysis of AarC levels by Western blotting. AarC levels were determined as described above for SixA except that the primary antibody was custom polyclonal rabbit α-AarCH6 (diluted 1:50,000; Cocalico Biologicals) and the Towbin buffer used for protein transfer was supplemented with 0.1% (w/v) sodium dodecyl sulfate (SDS) to prevent protein from remaining trapped in the polyacrylamide gel.

Preliminary analysis of AarA levels by Western blotting. AarA levels were determined as described above for AarC except that the primary antibody was custom polyclonal chicken α-AarA (diluted 1:50,000; Cocalico Biologicals) and the secondary antibody was rabbit α-chicken IgY (H+L) HRP conjugate (diluted 1:500,000; Thermo Scientific).

Heterologous production of AarCH6-C357Y. *E. coli* C41(DE3) cells transformed with pJK504 were propagated on LB medium containing 0.1 g/L ampicillin (LB/Amp). Production cultures (1 L LB/Amp) were inoculated with overnight cultures at a 1:500 dilution and grown at 37 °C to an OD_{600} = 0.6. Production of recombinant AarCH6-C357Y was then induced by addition of IPTG to 0.4 mM. Cells were grown at 15 °C an additional 16 h, harvested by centrifugation, and stored at –80 °C. All subsequent steps were performed at 4 °C. Cells (typically 5 g/L culture) were resuspended in 5 mL/g TK buffer and disrupted by three cycles of sonication. Lysate was cleared by centrifugation at 30,000*g* for 30 min, addition of streptomycin to 1% (w/v) from a 10% (w/v) stock, incubation for 15 min, and additional centrifugation at 30,000*g* for 30 min.

Analytical gel-filtration. Analytical gel-filtration was performed by K. L. Sullivan using an ÄKTA fast protein liquid chromatography (FPLC) system (Amersham Biosciences). SixAH6 (5 mg/mL in TK buffer but adjusted to 5% glycerol) was filtered through a low-retention nylon membrane (0.22 μm, Fisher) and then centrifuged at 16,000*g* and 4 °C for 10 min prior to injection (0.1 mL) onto a Superdex 200 column (1.6 cm × 60 cm, 120 mL). The column was developed at 4 °C and 1 mL/min in TK buffer. Solution sizes were determined by reference to size standards (Sigma MW-GF-1000, Blue Dextran, and acetone) using Equation 1, where V_e is the peak elution volume, V_0 is the void volume, V_t is the included volume of the gel bed, and K_{av} is the partition coefficient (proportional to the logarithm of the solution molecular weight).

$$K_{av} = \frac{V_e - V_0}{V_t - V_0} \quad (1)$$

RESULTS

Diauxic growth of *A. aceti*. Three *A. aceti* strains were propagated in YPD medium supplemented with 2% (v/v) ethanol. Both *A. aceti* strains 1023 and 10-8 [proline auxotroph derived from *A. aceti* strain 1023 by treatment with N-methyl-N′-nitro-N-nitrosoguanidine (MNNG)] exhibited biphasic growth (Figure 3.1). The first log phase for each of the strains coincided with ethanol oxidation and acetate accumulation (Figure

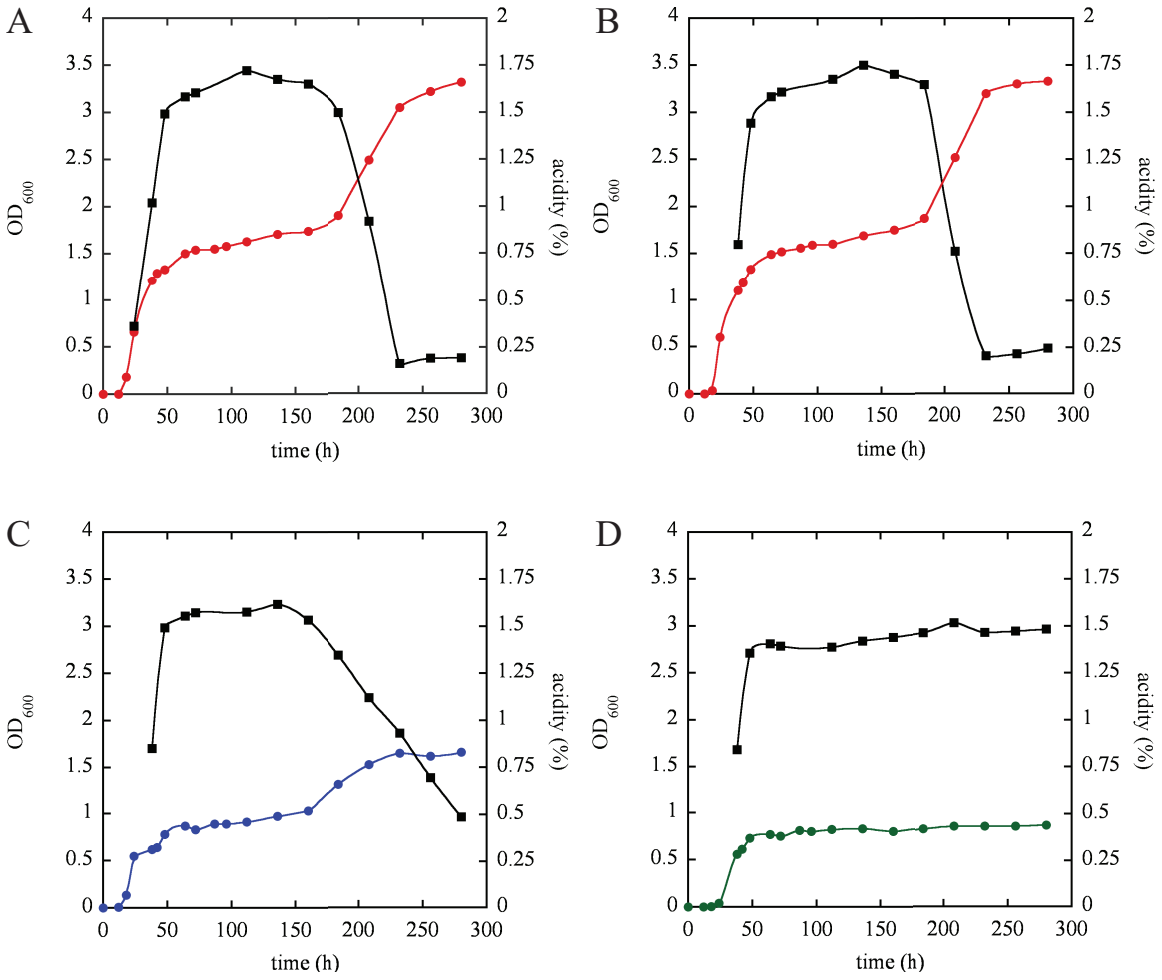

Figure 3.1. Propagation of *A. aceti* strains 1023, 10-8, and AS10. **(A)** *A. aceti* strain 1023. **(B)** *A. aceti* strain 1023 (biological replicate). **(C)** *A. aceti* strain 10-8. **(D)** *A. aceti* strain AS10. All strains were grown in YPDE medium at 30 °C. Cell density (colored circles) and culture acidity (black squares) were monitored throughout the 12-day growth period. The first and second log phases coincided with acetate accumulation and depletion, respectively, while acetate levels remained relatively constant in both stationary phases. *A. aceti* strain AS10 did not exhibit biphasic growth. Complete conversion of ethanol [2% (v/v), 0.34 M] to acetic acid [0.34 M] would correspond to 2.1% acidity.

3.1). *A. aceti* strains 1023 and 10-8 maintained relatively constant levels of acetate throughout the first stationary phase but rapidly depleted levels of acetate as the second log phase began. *A. aceti* strain AS10 (acetic-acid-sensitive derivative of *A. aceti* strain 10-8 produced by treatment with MNNG) did not undergo a diauxic shift, remaining in the first stationary phase and maintaining the concentration of acetate in the medium until the end of the growth period.

Enzyme activity assays. Cells were harvested from *A. aceti* cultures during the 12-day growth period, and SCACT and CS activities were assayed in soluble lysates (Figure 3.2). *A. aceti* strain 1023 exhibited moderate SCACT and CS activities in the first log phase and early first stationary phase as ethanol was being converted to acetate and glucose was presumably being used as the primary carbon source. SCACT and CS activities dropped dramatically (~100-fold decrease) during the first stationary phase and then spiked (> 200-fold increase) during the second log phase as acetate was depleted. Surprisingly, *A. aceti* strain 10-8 displayed very low SCACT and CS activities during both the first log and first stationary phases. Only upon onset of the second log phase did SCACT and CS activities rise to approximately those of *A. aceti* strain 1023. *A. aceti* strain AS10 exhibited SCACT and CS activities near the threshold of detection throughout the growth period, rising slightly at the last time point. The combination of greatly reduced SCACT and CS activities may account for the previously observed acetic acid sensitivity of *A. aceti* strain AS10.

Sequencing of the *aar* gene cluster. The *aar* gene cluster was amplified as a single amplicon from *A. aceti* strain 1023, 10-8, or AS10. Multiple-coverage sequencing

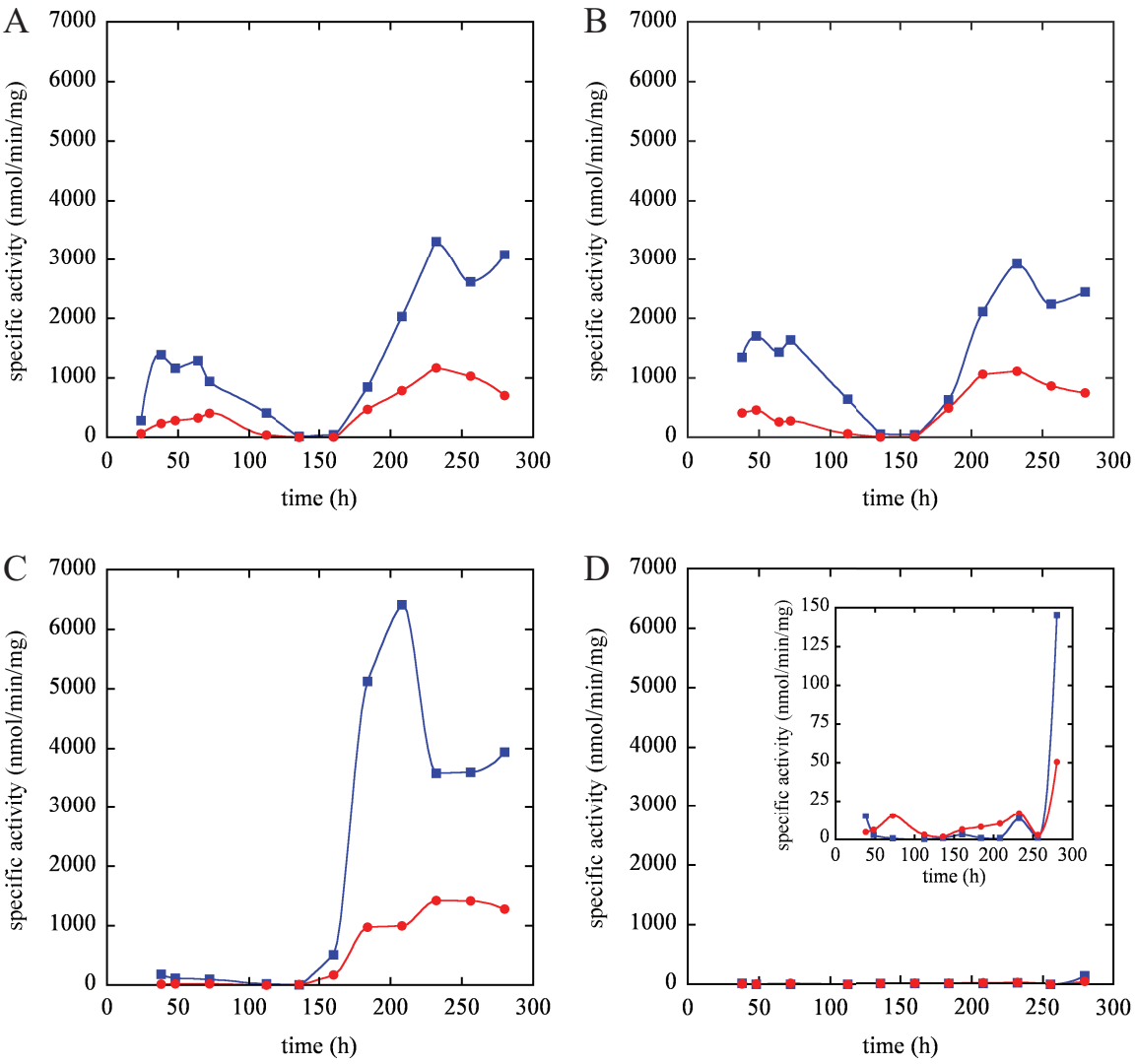

Figure 3.2. SCACT and CS activities in *A. aceti* lysates. **(A)** *A. aceti* strain 1023. **(B)** *A. aceti* strain 1023 (biological replicate). **(C)** *A. aceti* strain 10-8. **(D)** *A. aceti* strain AS10. **(D/inset)** Baseline zoom, ~50x. Cells were harvested from *A. aceti* cultures throughout the 12-day growth period, and SCACT (red circles) and CS (blue squares) specific activities were measured in soluble lysates. Vastly differing patterns of activity were observed among the strains: strain 1023 showed high levels of SCACT and CS activities in both log phases, strain 10-8 displayed high levels of SCACT and CS activities in only the second log phase, while strain AS10 exhibited SCACT and CS activities just above the limit of detection throughout the growth period.

identified three mutations relative to the deposited *aar* sequence from *A. aceti* strain 1023 (Table 3.3), encoding three mutants: AarA-A265V (*A. aceti* strain 10-8), AarA-E92K (*A. aceti* strain AS10), and AarC-C357Y (*A. aceti* strain AS10).

The *A. aceti* strain 1023 biological replicate was originally believed to be *A. aceti* strain 2002. However, sequencing revealed a nucleotide-perfect match to the *A. aceti* strain

Table 3.3. Mutations in the *aar* gene cluster[a]

Strain	Mutation	Mutant
A. aceti 10-8	619G→A	AarA-A265V
A. aceti AS10	1139C→T	AarA-E92K
A. aceti AS10	4602G→A	AarC-C357Y

[a] Mutations are relative to the deposited *aar* sequence from *A. aceti* strain 1023 (GenBank entry DQ631551).

1023 sequence in the *aar* gene cluster. *A. aceti* strain 2002 is the most phylogenetically distinct of the four strains discussed herein and should exhibit the most genotypic variance. All attempts to amplify *aarA*, *aarC,* or the complete *aar* gene cluster from authentic *A. aceti* strain 2002 gDNA failed. While undesirable, this failure is congruent with the expected sequence divergence of the industrial vinegar-production strain 1023 and the type strain 2002.

Characterization of AarA and AarC mutants. AarCH6-C357Y was heterologously overproduced in *E. coli* C41(DE3). While AarCH6-C357Y was abundant in the total lysate, no soluble enzyme remained after insoluble protein was removed by centrifugation (Figure 3.3). Furthermore, no SCACT activity was detected in the

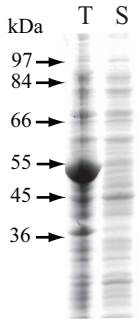

Figure 3.3. Overproduction of AarCH6-C357Y. The solubility of AarCH6-C357Y was assessed by SDS-PAGE and specific activity. Lane T: total lysate and lane S: soluble lysate. While AarCH6-C357Y was abundantly produced in recombinant *E. coli* C41(DE3), no enzyme remained after insoluble protein was removed by centrifugation. SCACT activity (VisR assay) was not detected in the soluble lysate. Lane S contains 5 µg protein. Size standard positions are indicated.

recombinant *E. coli* C41(DE3) lysate. Insolubility explains the lack of SCACT activity in the lysates of both recombinant *E. coli* C41(DE3) and *A. aceti* strain AS10. [Crystallographic analysis of AarC (Chapter 4) revealed that Cys357 is buried within a cluster of highly ordered hydrophobic residues. Introduction of a Cys357→Tyr mutation would disrupt hydrophobic packing interactions and likely hinder formation of the core β-sheet in the C-terminal domain.]

The effects of the mutations in AarA are unclear. Inspection of the hexameric structure of AarA (PDB entry 2h12) revealed that both Ala265 and Glu92 are located at the monomer-monomer interface, and neither residue has an obvious role in catalysis. Nonetheless, perturbation of the oligomeric structure could have profound implications for protein stability and catalytic activity. CS assays using lysate from *A. aceti* strain 10-8 or AS10 indicated that AarA-A265V retains most, if not all, activity, while AarA-E92K has greatly reduced activity. Activity assays using lysate from *A. aceti* strains, however, are likely influenced by overproduction of AarA, which would mask impaired catalytic activity. The effects of the mutations could be better assessed using pure enzyme. Unfortunately, efforts to duplicate the A265V or E92K mutation in plasmids encoding AarA were unsuccessful.

Purification and characterization of SixAH6. Despite the apparent toxicity of the gene product, SixAH6 was overproduced in *E. coli* C41(DE3) and purified by ammonium sulfate fractionation and immobilized metal affinity chromatography (Figure 3.4). Analytical gel-filtration and MALDI-TOF-MS indicated that SixAH6 is a predominantly monomeric (Figure 3.5), 183-residue protein retaining Met1 (Figure A.3; 19,821 ± 2 Da

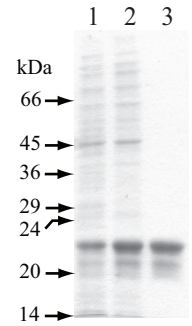

Figure 3.4. Purification of SixAH6. Purity was assessed throughout the purification by SDS-PAGE. Lane 1: clarified lysate, lane 2: 25 − 45% ammonium sulfate, and lane 3: Ni-NTA. SixAH6 migrates more slowly than expected (19.8 kDa) and smears. Both abnormalities could be caused by incomplete denaturation. MS analysis (Figure A.3) did not reveal peaks consistent with proteolysis products or contaminating proteins. Each lane contains 5 µg protein. Size standard positions are indicated.

observed; 19,822 Da expected). No peak corresponding to N-terminally processed SixAH6 lacking Met1 (19,690 Da expected) was observed by MALDI-TOF-MS analysis. Without the N-terminal methionine, SixA(H6) is predicted to have a fleeting *in vivo* half-life (2 min, ExPASy, http://web.expasy.org/protparam/) resulting from an N-terminal arginine (Arg2). Arginine is a secondary destabilizing residue in bacteria that marks proteins for ClpAP-dependent proteolysis (*12*).

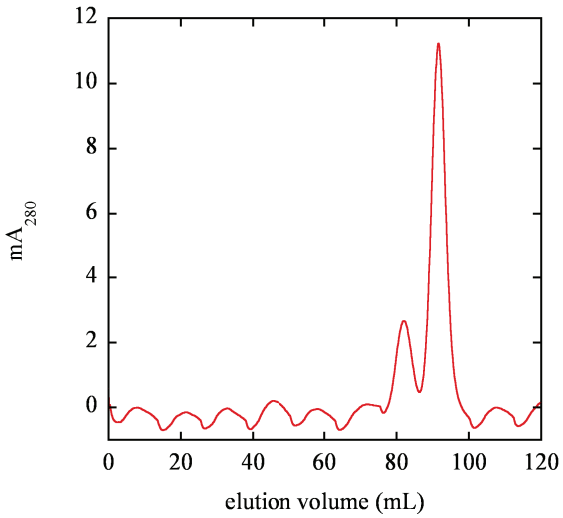

Figure 3.5. Analytical gel-filtration of SixAH6. The major peak at 91.6 mL corresponds to a monomeric solution state (21 kDa observed, 19.8 kDa expected), while the minor peak at 82.1 mL corresponds to a dimeric solution state (43 kDa observed, 39.6 kDa expected). A faulty mixer increased oscillation in the baseline but did not affect elution. Gel-filtration was performed by K. L. Sullivan.

Preliminary analyses of AarA, SixA, and AarC levels by Western blotting. Immunoblotting was performed to assess AarA, SixA, and AarC levels in *A. aceti* strain 1023 throughout the 12-day growth period (Figure 3.6). AarA and AarC levels were moderate in the first log phase, low in the mid first stationary phase, and highest in the second log phase when acetate was depleted from the medium. These protein levels correlate with SCACT and CS activities. SixA was not detected in lysate from *A. aceti* strain 1023 at any stage of the biphasic growth period. Pure SixAH6, however, strongly cross-reacted with the custom antibody under the same conditions. A limit-of-detection study indicated that SixA levels in the lysates were less than ~400 pg. [The limit-of-detection study was performed with lysate that had been transferred to the membrane in

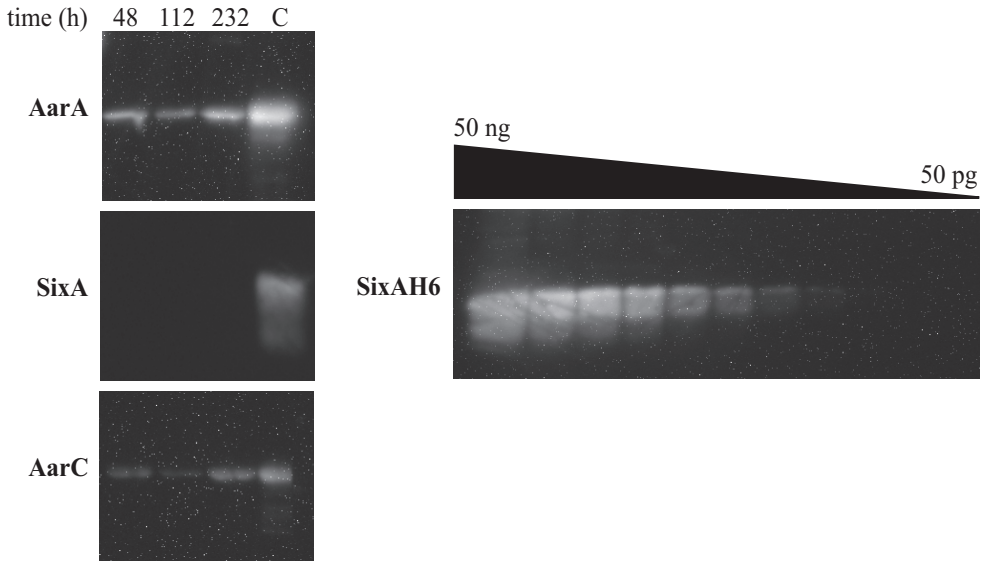

Figure 3.6. Western blot analysis of AarA, SixA, and AarC levels in *A. aceti* strain 1023. **(Left)** AarA, SixA, and AarC levels were measured in soluble lysates from *A. aceti* strain 1023 cells harvested throughout the 12-day growth period. Lanes 48, 112, and 232 each contain 5 μg total protein. Lane C contains 50 ng pure AarA, SixAH6, or AarCH6. AarA and AarC levels were highest during the first and second log phases (48 and 232 h), while both levels were considerably lower during the first stationary phase (112 h). SixA was not detected during any growth phase. **(Right)** Pure SixAH6 was two-fold serially diluted in *A. aceti* strain 1023 lysate (112 h, 1 mg/mL, 5 μg total protein per lane). The limit of detection was ~400 pg SixAH6. Transfer efficiency was improved relative to that of the SixA detection experiment, which may have slightly altered the limit of detection.

the presence of SDS, minimizing the amount of protein remaining embedded in the gel and likely slightly lowering the limit of detection beyond that of the original SixA immunoblot.] The lack of detectable levels of SixA is likely a consequence of the brief *in vivo* half-life resulting from an N-terminal arginine (Arg2). Rapid degradation is a common feature of regulatory proteins (*13*) like SixA. A short *in vivo* half-life allows for more responsive attenuation of regulator function as the rate of regulator synthesis is reduced.

Preliminary analyses of *aarA*, *sixA*, and *aarC* levels by RT-PCR. RT-PCR was performed to monitor expression of *aarA*, *sixA*, and *aarC* in *A. aceti* strain 1023 during growth in YPDE medium (Figure 3.7). Transcription of *aarA* and *aarC* increased as acetate was produced in the first log and early first stationary phases. Transcription of *aarC* further increased in the second log phase as acetate was consumed. The observed levels of expression correlate with AarA and AarC levels and CS and SCACT activities. Transcription of *sixA* peaked earlier in both log phases relative to levels of *aarA* and *aarC* and decreased earlier in both stationary phases. All three genes were weakly expressed in the second stationary phase. [RNA samples were not collected during the mid first stationary phase when protein levels and enzyme activities were lowest.] Transcription of the three *aar* genes appears to be differentially regulated.

Approximate mapping of *aar* transcripts by RT-PCR. RT-PCR primers were selected such that amplicons would span the intergenic regions in the *aar* gene cluster (Figure 3.8). RT-PCR products were observed for *sixA* − *tyrA* and *sixA* − *orf1* but not for *aarA* − *sixA*. Since *aarC* is divergently transcribed, the *aar* gene cluster appears to

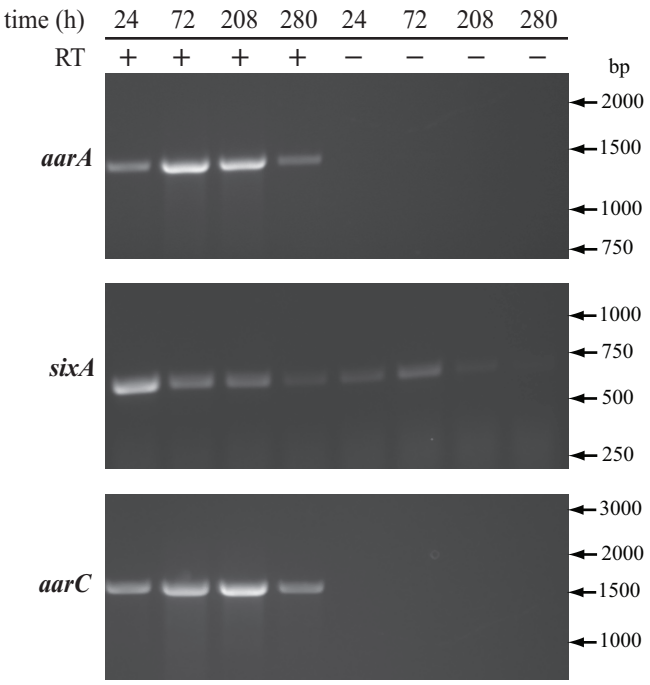

Figure 3.7. RT-PCR analysis of *aarA*, *sixA*, and *aarC* levels in *A. aceti* strain 1023. Levels of *aarA*, *sixA*, and *aarC* mRNA were measured in total RNA isolated from *A. aceti* strain 1023 cells harvested throughout the 12-day growth period. PCR controls lacking reverse transcriptase (RT) were performed to assess the effects of contaminating gDNA. While all three products were amplified from the same batches of total RNA, weak bands were only observed in *sixA* control reactions, suggesting a need for higher stringency in these reactions. Levels of *aarA* and *aarC* increased as acetate concentrations rose in the first log phase (24 h) and early first stationary phase (72 h). Levels of *aarC* further increased as acetate was depleted during the second log phase. Levels of *sixA* peaked earlier in both log phases relative to those of *aarA* and *aarC* and decreased earlier in both stationary phases. All three genes appear to be differentially expressed. Size standard positions are indicated.

produce three transcripts: a single polycistronic transcript encodes *sixA*, *tyrA*, and *orf1* and two monocistronic transcripts encode *aarA* and *aarC* (Figure 3.8). Each *aar* gene is transcribed separately from the two others, allowing for independent and potentially differential regulation.

Putative rho-independent terminator sequences are located downstream of *aarA* (TAA AAC AGA CTA ACC CAA AAA **GCC GAC TTC CCG TAA GGA AAG TCG GC**T TTT TGT TTG CAC) and *aarC* (TAA AAA **AGG GGT GGA TTT CCA CCT CT**T TTT TTC GGC TTC), defining the *aar* gene cluster. [Sequences begin with the stop codon and end with the expected T-rich region. Nucleotides shown in bold are predicted

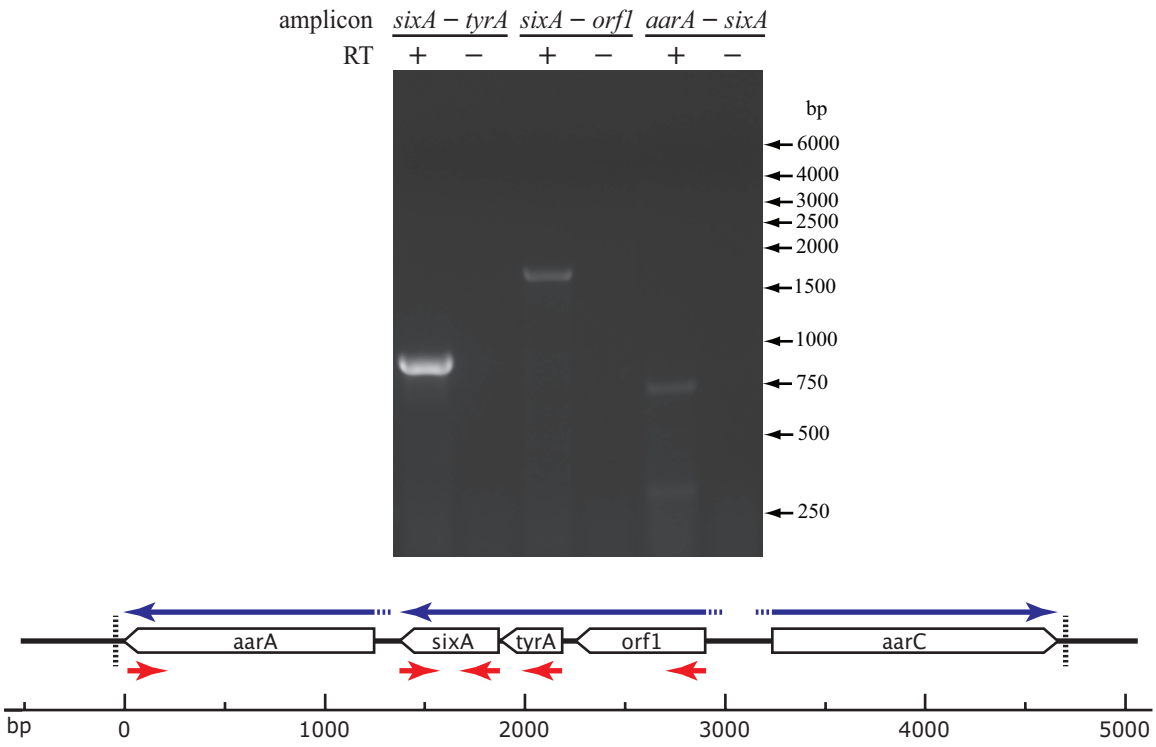

Figure 3.8. Transcriptional mapping of the *aar* gene cluster of *A. aceti* strain 1023. **(Top)** RT-PCRs were performed with ODN primers that produced amplicons spanning intergenic regions: *sixA* − *tyrA*, 833 bp expected; *sixA* − *orf1*, 1639 bp expected; and *aarA* − *sixA*, 2049 bp expected. The faint bands present in the *aarA* − *sixA* lane correspond to significantly shorter products than that expected for *aarA* − *sixA* and likely result from mispriming. No products were observed in PCR-control reactions lacking reverse transcriptase (RT). Conversely, all PCR-control reactions lacking RNA but containing gDNA produced the expected amplicons (not shown). [K. E. Nyffeler performed the latter control experiment.] Size standard positions are indicated. **(Bottom)** The *aar* gene cluster produces three transcripts (blue arrows), one of which is polycistronic. Red arrows indicate the expected annealing positions of ODN primers. The gene cluster is bookended by putative rho-independent terminator sequences (vertical dotted lines) downstream of *aarA* and *aarC*.

to constitute the stem (black) and loop (gray) structures that compose the characteristic hairpin motif. Terminator sequences were identified using the ARNold web server (http://rna.igmors.u-psud.fr/toolbox/arnold/).] A putative rho-independent terminator sequence is not present downstream of *sixA*, *tyrA*, or *orf1*, congruent with the proposed polycistronic nature of these genes. Termination of transcription after *sixA* is presumably rho dependent.

DISCUSSION

Over centuries, the repeated passaging of vinegar-producing cultures has selected for strains with the ability to rapidly accumulate and then prolongedly tolerate high concentrations of vinegar, while further overoxidizing little of the product to carbon dioxide (*4*). In the experiments performed in this study, the industrial vinegar strain *A. aceti* 1023 quickly produced acetate in the first two days of growth as cell density increased and then maintained and tolerated a high concentration of acetate (~280 mM from 340 mM ethanol) for five days as cell density remained constant. The lack of substantial acetate overoxidation during these periods could reasonably be attributed to modulation of CAC enzyme levels. However, the findings discussed below suggest that *A. aceti* strain 1023 employs an additional method, or methods, of regulating acetate overoxidation.

Modulation of CAC enzyme synthesis by SixA. Synthesis of CAC enzymes is regulated by the Arc two-component anoxic-redox-control system (*7*). The transmembrane sensor kinase ArcB autophosphorylates under anoxic and low redox conditions and then transphosphorylates ArcA (*14*), which in turn inhibits synthesis of CAC enzymes (*15*). The presence of extracellular acetate enhances autophosphorylation (*16*) and presumably further reduces CAC enzyme synthesis. However, by dephosphorylating ArcB (*7*), SixA may prevent inhibition of CAC enzyme synthesis. During vinegar production, when acetate levels in the medium can approach molar concentrations, SixA may be essential. [*A. aceti* strain 1023 derivatives with interrupted *sixA* sequences are sensitive to acetic acid (*5*).]

While the expectedly short *in vivo* half-life of SixA prevented detection of the enzyme by immunoblotting, RT-PCR revealed *sixA* expression was greatest in the early first and early second log phases. This finding reconciles the apparent need of logarithmically growing cells for high flux through the CAC and the high concentration of acetate in the medium during these periods.

Regulation of acetate overoxidation in *A. aceti* strain 1023. Enzyme activity assays and immunoblotting revealed that AarA and AarC were abundant during not only the depletion of acetate but also during the initial accumulation of acetate and much of the intervening conservation of acetate. The lack of substantial acetate overoxidation before the eighth day but the moderate levels of AarA and AarC present for most of the growth period imply that acetate catabolism during the initial stages of vinegar production was not minimized solely by reduction of the abundance of CAC enzymes.

Further diminution of acetate overoxidation during the acetic acid accumulation and conservation phases may result from the maintenance of a low cytoplasmic acetate concentration (Figure 3.9). Acetic acid efflux from the *A. aceti* cytoplasm is performed by an ABC transporter (*17*) and a proton-motive-force-dependent antiporter (*18*). Both systems require energy input that could be provided by ethanol oxidation. Periplasmic and cytoplasmic alcohol and aldehyde dehydrogenases are linked to a terminal oxidase and the oxidative phosphorylation pathway (*11*), respectively, providing the proton-motive-force required for active efflux of acetic acid and other cellular processes. While most ethanol was oxidized in the first log phase as acetic acid was being rapidly produced, the subsequent, slower accumulation of acetic acid (Figure 3.1) suggests that a

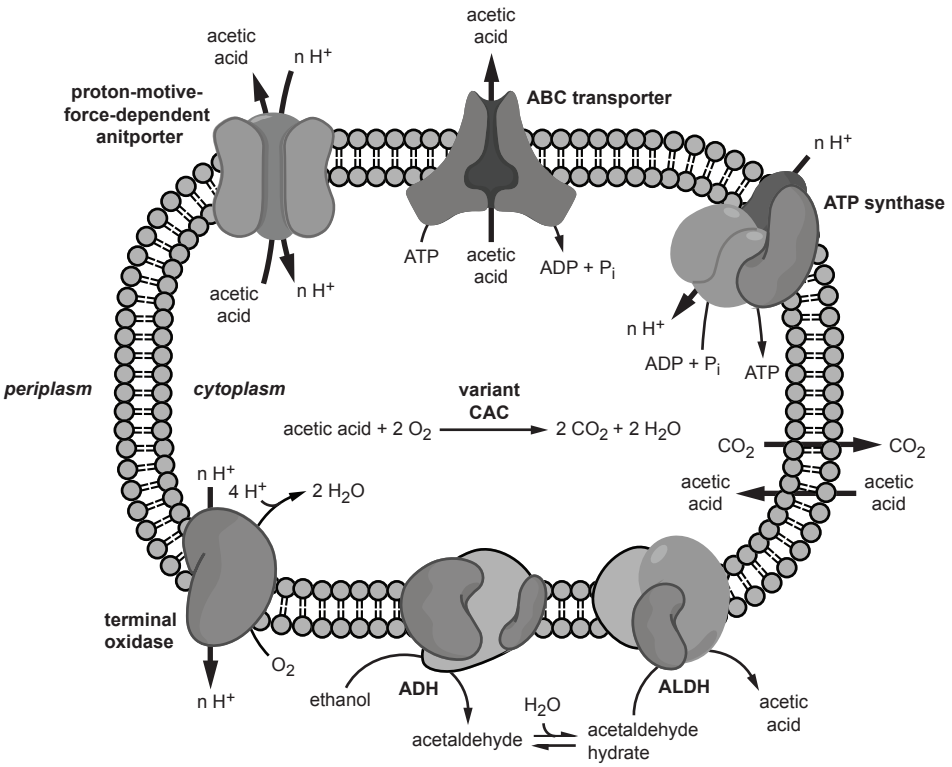

Figure 3.9. Regulation of acetate catabolism. Acetate overoxidation by the variant *A. aceti* CAC may in part be modulated by the cytoplasmic acetate concentration. Both a proton-motive-force-dependent antiporter and an ABC transporter counter the passive influx of acetic acid. Active efflux may be powered by periplasmic alcohol (ADH) and aldehyde (ALDH) dehydrogenases during acetic acid production. ADH and ALDH supply electrons for a terminal oxidase which provides the proton-motive-force required for synthesis of ATP and other cellular processes. Cytoplasmic NADH-dependent ADH and ALDH (not shown) may also support efflux of acetic acid.

small but significant amount of ethanol remained, providing a source of energy to support continued, active acetic acid efflux during the first stationary phase. The onset of the acetate depletion phase has been observed to occur only when all ethanol has been depleted (*2, 4, 19*) and ethanol oxidation can no longer provide the necessary proton-motive-force to support active acetic acid efflux. This metabolic shift may be delayed by the variable but low cytoplasmic pH of *A. aceti* (*20*), which should reduce diffusively trapped acetate (*21*). Additionally, the high acetate K_m in the AarC-catalyzed SCACT reaction (Chapters 2 and 4) may minimize background acetate overoxidation during the

acetate accumulation and acetate conservation phases (while a low cytoplasmic acetate concentration is maintained).

Acetic acid sensitivity in *A. aceti* strain AS10. *A. aceti* strain AS10 was previously found to be sensitive to acetic acid (*5*). This phenotype was attributed to an undefined mutation in *aarC*. This study shows that *A. aceti* strain AS10 encodes AarC-C357Y, a mutant with dramatically lower solubility than the wild-type enzyme. A previously unknown mutation in *aarA* was also identified. *A. aceti* strain AS10 encodes AarA-E92K. Both mutants supported greatly diminished enzymatic activities in lysates that would substantially slow, if not halt, acetate overoxidation. An inability to remove excess acetate from the cytoplasm by overoxidation would be consistent with the observed acetic-acid-sensitive phenotype. Furthermore, the lack of a second log phase suggests that acetate overoxidation and biphasic growth are linked in *A. aceti*.

Acetate metabolism in type and vinegar-production strains. *A. aceti* strain 1023 has a highly specialized CAC. While AarC facilitates acetate overoxidation by bypassing substrate-level phosphorylation and adenylation (Chapter 2), the lack of succinyl-CoA synthetase (SCS) makes flux through the CAC dependent upon the cytoplasmic acetate concentration. Recent sequencing of the genome of *A. aceti* strain NBRC 14818 (regarded as the "other" type strain) revealed far more versatile pathways of acetate metabolism (*3*) that avoid this limitation (Figure 3.10). SCS permits acetate-independent flux through the CAC, while isocitrate lyase and malate synthase provide an assimilatory pathway for acetate utilization. In this varied metabolic scheme, AarC may be relegated solely to acetic acid resistance.

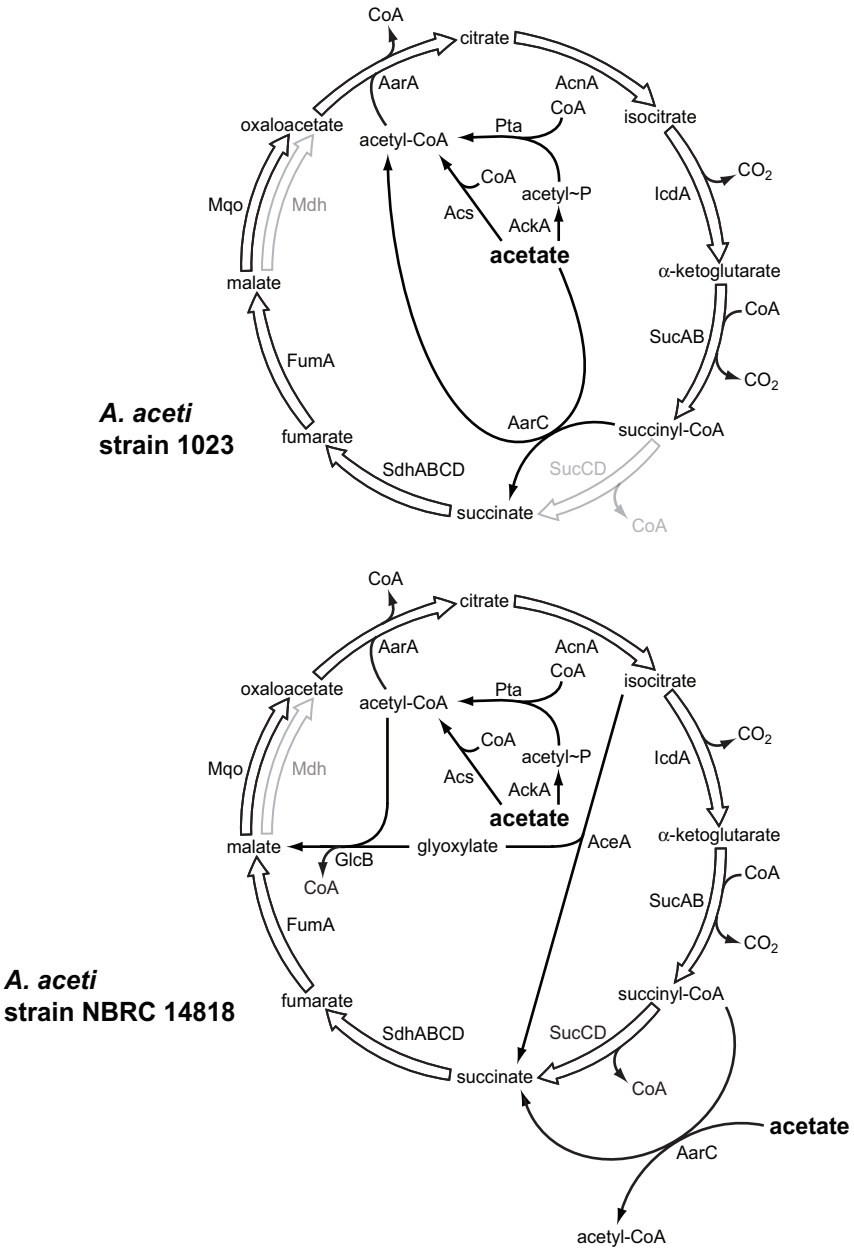

Figure 3.10. Acetate metabolism pathways in *A. aceti*. Gray arrows indicate enzymes that are not encoded in the genome sequences. **(Top)** *A. aceti* strain 1023 has a highly specialized CAC, conferring acetic acid resistance through efficient cytoplasmic acetate overoxidation. AarC preserves the cyclic nature of the CAC in the absence of SCS, isocitrate lyase, and malate synthase. **(Bottom)** *A. aceti* strain NBRC 14818 has a far more versatile CAC, maintaining the canonical route for acetate-independent flux while providing both dissimilatory and assimilatory pathways for acetate metabolism. SCS, both glyoxylate shunt enzymes, and AarC support recycling of oxaloacetate. Mdh is functionally replaced by Mqo in both strains. The *A. aceti* strain NBRC 14818 CAC was reproduced from (*3*).

Diverse pathways of acetate metabolism provide clear adaptive advantages in the complex, nutritionally variable fruit-associated niches in which *A. aceti* is commonly

found (*1*). In a defined industrial setting, however, a glyoxylate shunt may not be beneficial and may increase acetate consumption during ethanol oxidation. Selection for strains that produce the highest yield of vinegar may have eliminated those capable of acetate assimilation.

Conclusion. Biphasic growth in YPDE medium is accompanied by distinct stages of acetate accumulation, conservation, and depletion. While AarC is most abundant during the acetate overoxidation phase, the moderate levels of AarC present during the acetate accumulation and early acetate conservation phases seem to preclude direct modulation of enzyme levels from being the sole method by which acetate catabolism is regulated. Further reduction of acetate overoxidation prior to the acetate depletion phase may result from the active maintenance of a low cytoplasmic acetate concentration.

FUTURE DIRECTIONS

The work described herein was of a preliminary nature but established the methods necessary for a thorough study and made apparent the deficiencies in the current experimental design. [1] A more complete analysis of metabolite levels is needed. Ethanol and glucose concentrations should be measured enzymatically or chromatographically as described previously (*2*) to supplement the analysis of acetate levels. [2] Regulation of acetic acid influx and efflux is likely critical for acetate overoxidation and resistance. Cytoplasmic acetate concentrations should be determined throughout the biphasic growth period using a radiation-independent method described previously (*22*). [3] The MNNG-derived strains are largely genotypically uncharacterized

and potentially misleading. The presence of previously unidentified mutations in *aarA* (*A. aceti* strains 10-8 and AS10) and the lack of induction of AarA and AarC in the first log phase (*A. aceti* strains 10-8 and possibly AS10) suggest that a number of additional unidentified mutations may be present. Precise mutations, while challenging to generate in *A. aceti*, are needed if definitive conclusions are to be drawn. Alternatively, the *A. aceti* type strain NBRC 14818, which now has an available genome sequence, could be compared with *A. aceti* strain 1023 to examine the effects of directed evolution on acetic acid production, conservation, and resistance.

REFERENCES

1. Asai, T. (1968) *Acetic acid bacteria: classification and biochemical activities*, University of Tokyo Press, Tokyo.

2. Saeki, A., Matsushita, K., Takeno, S., Taniguchi, M., Toyama, H., Theeragool, G., Lotong, N., and Adachi, O. (1999) Enzymes responsible for acetate oxidation by acetic acid bacteria, *Biosci. Biotechnol. Biochem. 63*, 2102-2109.

3. Sakurai, K., Arai, H., Ishii, M., and Igarashi, Y. (2011) Transcriptome response to different carbon sources in *Acetobacter aceti*, *Microbiology 157*, 899-910.

4. Saeki, A., Taniguchi, M., Matsushita, K., Toyama, H., Theeragool, G., Lotong, N., and Adachi, O. (1997) Microbiological aspects of acetate oxidation by acetic acid bacteria, unfavorable phenomena in vinegar fermentation, *Biosci. Biotechnol. Biochem. 61*, 317-323.

5. Fukaya, M., Takemura, H., Okumura, H., Kawamura, Y., Horinouchi, S., and Beppu, T. (1990) Cloning of genes responsible for acetic acid resistance in *Acetobacter aceti*, *J. Bacteriol. 172*, 2096-2104.

6. Francois, J. A., Starks, C. M., Sivanuntakorn, S., Jiang, H., Ransome, A. E., Nam, J. W., Constantine, C. Z., and Kappock, T. J. (2006) Structure of a NADH-insensitive hexameric citrate synthase that resists acid inactivation, *Biochemistry 45*, 13487-13499.

7. Matsubara, M., and Mizuno, T. (2000) The SixA phospho-histidine phosphatase modulates the ArcB phosphorelay signal transduction in *Escherichia coli*, *FEBS Lett. 470*, 118-124.

8. Fukaya, M., Takemura, H., Tayama, K., Okumura, H., Kawamura, Y., Horinouchi, S., and Beppu, T. (1993) The *aarC* gene responsible for acetic acid assimilation confers acetic acid resistance on *Acetobacter aceti*, *J. Ferment. Bioeng. 76*, 270-275.

9. Francois, J. A., and Kappock, T. J. (2007) Alanine racemase from the acidophile *Acetobacter aceti*, *Protein Expr. Purif. 51*, 39-48.

10. Ausubel, F. M., Brent, R., Kingston, E., Moore, D. D., Siedman, J. D., Smith, J. A., and Struhl, K. (2000) *Current protocols in molecular biology*, John Wiley & Sons, New York, NY.

11. Chinnawirotpisan, P., Theeragool, G., Limtong, S., Toyama, H., Adachi, O., and Matsushita, K. (2003) Quinoprotein alcohol dehydrogenase is involved in catabolic acetate production, while NAD-dependent alcohol dehydrogenase in ethanol assimilation in *Acetobacter pasteurianus* SKU1108, *J. Biosci. Bioeng. 96*, 564-571.

12. Tobias, J. W., Shrader, T. E., Rocap, G., and Varshavsky, A. (1991) The N-end rule in bacteria, *Science 254*, 1374-1377.

13. Varshavsky, A. (1997) The N-end rule pathway of protein degradation, *Genes Cells 2*, 13-28.

14. Peña-Sandoval, G. R., and Georgellis, D. (2010) The ArcB sensor kinase of *Escherichia coli* autophosphorylates by an intramolecular reaction, *J. Bacteriol. 192*, 1735-1739.

15. Iuchi, S., and Lin, E. C. (1988) *arcA* (*dye*), a global regulatory gene in *Escherichia coli* mediating repression of enzymes in aerobic pathways, *Proc. Natl. Acad. Sci. USA 85*, 1888-1892.

16. Georgellis, D., Kwon, O., and Lin, E. C. C. (1999) Amplification of signaling activity of the Arc two-component system of *Escherichia coli* by anaerobic metabolites, *J. Biol. Chem. 274*, 35950-35954.

17. Nakano, S., Fukaya, M., and Horinouchi, S. (2006) Putative ABC transporter responsible for acetic acid resistance in *Acetobacter aceti*, *Appl. Environ. Microbiol. 72*, 497-505.

18. Matsushita, K., Inoue, T., Adachi, O., and Toyama, H. (2005) *Acetobacter aceti* possesses a proton motive force-dependent efflux system for acetic acid, *J. Bacteriol. 187*, 4346-4352.

19. Kornmann, H., Duboc, P., Niederberger, P., Marison, I., and von Stockar, U. (2003) Influence of residual ethanol concentration on the growth of *Gluconacetobacter xylinus* I 2281, *Appl. Microbiol. Biotechnol. 62*, 168-173.

20. Menzel, U., and Gottschalk, G. (1985) The internal pH of *Acetobacterium wieringae* and *Acetobacter aceti* during growth and production of acetic acid, *Arch. Microbiol. 143*, 47-51.

21. Russell, J. B. (1992) Another explanation for the toxicity of fermentation acids at low pH: anion accumulation versus uncoupling, *J. Appl. Bacteriol. 73*, 363-370.

22. Steiner, P., and Sauer, U. (2003) Long-term continuous evolution of acetate resistant *Acetobacter aceti*, *Biotechnol. Bioeng. 84*, 40-44.

23. Ohmori, S., Arima, K., Beppu, T., and Masai, H. (1980) Isolation and identification of acetic acid bacteria for submerged acetic acid fermentation at high temperature, *Agric. Biol. Chem. 44*, 2901-2906.

24. Miroux, B., and Walker, J. E. (1996) Over-production of proteins in *Escherichia coli*: mutant hosts that allow synthesis of some membrane proteins and globular proteins at high levels, *J. Mol. Biol. 260*, 289-298.

25. Laboratories, B. R. (1986) BRL pUC host: *E. coli* DH5α competent cells, *Focus 8*, 9.

Chapter 4.

Crystallographic, mechanistic, and further biophysical characterization of succinyl-CoA:acetate CoA-transferase (AarC)

INTRODUCTION

Coenzyme A (CoA)-transferases catalyze the reversible transfer of CoA from acyl-CoA thioesters to free acids and play diverse metabolic roles in organisms from all lines of descent. All three classes of CoA-transferase share mechanistic features, but only class I and II enzymes appear to have a common ancestor (*1*).

Class I CoA-transferases exhibit ping-pong kinetics and employ a substituted-enzyme mechanism (Scheme 4.1) (*2, 3*). Upon formation of the enzyme•acyl-CoA Michaelis complex, the protein undergoes a conformational shift that accelerates catalysis (*4*). Attack by the nucleophilic glutamate transiently produces the covalent acylglutamyl anhydride intermediate and the CoA thiolate (*4-6*), while subsequent attack by the nucleophilic CoA thiolate produces the glutamyl-CoA thioester intermediate and the

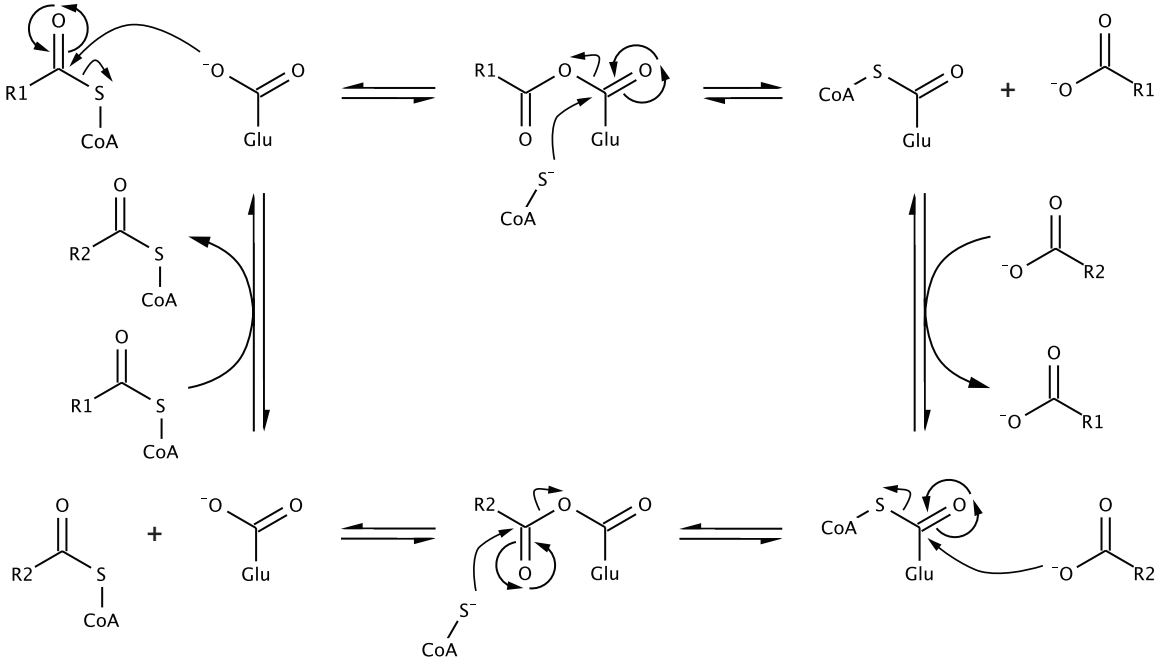

Scheme 4.1. Abbreviated class I CoA-transferase mechanism. The class I reaction proceeds through a series of anhydride, tetrahedral oxyanion (not shown), and thioester intermediates. Only the covalent thioester intermediate has been previously crystallographically observed. All individual steps and the overall reaction are fully reversible.

carboxylate product (*7*). The carboxylate product characteristically dissociates before the carboxylate substrate binds.

Kinetic experiments indicated that the acyl moiety of the acyl-CoA substrate, the first acylglutamyl anhydride intermediate, and the carboxylate product share a common binding pocket (*5*). Only the glutamyl-CoA thioester has been previously crystallographically observed for a class I enzyme (*8*). Both Michaelis complexes, both acylglutamyl anhydride intermediates, and both product complexes have remained elusive.

Class I CoA-transferases are frequently involved in fatty acid metabolism and often use acetyl-CoA or succinyl-CoA as a CoA donor (*8, 9*). In the acidophilic acetic acid bacterium *Acetobacter aceti*, the class I CoA-transferase and acetic-acid-resistance protein succinyl-CoA:acetate CoA-transferase (AarC, SCACT) facilitates metabolic "overoxidation" of acetic acid to carbon dioxide in a specialized citric acid cycle (Chapters 2 and 3).

This study shows that AarC is unusually stringent and catalytically rapid and appropriately acid tolerant. All catalytic residues and determinants of substrate specificity were identified in both the primary binding site and a previously unidentified secondary (carboxylate) binding site. A novel oxyanion hole configuration is utilized to stabilize tetrahedral oxyanion intermediates in what appears to be the archetypal mechanism for class I enzymes. Molecular modeling and molecular mechanics calculations were employed to augment crystallographic results, providing the first complete structural

description of the ground-state complexes and intermediates in a class I CoA-transferase reaction.

MATERIALS AND METHODS

Reagents and general analytical methods. Chemicals were purchased from Sigma-Aldrich or Fisher in the highest purity available unless otherwise noted. Dethiaacetyl-CoA was synthesized by H. Jiang as described previously (*10*). Oligodeoxynucleotide (ODN) primers were obtained from Integrated DNA Technologies and used without further purification. *A. aceti* citrate synthase with a C-terminal hexahistidine affinity tag (*Aa*CSH6) was isolated by C. Z. Constantine as described previously (*10*). Protein quantitation by the method of Bradford was performed as described previously (*11*). Absorbance measurements were recorded on an 8453 UV-visible spectrophotometer (Agilent Technologies). Plasmids were sequenced by the Purdue University Genomics Core Facility. Protein mass was determined using electrospray-ionization time-of-flight mass spectrometry (ESI-TOF-MS) by the Washington University Mass Spectrometry Resource.

Mutagenesis. Mutagenesis reactions were performed by T. J. Kappock using the QuikChange II Site-Directed Mutagenesis kit (Stratagene), pJK385 (Table 4.1), and appropriate ODN primers (Table 4.2).

Purification of wild-type and mutant AarCH6. *E. coli* C41(DE3) cells transformed with pJK385 and pREP4-*groELS* (Table 4.1) were propagated on Luria-Bertani (LB) medium containing 0.1 g/L ampicillin and 0.07 g/L kanamycin (LB/Amp/Kan).

Table 4.1. Bacterial strains and plasmids used in this study

Strain or plasmid	Description[a]	Source
Strains		
E. coli C41(DE3)	F′ *ompT hsdS*$_B$(r_B^- m_B^-) *gal dcm* (DE3)	Avidis[b]
E. coli DH5α	F′ φ80*lacZ*ΔM15 Δ(*lacZYA-argF*)U169 *deoR recA1 endA1 hsdR17*(r_K^- m_K^+) *phoA supE44 thi-1 gyrA96 relA1*	Invitrogen[c]
Plasmids		
pJK357	T7 promoter expression construct, encodes AarC, Ap^r	Chapter 2
pJK385	T7 promoter expression construct, encodes AarCH6, Ap^r	Chapter 2
pJK512	Derivative of pJK385, encodes AarCH6-R228E, Ap^r	This study
pJK513	Derivative of pJK385, encodes AarCH6-E294A, Ap^r	This study
pJK514	Derivative of pJK385, encodes AarCH6-E435A, Ap^r	This study
pJK516	Derivative of pJK385, encodes AarCH6-E435Q, Ap^r	This study
pJK517	Derivative of pJK385, encodes AarCH6-E435D, Ap^r	This study
pJK524	Derivative of pJK385, encodes AarCH6-N347A, Ap^r	This study
pJK564	Derivative of pJK385, encodes AarCH6-S71A, Ap^r	This study
pREP4-*groELS*	T7 promoter expression construct, encodes GroEL/ES, Km^r	P. Cole[d]

[a] Ampicillin resistant (Ap^r) and kanamycin resistant (Km^r). [b] Described in reference (*35*). [c] Described in reference (*36*). [d] Described in reference (*37*).

Production cultures (1 L LB/Amp/Kan) were inoculated with overnight cultures at a 1:500 dilution and grown at 37 °C to mid-log phase (OD_{600} = 0.6). Production of recombinant AarCH6 was then induced by addition of isopropyl-β-D-1-thiogalactopyranoside (IPTG) to 0.4 mM. Cells were grown at 15 °C an additional 16 h, harvested by centrifugation, and either used immediately or stored at –80 °C. All subsequent steps were performed at 4 °C. Cells (typically 5 g/L culture) were resuspended in 5 volumes of TK buffer (50 mM Tris•HCl, pH 8.0, and 100 mM potassium chloride) and disrupted by sonication. Lysate was cleared by centrifugation at

Table 4.2. ODN primers used in this study

ODN	Sequence (5′ → 3′)[a]	Product
2079	GCA CGA ATG ACC GGG ACG AGA ATG CCC CGT TTG CCG C	pJK512
2080	GCG GCA AAC GGG GCA TTC TCG TCC CGG TCA TTC GTG C	pJK512
2081	CTG GTG GGC TAT AGT GCG GTG ATT CAG GAT GGC	pJK513
2082	GCC ATC CTG AAT CAC CGC ACT ATA GCC CAC CAG	pJK513
2083	GAT TTT TGT AAC CGC GCA GGG GCT GGC GG	pJK514
2084	CCG CCA GCC CCT GCG CGG TTA CAA AAA TC	pJK514
2093	CAG ATT TTT GTA ACC CAG CAG GGG CTG GCG	pJK516
2094	CGC CAG CCC CTG CTG GGT TAC AAA AAT CTG	pJK516
2095	CAG ATT TTT GTA ACC GAT CAG GGG CTG GCG GAT C	pJK517
2096	GAT CCG CCA GCC CCT GAT CGG TTA CAA AAA TCT G	pJK517
2101	AGC AGG ATG TCA GCG CCA GCC CCG GCA TTA	pJK524
2102	TAA TGC CGG GGC TGG CGC TGA CAT CCT GCT	pJK524
2176	CAG CTG AGG GCC TGT GGC TGC GCC CGT AAT CAG	pJK564
2177	CTG ATT ACG GGC GCA GCC ACA GGC CCT CAG CTG	pJK564

[a] Changes in the coding region relative to the genomic sequence are underlined.

30,000*g* for 30 min, addition of streptomycin to 1% (w/v) from a 10% (w/v) stock, incubation for 15 min, and additional centrifugation at 30,000*g* for 30 min. Solid ammonium sulfate was then added to the cleared lysate to 35% saturation (208 g/L) over 30 min. After equilibrating an additional 30 min, solids were removed by centrifugation at 30,000*g* for 10 min. Solid ammonium sulfate was then added to the supernatant to 75% saturation (275 g/L) over 30 min. After equilibrating an additional 30 min, solids were collected by centrifugation at 30,000*g* for 10 min, dissolved in TK buffer, and applied to a Ni^{2+}-charged nitrilotriacetic acid (Ni-NTA) agarose column (1.5 cm × 2.5 cm, 4.4 mL) equilibrated in buffer A (50 mM Tris•HCl, pH 8.0, and 300 mM sodium chloride). The column was rinsed with 10 column volumes (CV) of buffer A containing 10 mM

imidazole and then developed in a linear gradient of imidazole (10 → 500 mM, 40 mL × 40 mL). Fractions containing AarCH6 were identified by sodium dodecyl sulfate polyacrylamide gel electrophoresis (SDS-PAGE), pooled, and concentrated to > 5 mg/ mL by ultrafiltration (Amicon Ultra-15, 30,000 MWCO). A portion of the pure AarCH6 solution (10 mg) was applied to a Sephadex G200 column (2.5 cm × 28.0 cm, 140 mL) equilibrated in TK buffer. Protein was then eluted with additional TK buffer, and fractions containing AarCH6 were identified by SDS-PAGE, pooled, and concentrated by ultrafiltration as described above. The portion of the pure AarCH6 solution that was not applied to the gel-filtration column was exchanged into TK buffer by several cycles of dilution and reconcentration. Single-use aliquots were flash-frozen and stored at –80 °C.

AarCH6-S71A, AarCH6-R228E, AarCH6-N347A, AarCH6-E435A, AarCH6-E435D, and AarCH6-E435Q were purified as described above for wild-type AarCH6 except that *E. coli* C41(DE3) cells were transformed with pJK564/pREP4-*groELS*, pJK512/pREP4-*groELS*, pJK524/pREP4-*groELS*, pJK514/pREP4-*groELS*, pJK516/pREP4-*groELS*, or pJK517/pREP4-*groELS* (Table 4.1). [AarCH6-S71A was isolated by K. E. Nyffeler.] AarCH6-E294A was purified similarly except that *E. coli* C41(DE3) cells were transformed with only pJK513; pREP4-*groELS* was not coexpressed. None of the AarCH6 mutants were gel-filtered.

Purification of AarC. *E. coli* C41(DE3) cells transformed with pJK357 (Table 4.1) were propagated on LB medium containing 0.1 g/L ampicillin (LB/Amp). Production cultures (1 L LB/Amp) were inoculated with overnight cultures at a 1:500 dilution and grown at 37 °C to mid-log phase (OD_{600} = 0.6). Production of recombinant AarC was

then induced by addition of IPTG to 0.4 mM. Cultures were grown at 15 °C an additional 16 h, harvested by centrifugation, and either used immediately or stored at –80 °C. All subsequent steps were performed at 4 °C. Cells (typically 5 g/L culture) were resuspended in 5 volumes of buffer B (50 mM potassium phosphate, pH 6.0, and 100 mM potassium chloride) and disrupted by sonication. Lysate was cleared by centrifugation at 30,000*g* for 30 min, addition of streptomycin to 1% (w/v) from a 10% (w/v) stock, incubation for 15 min, and additional centrifugation at 30,000*g* for 30 min. Solid ammonium sulfate was then added to the cleared lysate to 43% saturation (263 g/L) over 30 min. After equilibrating an additional 30 min, solids were removed by centrifugation at 30,000*g* for 10 min. Solid ammonium sulfate was then added to the supernatant to 68% saturation (167 g/L) over 30 min. After equilibrating an additional 30 min, solids were collected by centrifugation at 30,000*g* for 10 min, dissolved in buffer C (20 mM potassium phosphate, pH 7.0), and applied to a Sephadex G25 column (2.5 cm × 40.0 cm, 200 mL) equilibrated in buffer C. Protein was eluted with additional buffer C, and fractions containing protein or salt were identified by absorbance (280 nm) and conductivity measurements, respectively. Fractions containing protein were pooled, concentrated by ultrafiltration as described above, and applied to a diethylaminoethyl (DEAE) Sepharose CL-6B column (2.5 cm × 8.0 cm, 39 mL) equilibrated in buffer C. The column was rinsed with ~1 CV of buffer C and then developed in a linear gradient of salt (0 → 1.2 M potassium chloride, 400 mL × 400 mL). Fractions containing AarC were identified by SDS-PAGE, pooled, concentrated by ultrafiltration as described above, exchanged into buffer D (50 mM MES, pH 6.2, 5 mM magnesium chloride, and 20 mM

potassium chloride) by several cycles of dilution and reconcentration, and applied to a Cibacron Blue 3GA agarose column (2.5 cm × 12.5 cm, 61 mL) equilibrated in buffer D. The column was rinsed with ~1 CV of buffer D and then developed in a linear gradient of salt (0.02 → 1.2 M potassium chloride, 350 mL × 350 mL). Fractions containing AarC were identified by SDS-PAGE, pooled, concentrated by ultrafiltration as described above, and exchanged into 50 mM potassium phosphate, pH 8.0, and 100 mM potassium chloride by several cycles of dilution and reconcentration. Single-use aliquots were flash-frozen and stored at –80 °C.

SCACT assays. Citrate synthase-dependent VisF/VisR assays and high performance liquid chromatography (HPLC)-coupled LCF/LCR assays were performed as described previously (Chapter 2) except that the concentrations of the enzymes and substrates and the durations of the reactions were adjusted as required for the AarCH6 mutants. A unit is defined as the amount of enzyme that forms 1 μmole of product per minute.

Alternate substrate screen. Alternate CoA-acceptors were screened in modified LCR assays containing 50 mM potassium phosphate, pH 8.0, 100 mM potassium chloride, 20 mM carboxylate, pH 8.0, 1.0 mM acetyl-CoA, and 5,000 ng AarCH6. Aliquots (0.1 ml) were withdrawn prior to the addition of enzyme and 5 and 30 min after the addition of enzyme, quenched with 6.25% trichloroacetic acid (0.4 ml), vortexed briefly, and centrifuged at 16,100*g* for 3 min. The soluble portion was transferred to an autosampler vial and analyzed by reverse-phase ion-pair HPLC. Compounds identified as alternate substrates were examined in saturation experiments employing modified LCR assays in which succinate was replaced by the new CoA-acceptor.

HPLC analysis. CoA and CoA thioesters were resolved on a Breeze HPLC system (Waters) equipped with a Symmetry C18 column (4.6 mm × 75 mm, 3.5 μm; Waters). Elution was performed at 30 °C and a flow rate of 0.8 mL/min with detection at 260 nm. A mixture of 200 mM sodium phosphate and 150 mM sodium acetate, pH 4.6, was used in a water/methanol solvent system. The gradient program was 0 – 5 min, 4.5% methanol (isocratic); 5 – 15 min, 4.5 → 15% methanol (linear gradient); 15 – 17 min, 15% methanol (isocratic); 17 – 22 min, 15 → 4.5% methanol (linear gradient); and 22 – 27 min, 4.5% methanol (isocratic). The intermediate isocratic phase was extended by 5 min for elution of samples containing butyrate, while the initial and final isocratic phases were stripped of methanol for elution of samples containing formate, glycolate, glyoxylate, oxalate, or tartrate. Injections (25 – 100 μL) were performed by a 717plus autosampler (Waters). Acyl-CoA peak areas were compared to an acetyl-CoA calibration curve as described previously (Chapter 2).

Thermal denaturation. Temperature-induced changes in the structures of AarC and AarCH6 were monitored using a Chirascan circular dichroism (CD) spectropolarimeter (Applied Photophysics). AarC or AarCH6 (19 μg/mL, 0.34 μM) was equilibrated at 20 °C for 30 min in a 10-mm pathlength quartz cuvette containing 50 mM potassium phosphate, pH 3.5 – 8.5, and 100 mM potassium chloride before a far-UV spectrum (3 scans, 200 – 260 nm, 1 nm bandwidth, 1 nm step, 1 s/point) was recorded. [Each spectrum was corrected by subtracting a buffer-only background spectrum.] The sample was then heated from 20 – 90 °C at a continuous rate of 0.5 °C/min. Ellipticity was monitored at 222 nm (1 nm bandwidth, 0.5 °C step, 12 s/point), and solution temperature was directly

measured using a probe inserted through the cuvette stopper. Melting profiles were fit to a double-sigmoid equation using Pro-Data Viewer (Applied Photophysics) and the steepest point of each profile was taken as the melting temperature (T_m).

Crystallization and cryoprotection. A sparse-matrix screen of AarCH6 crystallization conditions was performed using Wizard I and II kits (Emerald BioSystems) in hanging-drop vapor-diffusion experiments. Reservoirs contained 0.5 mL Wizard solution supplemented with 25 mM 2-mercaptoethanol. Drops contained 2 µL AarCH6 (6.0 mg/ mL protein, 45 mM Tris•HCl, pH 8.0, 90 mM potassium chloride, and 2.0 mM CoA) and 2 µL reservoir solution. Trays were incubated at room temperature (~22 °C). Two promising conditions (I-36 and II-4) identified in the sparse-matrix screen were used to grow large numbers of AarCH6 crystals. Reservoirs contained either 1.7 – 2.0 M ammonium sulfate, 0.2 M sodium chloride, 0.1 M sodium cacodylate, pH 6.5, and 25 mM 2-mercaptoethanol or 0.8 – 1.0 M sodium citrate, 0.1 M imidazole, pH 8.2, and 25 mM 2-mercaptoethanol. Drops were prepared as described above. AarC (5.6 mg/mL protein, 45 mM potassium phosphate, pH 8.0, 90 mM potassium chloride, and 2.0 mM CoA) was crystallized in the same manner. Additional crystallization experiments were performed in which sodium citrate was replaced by 0.5 – 1.4 M sodium succinate, sodium L-malate, or sodium acetate.

Crystals were soaked for 24 h at room temperature in either 15% (w/v) sorbitol, 2.2 M ammonium sulfate, 0.1 M sodium cacodylate, pH 6.5, 0.25 M sodium chloride, 25 mM 2-mercaptoethanol, and 2.0 mM CoA or 15% (w/v) sorbitol, 1.1 M sodium citrate, 0.1 M imidazole, pH 8.2, 25 mM 2-mercaptoethanol, and 2.0 mM CoA and then flash-cooled by

immersion in liquid nitrogen. Acetyl-CoA (2.0 mM), succinyl-CoA (2.0 mM), dethiaacetyl-CoA (10 mM), or water was substituted for CoA in drops and cryoprotectants in an effort to obtain alternate ligand-bound or unliganded structures. Alternatively, crystals grown without substrate or inhibitor present were soaked in cryoprotectant lacking ligand for 22 h and then transferred to cryoprotectant containing acetyl-CoA for 2 h before being flash-cooled as described above.

Crystallographic data collection and refinement. X-ray diffraction data were collected at the Advanced Photon Source, Argonne National Laboratory. Diffraction data were indexed, integrated, and scaled in HKL2000 (*12*). The structure of AarCH6•CoA•citrate was solved by molecular replacement using a threaded AarC model (monomer, residues 3 – 505) generated with SWISS-MODEL (*13*). The homology model was an uncharacterized CoA-transferase (PDB entry 2g39, 48% identity) from *Pseudomonas aeruginosa*. For all subsequent AarC(H6) models, AarCH6•CoA•citrate (subunit A, residues 2 – 514) was used as the search model for molecular replacement. All refinement was performed with PHENIX (*14*). Automated building (PHENIX AutoBuild) was used to improve the starting structures of AarCH6•CoA•citrate and AarCH6-S71A•CoA. Subsequent early rounds of refinement for each model consisted of rigid-body refinement, simulated annealing, coordinate optimization, isotropic temperature-factor refinement, and automated water picking. Later rounds of refinement for each model included only coordinate optimization, isotropic temperature-factor refinement, and occupancy refinement. Noncrystallographic symmetry (NCS) restraints were applied for automated building of the AarCH6•CoA•citrate model and for all stages

of refinement of the medium-resolution AarCH6•CoA, AarCH6-R228E•CoA [anomalous], and AarCH6-E294A•dethiaacetyl-CoA models. Manual building and water picking were conducted in Coot (*15*) following each round of automated refinement. Ligand coordinates and restraints were obtained from HIC-Up (*16*) and manually modified using PHENIX. All structural images were generated with PyMOL (*17*).

Molecular mechanics calculations. Michaelis complexes and the glutamylsuccinyl anhydride intermediate were manually constructed in active sites containing the crystallographically observed acetylglutamyl anhydride and glutamyl-CoA thioester intermediates (AarCH6•CoA•acetate). A single water (HOH517) and all residues (Phe35, Thr36, Ala70, Ser71, Phe92, Leu114, Gln267, Gly269, Val270, Glu294, Val295, Asn361, Gly387, Gly388, and Ser389) directly contacting modeled atoms were included during building and subsequent energy minimization. Hydrogen atoms were added in appropriate riding positions before equilibrium conformer calculations incorporating a Monte Carlo search method (5,000 K) and MMFF94 force field were performed. Only the positions of hydrogen atoms and modeled nonhydrogen atoms were refined during energy minimization. All nonhydrogen protein atoms and selected ligand atoms were "frozen." Corrections for implicit solvent were not applied at any point during refinement. All calculations were performed with Spartan '02 (Wavefunction).

RESULTS

Isolation of wild-type and mutant AarCH6. Earlier attempts to increase the solubility of AarCH6 by employing *E. coli* C41(DE3) for protein production and/or lowering the

induction temperature were only marginally successful as ~90% of total AarCH6 remained insoluble (Chapter 2). Co-overproducing AarCH6 with the chaperonins GroEL/ES, however, increased soluble AarCH6 by ~10-fold (Figure 4.1). While total AarCH6 was lessened, presumably as a result of competitive synthesis of GroEL/ES, solubility was greatly improved. Purification of AarCH6 was performed as described previously (Chapter 2) except that gel-filtration chromatography was introduced to facilitate crystallization.

AarCH6 mutants were purified as described previously for the wild-type enzyme (Chapter 2, Figure 4.1). Co-overproduction of GroEL/ES improved the solubility of AarCH6-S71A, AarCH6-R228E, AarCH6-N347A, and AarCH6-E435D, but failed to relieve the complete insolubility of AarCH6-E435A and AarCH6-E435Q. AarCH6-E294A was overproduced without co-overproduction of GroEL/ES and displayed solubility similar to that of the wild-type enzyme. ESI-TOF-MS analysis of the AarCH6

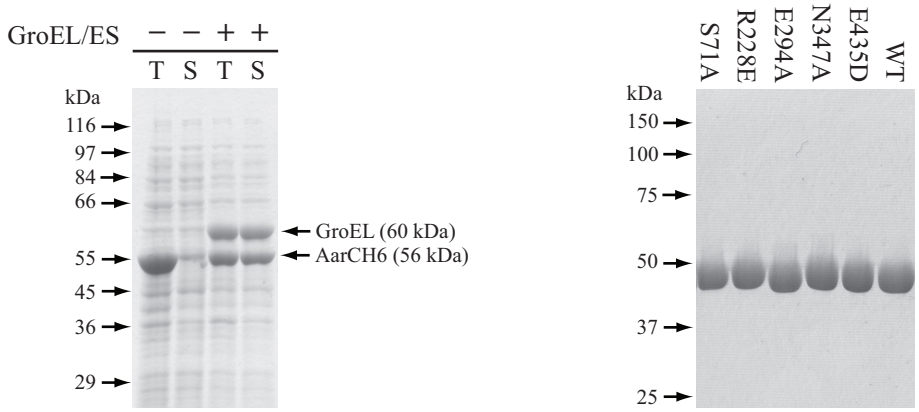

Figure 4.1. Overproduction and purification of wild-type (WT) and mutant AarCH6. **(Left)** AarCH6 was overproduced in *E. coli* C41(DE3). Limited solubility was dramatically improved by co-overproduction of GroEL/ES. Lane T: total lysate and lane S: soluble lysate. GroES (10 kDa) presumably runs with the dye front. **(Right)** AarCH6 mutants were purified by ammonium sulfate fractionation and immobilized metal affinity chromatography as described in the Materials and Methods. [K. E. Nyffeler purified AarCH6-S71A.] Even when co-overproduced with GroEL/ES, AarCH6-E435A and AarCH6-E435Q were insoluble (not shown). Each lane contains 5 μg protein. Size standard positions are indicated.

mutants was consistent with the expected alterations in 513-residue proteins lacking Met1: AarCH6-S71A (55,831 Da observed; 55,831 Da expected; Figure A.4), AarCH6-R228E (55,821 Da observed; 55,820 Da expected; Figure A.5), AarCH6-E294A (55,789 Da observed; 55,789 Da expected; Figure A.6), AarCH6-N347A (55,804 Da observed; 55,804 Da expected; Figure A.7), and AarCH6-E435D (55,833 Da observed; 55,833 Da expected; Figure A.8).

Isolation and partial kinetic characterization of AarC. AarC was purified to near homogeneity by ammonium sulfate fractionation, gel-filtration chromatography, ion exchange chromatography, and dye affinity chromatography (Figure 4.2 and Table 4.3). ESI-TOF-MS analysis of AarC was consistent with a 504-residue protein lacking Met1 (54,695 Da observed; 54,695 Da expected; Figure A.9).

Acetate saturation experiments using AarC produced kinetic constants [k_{cat} = 290 ± 30 s^{-1}, K_m = 110 ± 20 mM, k_{cat}/K_m = (2.6 ± 0.5) × 10^3 M^{-1} s^{-1}, and K_i = 1600 ± 500 mM] that are similar to those of AarCH6 (Chapter 2), suggesting the C-terminal hexahistidine tag does not significantly affect binding affinity or catalytic activity.

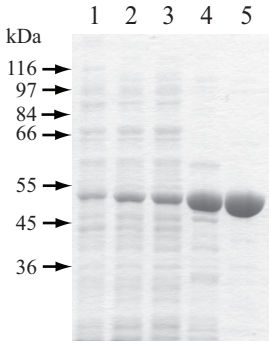

Figure 4.2. Purification of AarC. Purity was assessed throughout the purification by SDS-PAGE and specific activity (Table 4.3). Lane 1: clarified lysate, lane 2: 43 – 68% ammonium sulfate, lane 3: G25, lane 4: DEAE, and lane 5: Cibacron Blue 3GA. Each lane contains 5 μg protein. Size standard positions are indicated.

Table 4.3. AarC purification chart[a]

Stage	Protein (mg)	Activity (U)[b]	Sp. activity (U/mg)	Fold purification	Yield (%)
Clarified lystate	550	3200	5.9	1.0	100
43 − 68% $(NH_4)_2SO_4$	260	2600	10	1.7	81
G25	200	2400	12	2.0	75
DEAE	33	2000	60	10	63
Cibacron Blue 3GA	5.7	400	71	12	13

[a] AarC was purified from 4 1-L production cultures (~20 g cell paste). [b] SCACT activity was measured using the VisR assay.

Substrate specificity. Twenty-four carboxylates (formate, trifluoroacetate, glycolate, glyoxylate, oxalate, propionate, L-lactate, DL-lactate, pyruvate, malonate, butyrate, acetoacetate, maleate, fumarate, D-malate, L-malate, oxaloacetate, D-tartrate, L-tartrate, DL-methylsuccinate, glutarate, α-ketoglutarate, citrate, and DL-isocitrate; Figure A.10) were screened as possible alternate CoA-acceptors in modified LCR assays. Only nine supported specific activity above that of the limit of detection (~0.01 U/mg), and none supported activity above 10% of that produced by acetate or succinate (Figure 4.3A). Saturation experiments revealed a substantial gap between the catalytic efficiencies of the physiological substrates and those of the alternate substrates (Figure 4.3B and Table A.1). This gap largely resulted from consistently lower turnover numbers. Conversely,

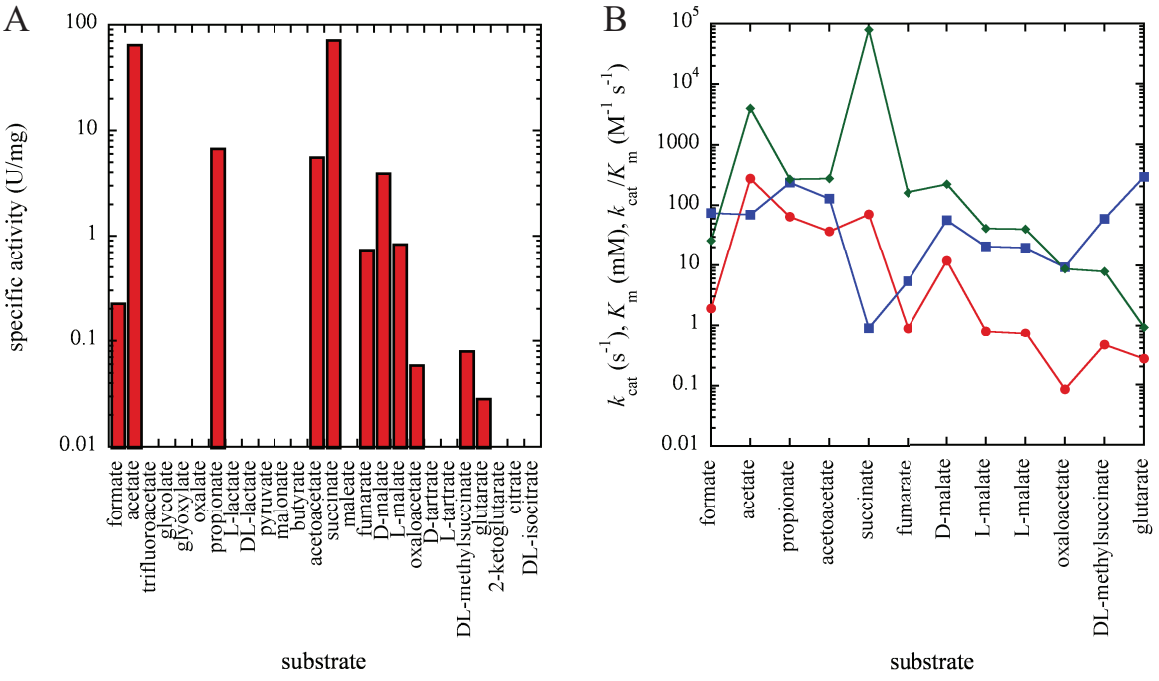

Figure 4.3. Alternate substrate screen. **(A)** Twenty-four carboxylates were screened as possible alternate CoA-acceptors in modified LCF/LCR assays. Only nine supported detectable CoA-transferase activity. The limit of detection was ~0.01 U/mg. **(B)** Kinetic constants [k_{cat} (red circles), K_m (blue squares), and k_{cat}/K_m (green diamonds)] were determined for the alternate substrates using modified LCF/LCR assays. The highest catalytic efficiencies were observed with the physiological substrates acetate and succinate. L-malate produced two acyl-CoA/acyl-isoCoA product pairs that are likely constitutional isomers. Kinetic parameters (Table A.1) are provided in Appendix A.

Michaelis constants varied dramatically (but remained consistently higher than that of succinate).

Crystallization, cryoprotection, and data collection. A sparse-matrix screen yielded AarCH6 crystals with two distinct morphologies. Hexagonal crystals were produced in ammonium sulfate, while orthorhombic crystals were generated in sodium citrate (Figure 4.4). Crystals routinely grew to full size in 2 – 14 days with growth occurring most rapidly from AarCH6 that had been coproduced with GroEL/ES and subsequently gel-filtered. Crystals of both morphologies were soaked in cryoprotectant for 24 h without noticeable deterioration. Soaking of the hexagonal crystals for shorter periods produced diffraction patterns with dark ice rings. Shorter soaks were not attempted with the orthorhombic crystals.

Despite the pleasing appearance of the hexagonal crystals, diffraction data never extended beyond 2.8 Å and often failed to extend beyond 3.5 Å. The aesthetically less attractive orthorhombic crystals regularly diffracted to 2.0 Å and often approached 1.5 Å. The orthorhombic crystals, however, were plagued by microscopic heterogeneity and a

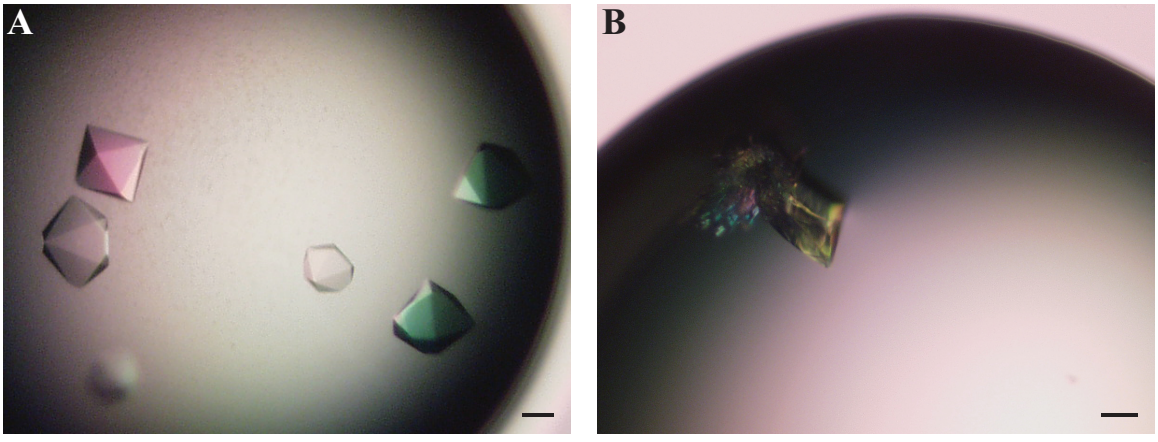

Figure 4.4. AarCH6 crystals. **(A)** Hexagonal crystals grown in ammonium sulfate. **(B)** Orthorhombic crystals grown in sodium citrate. Black bars represent 0.1 mm.

propensity to grow in clusters. Attempts to circumvent these shortcomings by employing altered precipitant concentrations and/or pH conditions failed, while efforts to grow AarCH6 crystals in sodium acetate, sodium L-malate, or sodium succinate produced only microcrystals. Despite these failures, usable high-resolution datasets were obtained by screening large numbers of orthorhombic crystals in carefully selected orientations.

Secondary, tertiary, and quaternary structures. In sodium citrate, AarCH6 crystallized in the space group $P2_12_12_1$ with an asymmetric unit containing the expected biological dimer. Each monomer is composed of distinct N-terminal (residues 2 – 170, 216 – 223) and C-terminal (residues 179 – 181, 236 – 505) domains displaying open α/β-folds (Figures 4.5A and 4.6). The N-terminal domain possesses a three layer architecture. A core seven-strand parallel β-sheet (β9, β7, β5, β1, β2, β3, β4) with a single antiparallel edge (β6) is sandwiched between four surface-exposed α-helices (α1 – α4) and two semi-buried α-helices (α5 and α6) at the subunit interface. The C-terminal domain is similarly arranged. A core eight-strand parallel β-sheet (β8, β13, β12, β11, β10, β14, β19, β22) with a single antiparallel edge (β23) is sandwiched between five surface-exposed α-helices (α7 – α11) and three buried α-helices (α12 – α14) at the subunit interface. The C-terminal domain is additionally composed of a two-strand antiparallel β-sheet (β16 and β17), a four-strand mixed β-sheet (β15, β16, β20, and β21), and three flanking α-helices (α15 – α17). The domains are joined by two rigid loops (residues 171 – 178 and 182 – 215) and a single flexible domain linker (residues 224 – 235) spanning a deep, funnel-shaped cleft.

The extensive, highly hydrated monomer-monomer interface buries 3,500 $Å^2$ per subunit (17% of the total surface area). Four chloride ions are present at the interface,

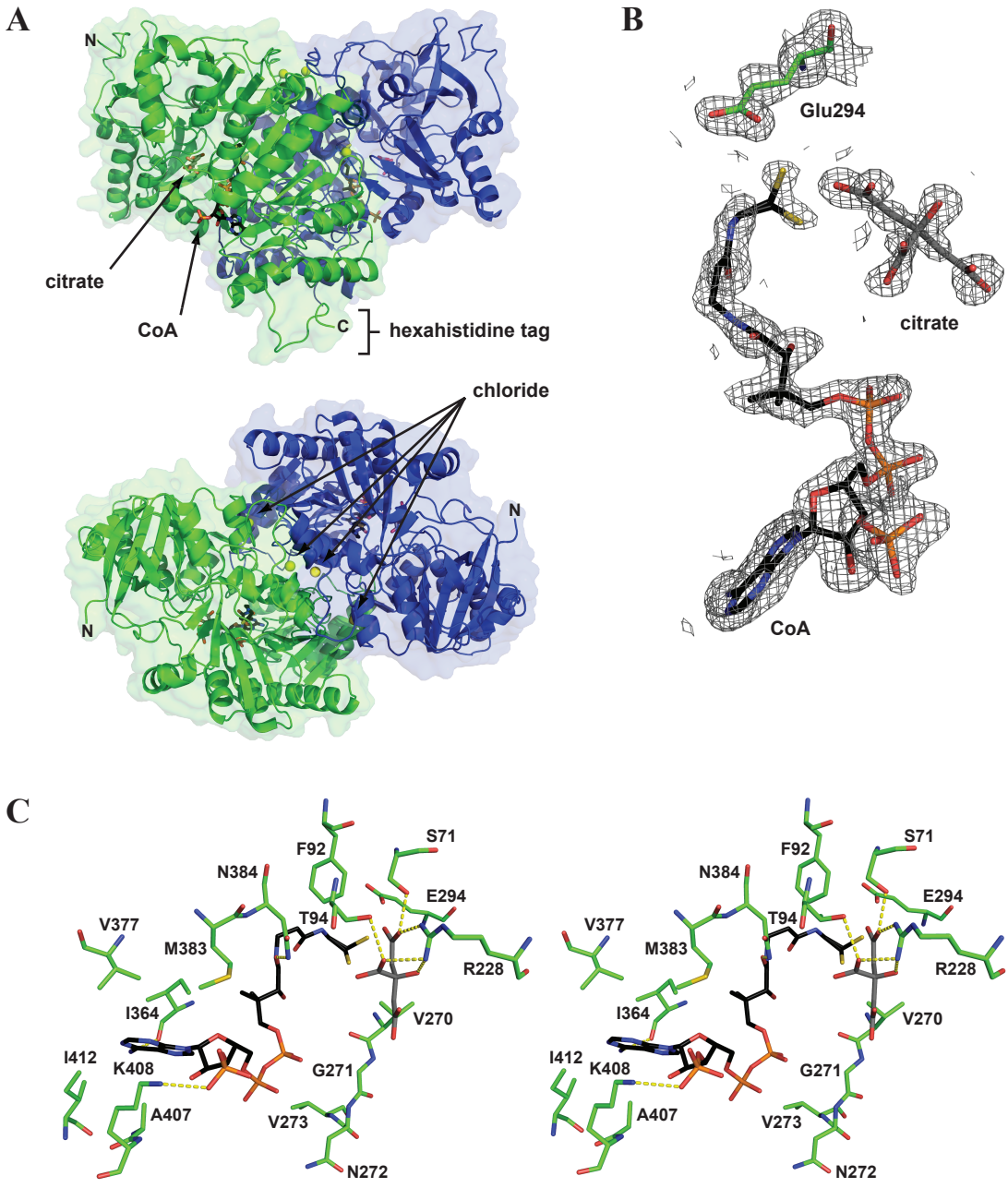

Figure 4.5. Crystallographic characterization of AarCH6•CoA•citrate (PDB entry 4eu7). **(A)** AarCH6 possesses a dimeric quaternary structure (green and blue subunits) with four chloride ions (yellow spheres) associated with buried arginine residues at the monomer-monomer interface. CoA (black) and citrate (gray) are bound in a deep, funnel-shaped active-site cleft between the N- and C-terminal domains of each subunit. **(B)** Ligands were identified based upon strong and unambiguous electron density. The subterminal methylene carbon and terminal thiol sulfur of CoA were modeled in two alternate conformations. The σ_A-weighted $2mF_o - DF_c$ map, calculated with CoA, citrate, and Glu294 omitted, is contoured at 1.0 sigma and carved with a 2-Å radius. **(C)** CoA and citrate are bound near the catalytic glutamate Glu294 (divergent stereodiagram). Citrate forms electrostatic and/or hydrogen-bonding interactions (yellow dotted lines) with Ser71, Thr94, and Arg228. The much larger CoA forms hydrogen-bonding interactions with only Ile364, Asn384, and Lys408. All other hydrogen-bonding interactions are mediated by water (not shown).

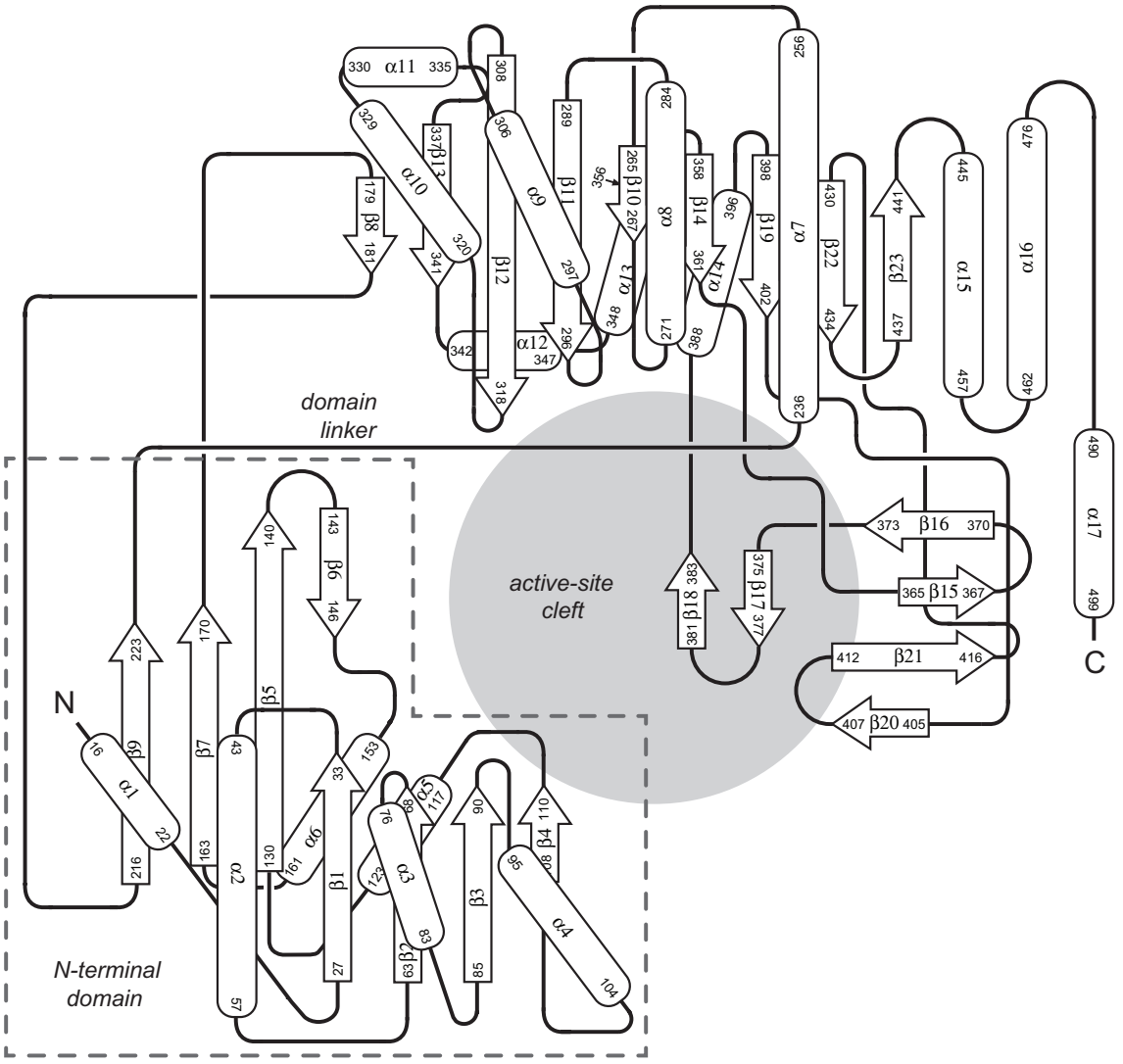

Figure 4.6. AarC(H6) topology diagram. Each subunit is composed of distinct N- and C-terminal domains displaying open α/β folds. The domains are joined by two static loops and a single dynamic domain linker that spans a deep active-site cleft. All 3_{10}-helices are omitted.

associated with buried and otherwise uncompensated arginine residues [Arg120 (A/B) and Arg354 (A/B)]. When the chloride ions were modeled as water molecules, corresponding B-factors were substantially lower than those of surrounding protein atoms and residual density remained in the σ_A-weighted $mF_o - DF_c$ difference map. The presence of heavy atoms was further substantiated by anomalous density centered around the chloride ions (AarCH6-R228E•CoA [anomalous], PDB entry 4eua, Tables 4.6 and

4.7; Figure 4.7). Given the buried locations of Arg120 and Arg354 in the dimer and the lack of nearby negatively charged residues, the four chloride ions are likely necessary for oligomerization of AarC(H6).

In ammonium sulfate, AarCH6 (AarCH6•CoA, PDB entry 4eu4, Tables 4.4 and 4.5) crystallized in the space group $P6_222$ with the same asymmetric unit as crystals grown in sodium citrate. Despite the vastly different solvent contents of the two crystal forms (orthorhombic, ~40%; hexagonal, ~70%), corresponding AarCH6 structures were highly similar (Rmsd = 0.54 Å for all Cα atoms, residues 2 – 505). Only the conformation of the hexahistidine tag of subunit A from the orthorhombic crystals was distinct. Formation of a 3_{10}-helix and favorable crystal packing interactions with an adjacent asymmetric unit allowed the complete hexahistidine tag (residues 506 – 514) to be observed. Ordered hexahistidine tags are rare and are often attributed to stabilizing packing contacts (*18*). Such interactions were lacking for subunit B in the orthorhombic crystals and both

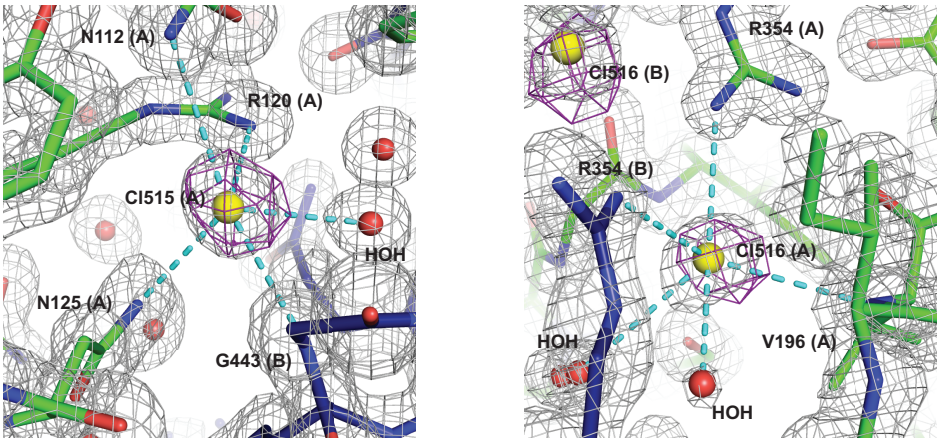

Figure 4.7. Chloride ions at the monomer-monomer interface. Four chloride ions (yellow spheres) are associated with buried and otherwise uncompensated arginine residues at the subunit interface (subunit A, green; subunit B, blue). The σ_A-weighted $2mF_o - DF_c$ map (gray, AarCH6-R228E•CoA, PDB entry 4eu9) is contoured at 1.5 sigma. The NCS-averaged, σ_A-weighted anomalous map (purple, AarCH6-R228E•CoA [anomalous], PDB entry 4eua) is contoured at 2.8 sigma. Neither map is carved in the region shown. All indicated electrostatic interactions (cyan dotted lines) occur over 2.8 − 3.5 Å.

subunits in the more sparsely packed hexagonal crystals. The similarity of the structures observed in the two different crystal forms suggests that crystal-packing interactions do not significantly perturb the solution-state conformation of AarCH6.

AarC crystals grown in sodium citrate closely resemble AarCH6 crystals grown in sodium citrate. Moreover, the structure of AarC (AarC•CoA•citrate, PDB entry 4eud, Tables 4.8 and 4.9) closely resembles the structure of AarCH6 (AarCH6•CoA•citrate, PDB entry 4eu7, Rmsd = 0.17 Å for all Cα atoms, residues 2 – 505). A high degree of structural similarity is congruent with the nearly identical kinetic constants obtained with AarC and AarCH6.

Active site. Electron density consistent with CoA and citrate was observed in the funnel-shaped cleft between the N- and C-terminal domains of AarCH6 (AarCH6•CoA•citrate, PDB entry 4eu7, Tables 4.4 and 4.5; Figure 4.5B). The adenine moiety of CoA is located in a hydrophobic pocket (Ile364, Val377, Met383, Ala407, and Ile412) near the entrance to the cleft, while the pantetheine arm extends into the active site, terminating near Glu294 (Figure 4.5B/C). Only three direct hydrogen bonds are present between CoA and the protein (Ile364, Asn384, and Lys408), while all other hydrogen bonds are water mediated. Other than a single hydrophobic contact between the panthetheine arm and Phe92, CoA exclusively contacts residues in the C-terminal domain. Conversely, citrate contacts only residues in the N-terminal domain and the domain linker, forming extensive electrostatic and/or hydrogen-bonding interactions with the side chains of Ser71, Thr94, and Arg228.

Proposed role of Glu294. Glu294 seems ideally positioned to form the covalent mixed anhydride and thioester intermediates characteristic of class I (and III) CoA-transferase reactions. Moreover, introduction of a Glu294→Ala mutation reduced specific activity to a level that could not be detected at a threshold 10,000-fold below the activity of wild-type enzyme. AarCH6-E294A (AarCH6-E294A•CoA, PDB entry 4eub, Tables 4.8 and 4.9) did not undergo structural rearrangements that could account for the observed loss of activity.

Proposed role of Glu435. A previously published multiple sequence alignment predicted that Glu435 is the reactive active-site glutamate in AarC (*19*). Glu435, however, is located outside the active-site cleft and constitutes part of a highly conserved β-hairpin motif. Furthermore, AarCH6-E435D possesses catalytic properties similar to those of AarCH6 (Table 4.10). Insolubility prevented kinetic characterization of AarCH6-E435A and AarCH6-E435Q but supports relegation of Glu435 to a purely structural role.

Proposed role of Arg228. The structural similarity between citrate and succinate could imply that Thr94 and Arg228 (and Ser71) participate in recognition of the physiological carboxylate substrates. The significant gap between citrate and Glu294, however, seems to preclude participation of either residue in Michaelis complexes. Alternatively, Thr94 and Arg228 (and Ser71) may comprise an auxiliary binding site.

AarCH6-R228E exhibited a pronounced defect in apparent binding of carboxylate substrates. At concentrations in excess of 0.5 M, neither acetate nor succinate could saturate AarCH6-R228E (Figure 4.8 and Table 4.10). Catalytic activity and apparent binding of acyl-CoA substrates were relatively unimpaired. While the side chain of

Table 4.4. Data-collection statistics for wild-type AarCH6[a]

	AarCH6 (4eu3)	AarCH6•CoA (4eu4)	{AarCH6}•CoA (4eu5)	AarCH6•CoA•acetate (4eu6)	AarCH6•CoA•citrate (4eu7)
Beamline	21-ID-F	21-ID-G	23-ID-D	21-ID-F	21-ID-G
Wavelength (Å)	0.97872	0.97856	1.0331	0.97872	0.97856
Space group	$P2_12_12_1$	$P6_222$	$P2_12_12_1$	$P2_12_12_1$	$P2_12_12_1$
Unit-cell dimensions (Å)	a = 67.5, b = 110.3, c = 119.8	a = b = 150.2, c = 290.4	a = 67.6, b = 110.6, c = 119.5	a = 67.2, b = 110.4, c = 119.8	a = 67.4, b = 110.9, c = 120.4
Solvent content (%)[b]	38.4	70.9	38.5	38.1	38.9
Matthews coefficient (Å^3/Da)[b]	2.00	4.23	2.00	1.99	2.01
Resolution (Å)	50 – 1.58 (1.61 – 1.58)	50 – 2.80 (2.85 – 2.80)	50 – 1.75 (1.81 – 1.75)	50 – 1.99 (2.02 – 1.99)	50 – 1.70 (1.73 – 1.70)
Measured reflections	1,502,448	845,333	865,507	787,079	1,319,072
Unique reflections	121,024 (5,211)	46,836 (2,173)	91,574 (9,057)	61,848 (3,022)	99,312 (4,801)
Redundancy	12.4 (4.9)	18.0 (12.5)	9.5 (7.3)	12.7 (12.1)	13.3 (8.4)
Completeness (%)	98.4 (86.0)	97.1 (92.2)	100.0 (100.0)	99.7 (99.1)	99.8 (97.6)
$\langle I/\sigma(I)\rangle$	21.4 (2.1)	34.1 (3.9)	27.5 (3.6)	34.1 (7.2)	30.0 (2.9)
R_{sym}[c] (%)	10.3 (44.2)	11.4 (71.8)	12.4 (62.3)	11.0 (53.0)	10.5 (54.2)

[a] Values in parentheses are for the outermost resolution shell. [b] Solvent contents and Matthews coefficients were calculated using a web applet (http://www.ruppweb.org/Mattprob/) (*38, 39*). [c] $R_{sym} = \sum_{hkl} \sum_i |I_i(hkl) - \langle I_i(hkl)\rangle| / \sum_{hkl} \sum_i I_i(hkl)$, where $I_i(hkl)$ is the intensity of the ith observation of reflection hkl and $\langle I_i(hkl)\rangle$ is the mean intensity of all observations i of reflection hkl.

Table 4.5. Refinement statistics for wild-type AarCH6[a]

	AarCH6[d] (4eu3)	AarCH6•CoA (4eu4)	{AarCH6}•CoA (4eu5)	AarCH6•CoA•acetate[e] (4eu6)	AarCH6•CoA•citrate (4eu7)
Resolution (Å)	40.2 – 1.58 (1.60 – 1.58)	41.5 – 2.80 (2.90 – 2.80)	42.8 – 1.74 (1.81 – 1.74)	34.8 – 1.99 (2.02 – 1.99)	28.8 – 1.70 (1.76 – 1.70)
Reflections (working/test)	109,938/5,768	42,623/2,273	83,914/4,400	58,685/3,092	91,142/4,802
Total atoms	9,106	8,179	8,870	8,488	9,207
Protein atoms	7,817	7,684	7,789	7,786	7,843
Water atoms	1,272	295	981	595	1,236
Ligand atoms	17	200	100	107	128
R_{cryst}[b] **(%)**	15.6 (25.8)	17.8 (28.7)	16.7 (21.8)	16.4 (16.5)	15.6 (22.3)
R_{free}[c] **(%)**	18.9 (29.8)	22.3 (35.9)	20.9 (28.3)	20.9 (24.3)	19.4 (26.7)
Average B-factor (Å²)					
Protein	12.6	49.7	17.0	22.4	17.0
Water	24.8	45.0	25.9	27.9	29.4
Ligand	18.5	58.7	18.9	26.3	24.1
Rmsd from ideal geometry					
Bond lengths (Å)	0.006	0.008	0.006	0.007	0.006
Bond angles (°)	1.07	1.20	1.06	1.05	1.04
Ramachandran plot (%)					
Favored regions	97.0	92.5	97.0	96.8	96.6
Additionally allowed regions	2.9	6.9	2.7	2.8	3.2
Outlying regions	0.1	0.6	0.3	0.4	0.2

[a] Values in parentheses are for the outermost resolution shell. [b] $R_{cryst} = \sum_{hkl} |F_o - F_c| / \sum_{hkl} F_o$, where F_o and F_c are the observed and calculated structure factors, respectively. [c] R_{free} was calculated in the same manner as R_{cryst} using the 5% of reflections excluded from refinement. With the exception of the AarCH6-S71A•CoA, AarCH6-R228E•CoA [anomalous], and AarCH6-E294A•dethiaacetyl-CoA datasets, a consistent set of reflections was set aside for all datasets of the space group $P2_12_12_1$, including those datasets described in Tables 4.7 and 4.9. [d] Citrate was modeled in the active site of subunit B. [e] The covalent acetylglutamyl anhydride and glutamyl-CoA thioester intermediates were modeled in subunits A and B, respectively.

Table 4.6. Data-collection statistics for mutant AarCH6[a]

	AarCH6-S71A•CoA (4eu8)	AarCH6-R228E•CoA (4eu9)	AarCH6-R228E•CoA [anomalous] (4eua)
Beamline	21-ID-F	21-ID-F	21-ID-D
Wavelength (Å)	0.97872	0.97872	1.9075
Space group	$P2_12_12_1$	$P2_12_12_1$	$P2_12_12_1$
Unit-cell dimensions (Å)	a = 67.3, b = 109.7, c = 120.1	a = 67.1, b = 110.1, c = 119.8	a = 67.4, b = 110.5, c = 119.2
Solvent content (%)[b]	38.0	37.9	38.1
Matthews coefficient (Å^3/Da)[b]	1.99	1.98	1.99
Resolution (Å)	50 – 1.81 (1.84 – 1.81)	50 – 1.48 (1.51 – 1.48)	50 – 2.40 (2.49 – 2.40)
Measured reflections	968,154	2,010,407	201,712
Unique reflections	81,672 (4,005)	148,137 (7,318)	34,893 (3,477)
Redundancy	11.9 (11.7)	13.6 (12.9)	5.8 (5.7)
Completeness (%)	100.0 (100.0)	99.9 (99.8)	98.2 (100.0)
$\langle I/\sigma(I)\rangle$	40.3 (5.9)	38.4 (4.4)	54.6 (33.5)
R_{sym}[c] **(%)**	8.3 (48.2)	7.9 (57.4)	6.3 (10.9)

[a] Values in parentheses are for the outermost resolution shell. [b] Solvent contents and Matthews coefficients were calculated using a web applet (http://www.ruppweb.org/Mattprob/). [c] $R_{sym} = \sum_{hkl} \sum_i |I_i(hkl) - \langle I_i(hkl)\rangle| / \sum_{hkl} \sum_i I_i(hkl)$, where $I_i(hkl)$ is the intensity of the ith observation of reflection hkl and $\langle I_i(hkl)\rangle$ is the mean intensity of all observations i of reflection hkl.

Table 4.7. Refinement statistics for mutant AarCH6[a]

	AarCH6-S71A•CoA (4eu8)	AarCH6-R228E•CoA[d] (4eu9)	AarCH6-R228E•CoA [anomalous] (4eua)
Resolution (Å)	34.7 – 1.81 (1.83 – 1.81)	31.0 – 1.48 (1.50 – 1.48)	44.6 – 2.40 (2.43 – 2.40)
Reflections (working/test)	77,516/4,077	140,548/7,386	62,276/3,330
Total atoms	8,513	9,290	8,364
Protein atoms	7,724	7,862	7,764
Water atoms	689	1,326	500
Ligand atoms	100	102	100
R_{cryst}[b] **(%)**	18.0 (24.0)	15.7 (19.1)	15.2 (15.3)
R_{free}[c] **(%)**	22.6 (29.6)	17.9 (22.1)	20.9 (23.6)
Average B-factor (Å²)			
Protein	20.1	13.3	16.9
Water	27.7	26.3	19.0
Ligand	27.1	20.0	31.3
Rmsd from ideal geometry			
Bond lengths (Å)	0.007	0.006	0.007
Bond angles (°)	1.11	1.14	1.02
Ramachandran plot (%)			
Favored regions	96.5	97.0	96.5
Additionally allowed regions	3.0	2.9	3.4
Outlying regions	0.5	0.1	0.1

[a] Values in parentheses are for the outermost resolution shell. [b] $R_{cryst} = \sum_{hkl} |F_o - F_c| / \sum_{hkl} F_o$, where F_o and F_c are the observed and calculated structure factors, respectively. [c] R_{free} was calculated in the same manner as R_{cryst} using the 5% of reflections excluded from refinement. With the exception of the AarCH6-S71A•CoA, AarCH6-R228E•CoA [anomalous], and AarCH6-E294A•dethiaacetyl-CoA datasets, a consistent set of reflections was set aside for all datasets of the space group $P2_12_12_1$, including those datasets described in Tables 4.5 and 4.9. [d] Both the glutamyl-CoA thioester intermediate and glutamate/CoA were modeled in the active site of subunit B.

Table 4.8. Data-collection statistics for mutant AarCH6 and wild-type AarC[a]

	AarCH6-E294A•CoA (4eub)	**AarCH6-E294A•dethiaacetyl-CoA (4euc)**	**AarC•CoA•citrate (4eud)**
Beamline	21-ID-F	21-ID-G	23-ID-B
Wavelength (Å)	0.97872	0.97856	1.0332
Space group	$P2_12_12_1$	$P2_12_12_1$	$P2_12_12_1$
Unit-cell dimensions (Å)	a = 67.4, b = 110.3, c = 120.2	a = 79.5, b = 104.1, c = 120.1[d]	a = 67.7, b = 110.6, c = 119.9
Solvent content (%)[b]	38.6	44.8	40.1
Matthews coefficient (Å^3/Da)[b]	2.00	2.23	2.05
Resolution (Å)	50 – 1.97 (2.00 – 1.97)	50 – 2.65 (2.70 – 2.65)	50 – 1.94 (2.01 – 1.94)
Measured reflections	904,072	438,134	605,583
Unique reflections	63,807 (3,167)	29,835 (1,441)	64,164 (6,136)
Redundancy	14.2 (13.4)	14.7 (14.9)	9.4 (6.5)
Completeness (%)	100.0 (99.9)	100.0 (100.0)	97.3 (94.8)
$\langle I/\sigma(I)\rangle$	28.4 (6.3)	33.9 (6.2)	20.0 (3.9)
R_{sym}[c] **(%)**	12.0 (49.1)	14.0 (75.4)	21.4 (60.0)

[a] Values in parentheses are for the outermost resolution shell. [b] Solvent contents and Matthews coefficients were calculated using a web applet (http://www.ruppweb.org/Mattprob/). [c] $R_{sym} = \sum_{hkl} \sum_i |I_i(hkl) - \langle I_i(hkl)\rangle| / \sum_{hkl} \sum_i I_i(hkl)$, where $I_i(hkl)$ is the intensity of the ith observation of reflection hkl and $\langle I_i(hkl)\rangle$ is the mean intensity of all observations i of reflection hkl. [d] Altered unit-cell dimensions resulted from a unique crystal-packing arrangement.

Table 4.9. Refinement statistics for mutant AarCH6 and wild-type AarC[a]

	AarCH6-E294A•CoA (4eub)	AarCH6-E294A•dethiaacetyl-CoA (4euc)	AarC•CoA•citrate[d] (4eud)
Resolution (Å)	40.2 – 1.97 (2.00 – 1.97)	43.5 – 2.64 (2.73 – 2.64)	42.8 – 1.95 (2.02 – 1.95)
Reflections (working/test)	60,553/3,179	28,286/1,489	57,803/3,021
Total atoms	8,583	7,987	8,544
Protein atoms	7,686	7,676	7,686
Water atoms	795	205	745
Ligand atoms	102	106	113
R_{cryst}[b] **(%)**	15.4 (18.2)	16.8 (22.2)	15.9 (17.8)
R_{free}[c] **(%)**	20.9 (26.4)	22.5 (29.7)	20.6 (26.0)
Average B-factor (Å²)			
Protein	17.9	46.9	18.8
Water	25.1	36.8	25.5
Ligand	14.3	43.9	29.1
Rmsd from ideal geometry			
Bond lengths (Å)	0.007	0.009	0.007
Bond angles (°)	1.07	1.07	1.03
Ramachandran plot (%)			
Favored regions	97.6	95.4	96.7
Additionally allowed regions	2.1	4.5	3.0
Outlying regions	0.3	0.1	0.3

[a] Values in parentheses are for the outermost resolution shell. [b] $R_{cryst} = \sum_{hkl} |F_o - F_c| / \sum_{hkl} F_o$, where F_o and F_c are the observed and calculated structure factors, respectively. [c] R_{free} was calculated in the same manner as R_{cryst} using the 5% of reflections excluded from refinement. With the exception of the AarCH6-S71A•CoA, AarCH6-R228E•CoA [anomalous], and AarCH6-E294A•dethiaacetyl-CoA datasets, a consistent set of reflections was set aside for all datasets of the space group $P2_12_12_1$, including those datasets described in Tables 4.5 and 4.7. [d] Citrate was only modeled in the active site of subunit B.

Table 4.10. Wild-type and mutant AarCH6 kinetic constants[a]

Substrate	Parameter	WT	S71A[c]	R228E	N347A	E435D
acetate	k_{cat} (s^{-1})	280 ± 40	4.85 ± 0.07	3.4 ± 0.1[e]	12.2 ± 0.2	370 ± 50
	K_m (mM)	70 ± 20	167 ± 6	6 ± 1	78 ± 5	110 ± 30
	k_{cat}/K_m (M^{-1} s^{-1})	(4 ± 1) × 10^3	(2.9 ± 0.1) × 10^1	(6 ± 1) × 10^2	(1.6 ± 0.1) × 10^2	(3 ± 1) × 10^3
	K_i (mM)	1,600 ± 800	NA[d]	NA	NA	2,000 ± 2,000
succinyl-CoA	k_{cat} (s^{-1})	201 ± 8	6.2 ± 0.6	16.0 ± 0.4[f]	12.1 ± 0.9	340 ± 10
	K_m (μM)	22 ± 4	90 ± 20	122 ± 9	38 ± 7	40 ± 5
	k_{cat}/K_m (M^{-1} s^{-1})	(9 ± 2) × 10^6	(7 ± 2) × 10^4	(1.3 ± 0.1) × 10^5	(3.2 ± 0.6) × 10^5	(9 ± 1) × 10^6
	K_i (μM)	NA	700 ± 200	NA	4000 ± 2000	NA
succinate	k_{cat} (s^{-1})	71 ± 2	6.2 ± 0.1	800 ± 500	2.07 ± 0.02[h]	153 ± 2
	K_m (mM)	0.9 ± 0.1	21 ± 2	3000 ± 2000	0.76 ± 0.03	2.1 ± 0.1
	k_{cat}/K_m (M^{-1} s^{-1})	(7.9 ± 0.9) × 10^4	(3.0 ± 0.3) × 10^2	(3 ± 3) × 10^2	(2.7 ± 0.1) × 10^3	(7.3 ± 0.4) × 10^4
acetyl-CoA	k_{cat} (s^{-1})	75 ± 2	40 ± 20	105 ± 3[g]	1.97 ± 0.07	129 ± 3
	K_m (μM)	22 ± 2	500 ± 300	45 ± 5	3.0 ± 0.4	25 ± 3
	k_{cat}/K_m (M^{-1} s^{-1})	(3.4 ± 0.3) × 10^6	(8 ± 6) × 10^4	(2.3 ± 0.3) × 10^6	(6.6 ± 0.9) × 10^5	(5.2 ± 0.6) × 10^6
	K_i (μM)	NA	70 ± 40	NA	5000 ± 2000	NA
---	K_{eq}[b]	0.14 ± 0.05	0.08 ± 0.06	0.1 ± 0.1	0.03 ± 0.01	0.07 ± 0.03

[a] SCACT activities were measured using LCF/LCR assays. Saturation experiments were performed in duplicate for the mutant enzymes. No activity was detected with AarCH6-E294A. Kinetic constants for the wild-type (WT) enzyme were taken from Chapter 2. [b] Haldanes were calculated as described in Chapter 2. [c] Assays were shortened to 17 − 35 s. [d] Substrate inhibition was not observed (not applicable). [e] The concentration of succinyl-CoA was 500 μM. The data were fit to a modified Michaelis-Menten equation (Figure 4.8). [f] The concentration of acetate was 750 mM. [g] The concentration of succinate was 550 mM. [h] The concentration of acetyl-CoA was 100 μM.

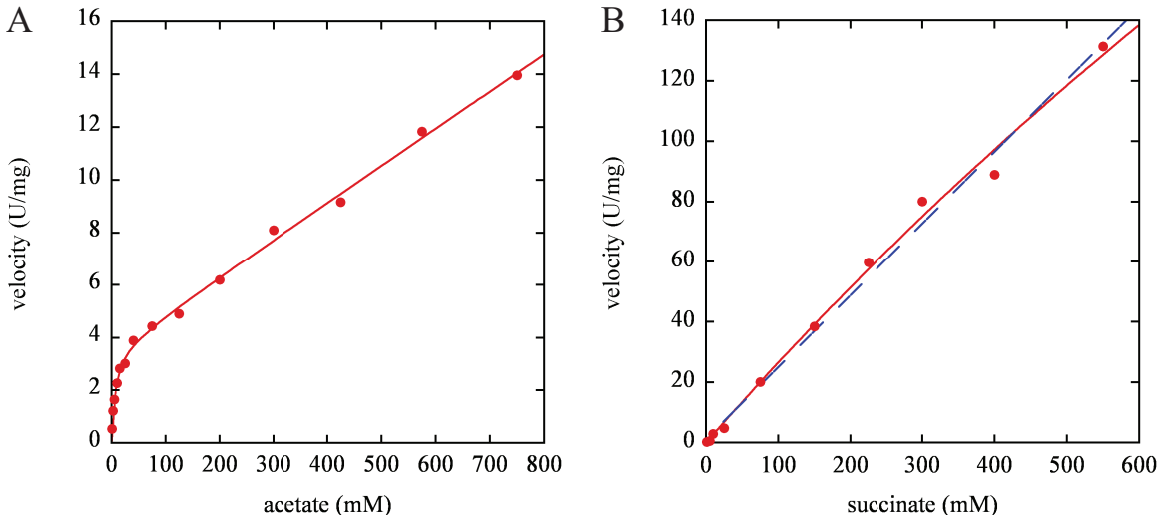

Figure 4.8. Kinetic characterization of AarCH6-R228E. Both physiological carboxylate substrates failed to saturate AarCH6-R228E. **(A)** Acetate "saturation" plot. Kinetic data were only satisfactorily fit when an additional linear-slope term was added to the Michaelis-Menten equation ($v = V_{max} \times [acetate]/(K_m + [acetate]) + slope \times [acetate]$). **(B)** Succinate "saturation" plot. Kinetic data were equally well fit by the Michaelis-Menten equation (red solid line) and a linear equation (blue dashed line). Potassium succinate is insoluble above ~650 mM at pH 8. Kinetic constants are given in Table 4.10.

Glu228 is well-removed from the proposed auxiliary binding site (AarCH6-R228E•CoA, PDB entry 4eu9, Tables 4.6 and 4.7), the charge reversal appears to have partially neutralized much of the positively charged active-site cleft (Figure 4.9). Altered electrostatic interactions could be responsible for much, if not all, of the loss of apparent binding affinity.

Substrate specificity (AarCH6-R228E). Four zwitterionic carboxylates (3-aminopropionate, 4-aminobutyrate, glycylglycine, and 4-guanidinobutyrate; Figure A.11) were screened as possible alternate CoA-acceptors in modified VisR and LCR assays containing AarCH6-R228E. None of the substrates produced detectable CoA-transferase activity, suggesting charge complementation alone is not sufficient to alter specificity.

Citrate inhibition. While citrate was unable to support CoA-transferase activity, SCACT activity was competitively inhibited by citrate in modified LCR assays

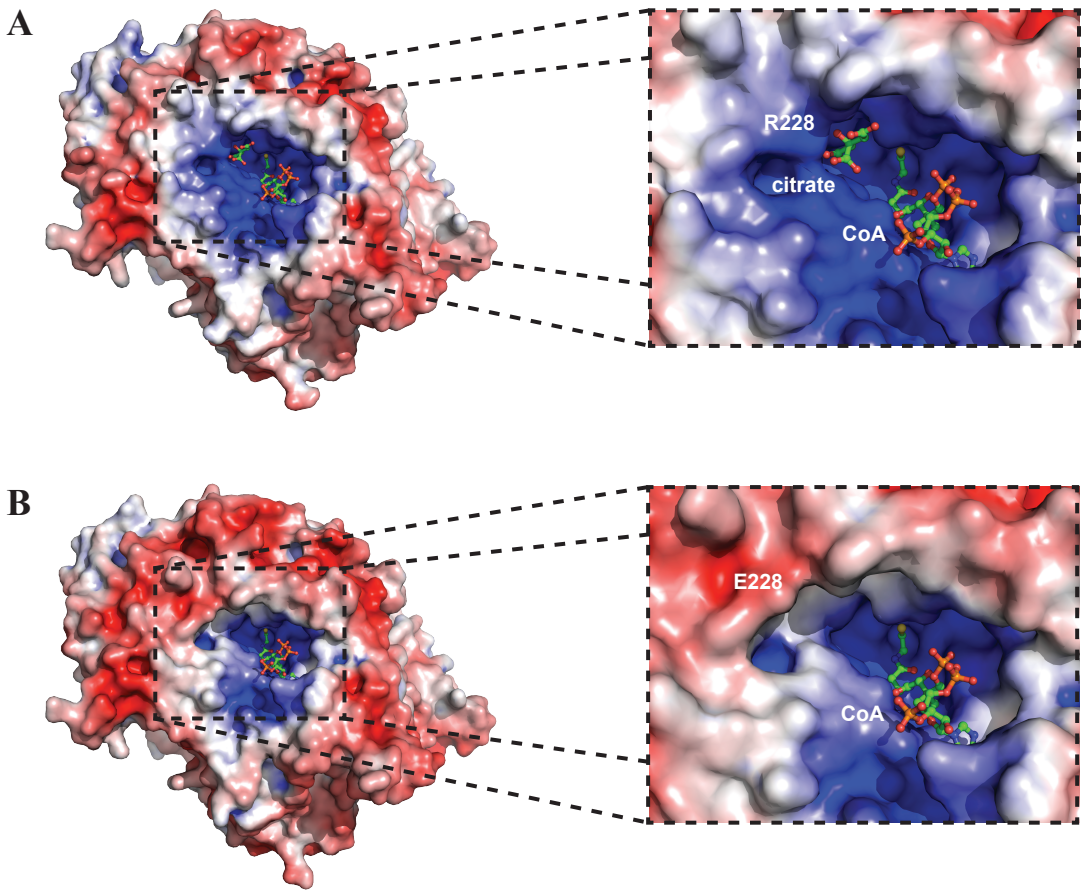

Figure 4.9. Electrostatic surfaces surrounding the auxiliary binding sites of AarCH6 and AarCH6-R228E. **(A)** AarCH6 (PDB entry 4eu6). **(B)** AarCH6-R228E (PDB entry 4eu9). The protein surfaces are colored red for negatively charged areas and blue for positively charged areas. The saturation of the colors is proportional to the degree of electrostatic charge from −7 *kT/e* to +7 *kT/e*. The charge surfaces were computed at pH 7 using the PDB2PQR (*40*) web server and the APBS (*41*) plugin for PyMOL. CoA and citrate are depicted in ball-and-stick representation.

containing a varied concentration of succinate and a fixed concentration of acetyl-CoA (Figure 4.10). Inhibition was too weak to be physiologically relevant (K_i = 150 ± 30 mM) but supports the proposed role of Thr94 and Arg228 in auxiliary binding of carboxylate substrates.

Conformational dynamics. Wild-type and mutant AarCH6 adopted several distinct conformations ranging from fully open to fully closed (Figure 4.11). The most open conformation was assumed by unliganded AarCH6 (AarCH6, PDB entry 4eu3, Tables 4.4 and 4.5), making the active site readily accessible to acyl-CoA substrates. Upon binding

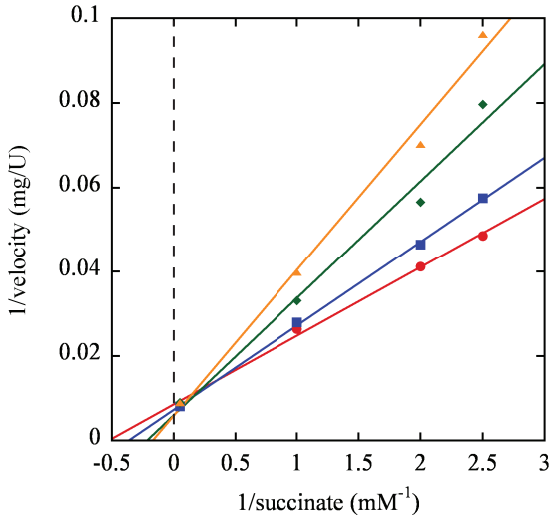

Figure 4.10. Citrate-dependent inhibition of SCACT activity. Citrate was a competitive inhibitor in modified LCR assays containing a variable concentration of succinate (0.4 – 20 mM) and fixed concentrations of acetyl-CoA (0.5 mM) and citrate [0 (red circles), 25 (blue squares), 75 (green diamonds), or 125 mM (orange triangles)]. Kinetic constants and error estimates were determined by global nonlinear fitting using gnuplot 4.4.

CoA, AarCH6 proceeded through three stages of constriction. The first stage left the active site largely open but through small, local structural shifts improved hydrogen-bonding, electrostatic, and hydrophobic interactions with the adenine and ribose rings, the 3′-phosphate, and the proximal carbonyl oxygen of the pantetheine arm. The second stage greatly narrowed the active site. Helices α8 – α11 and the loop connecting β10 and α8 translated toward CoA to maximize hydrogen-bonding and electrostatic interactions with the diphosphate moiety and the proximal amide nitrogen and adjacent hydroxyl of the pantetheine arm ({AarCH6}•CoA, PDB entry 4eu5, Tables 4.4 and 4.5; Figure 4.12B/C). The concomitant relocation of Val270 created a closed reaction pocket defined by the hydrophobic residues Phe35, Thr36, Ala70, Phe92, Leu114, and Val295, isolating the catalytic glutamate and CoA thiol from bulk solvent (Figure 4.12A). An accompanying rotation of the domain linker placed the side chain of Phe232 between α9 and the mobile loop connecting β10 and α8. The third and final stage appears to be an incremental

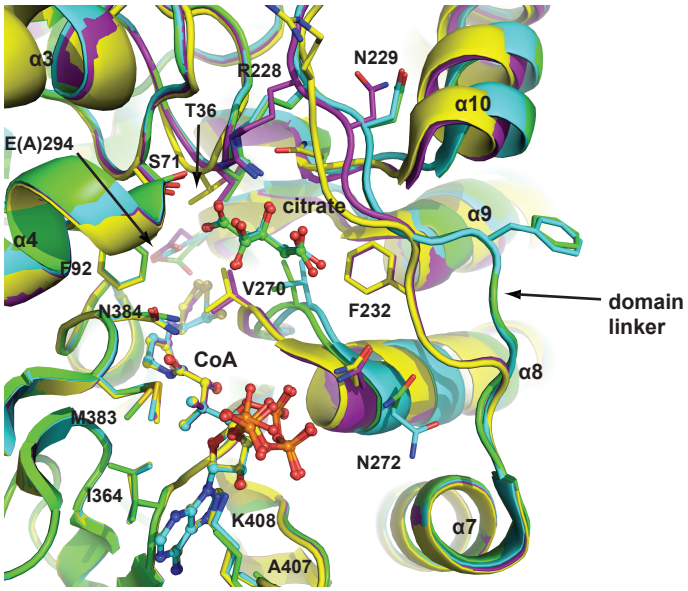

Figure 4.11. Stepwise constriction of AarCH6 (and AarCH6-E294A). The active-site cleft of AarCH6 narrows upon binding CoA. Helices α8 − α11 translate toward CoA, maximizing hydrogen-bonding and electrostatic interactions with the diphosphate moiety and the pantetheine arm. Concomitantly, the side chain of Val270 forms an isolated hydrophobic pocket around the catalytic residues and CoA thiol, while the domain linker rotates, pushing Asn229 and Phe232 into the active-site cleft and pulling Arg228 onto the protein surface. Residues in the fully open conformation are colored green (PDB entry 4eu3), residues in the mostly open conformation are colored cyan (PDB entry 4eu7), residues in the predominantly closed conformation are colored purple (PDB entry 4eu5), and residues in the fully closed conformation are colored yellow (PDB entry 4eub). CoA and citrate from all models are depicted in ball-and-stick representation.

continuation of the second stage (AarCH6-E294A•CoA, PDB entry 4eub, Tables 4.8 and 4.9). Rotation of the domain linker continued toward the N-terminal domain, pushing the side chain of Asn229 into the active site while pulling the side chain of Arg228 onto the protein surface, effectively removing the auxiliary binding site.

Relatively high B-factors in the dynamic portions of all structures, including the unliganded structure, suggest an equilibrium between the open and closed conformations. CoA seems to shift the equilibrium toward the closed conformation by forming favorable hydrogen-bonding and electrostatic interactions with the loop connecting β10 and α8 and the N-terminus of α8 that constrict the active site. Conversely, citrate seems to shift the equilibrium toward the open conformation by forming favorable hydrogen-bonding and

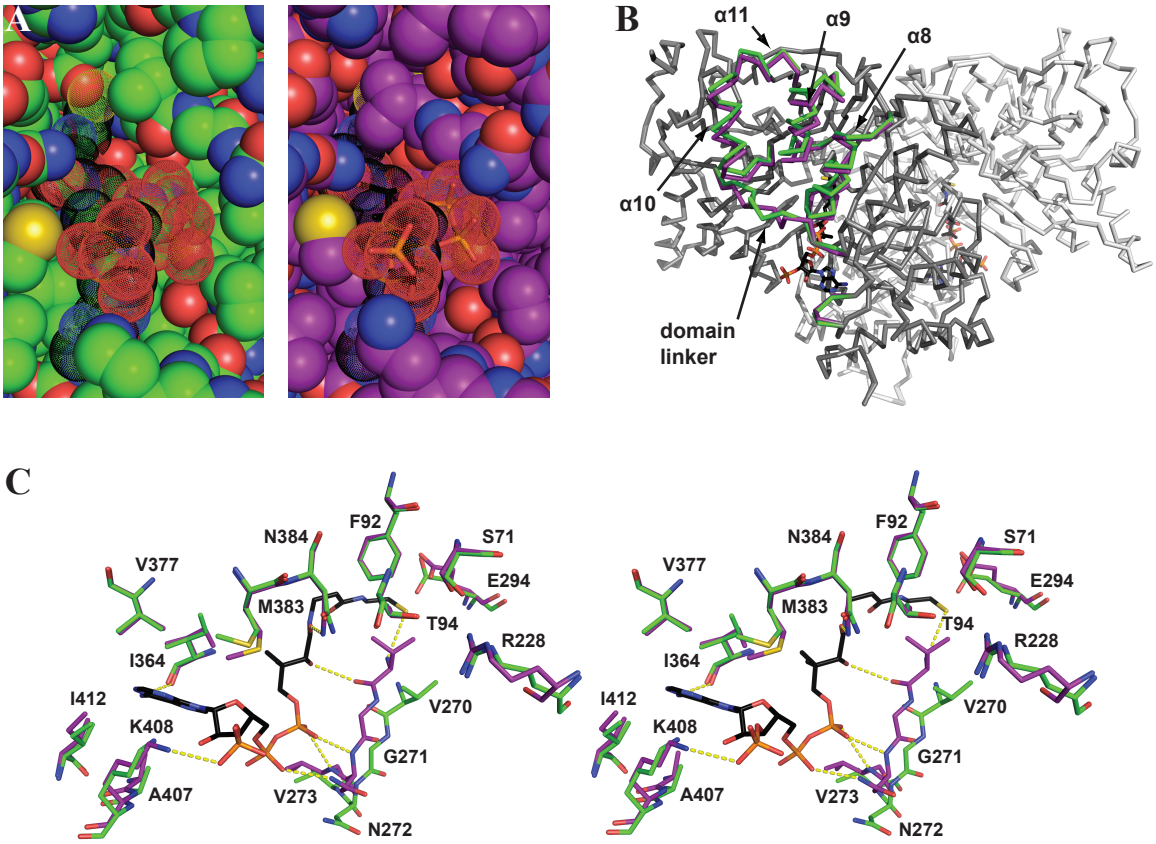

Figure 4.12. Conformational motions in AarCH6. **(A)** The active-site cleft of AarCH6 constricts upon binding CoA, isolating the catalytic glutamate and CoA thiol from bulk solvent. For reference, CoA from the closed structure was superposed onto the open, unliganded structure. **(B)** Changes in the active site are accompanied by significant shifts in surrounding loops and helices. Dynamic regions (Rmsd ≥ 0.5 Å for Cα atoms) are differentially colored. **(C)** Constriction of the active-site cleft maximizes electrostatic and hydrogen-bonding interactions (yellow dotted lines) with CoA (divergent stereodiagram). In all panels, residues in the open conformation are colored green (PDB entry 4eu3), residues in the closed conformation are colored purple (PDB entry 4eu5), and CoA is colored black.

electrostatic interactions with the side chain of Arg228 that inhibit rotation of the domain linker.

Characterization of a pseudo Michaelis complex. AarCH6-E294A was cocrystallized with dethiaacetyl-CoA (AarCH6-E294A•dethiaacetyl-CoA, PDB entry 4euc, Tables 4.8 and 4.9), and clear electron density was observed in the closed active-site cleft consistent with the complete and ordered ligand (Figure 4.13). [Dethiaacetyl-CoA is an unreactive analogue of acetyl-CoA in which the thioester sulfur is replaced by a methylene group.] The CoA moiety of dethiaacetyl-CoA is bound in the same extended

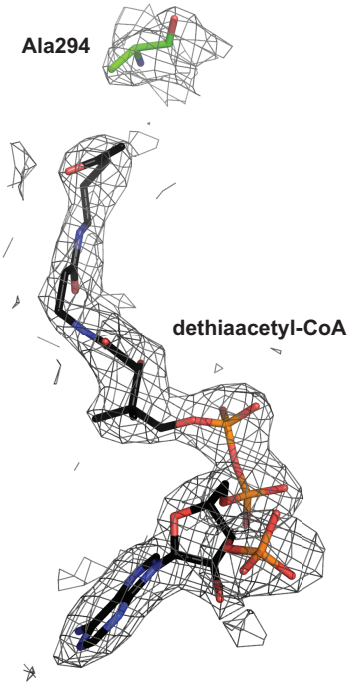

Figure 4.13. Pseudo Michaelis complex between AarCH6-E294A and dethiaacetyl-CoA (PDB entry 4euc). Electron density consistent with dethiaacetyl-CoA was observed in the active site of AarCH6-E294A. The NCS-averaged, σ_A-weighted $2mF_o - DF_c$ map, calculated with dethiaacetyl-CoA and Ala294 omitted, is contoured at 1.0 sigma and carved with a 2.6-Å radius.

conformation as described above for CoA. The "acetyl" group, however, does not continue toward Ala294 but wraps back toward the pantetheine arm, forming hydrogen-bonding interactions with the backbone nitrogen of Gly388 and the distal amide nitrogen of the CoA moiety (Figure 4.14). [This conformation would seemingly prepare acetyl-CoA for nucleophilic attack by Glu294 and stabilize the resulting tetrahedral oxyanion intermediate.] The terminal methyl group forms hydrophobic contacts with the side chains of Phe35, Thr36, Ala70, Phe92, Leu114, Val270, Ala294, and Val295.

Freeze-trapping of covalent intermediates. Multiple experimental conditions were screened in an effort to obtain covalent anhydride and thioester intermediates. While cocrystallization and prolonged soaking in drops and cryoprotectants supplemented with acetyl-CoA (or succinyl-CoA) failed, a 22-h soak in cryoprotectant without ligand

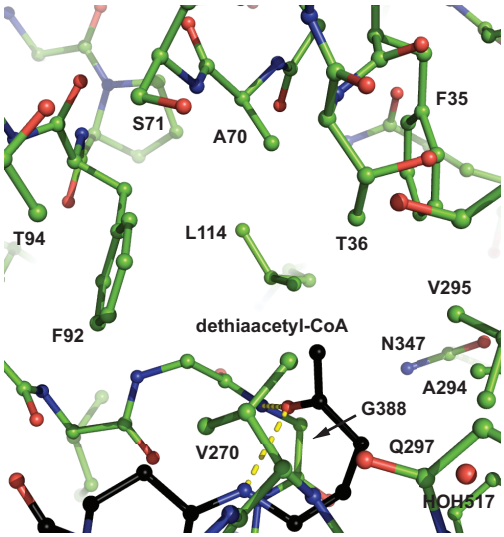

Figure 4.14. Pseudo Michaelis complex between AarCH6-E294A and dethiaacetyl-CoA (PDB entry 4euc) [2]. Dethiaacetyl-CoA (black) binds in a curled conformation. The ketone carbonyl oxygen forms hydrogen-bonding interactions (yellow dotted lines) with the backbone nitrogen of Gly388 and the distal amide nitrogen of the CoA moiety, while the terminal methyl group forms hydrophobic contacts with the side chains of Phe35, Thr36, Ala70, Phe92, Leu114, Val270, Ala294, and Val295. In the fully closed conformation, Arg228 (not shown) is pulled from the active site and the side chain of Gln297 reorients to form hydrogen-bonding interactions with the backbone carbonyl oxygen of Gly269 and the backbone nitrogen of Gly271.

followed by a short 2-h soak in cryoprotectant supplemented with acetyl-CoA was successful. [Under conditions similar to those employed for crystallization and cryoprotection the acyl-CoA substrates have ~10 h half-lives (Chapter 2).]

Electron density consistent with the acetylglutamyl anhydride/CoA thiolate and glutamyl-CoA thioester was observed in both active sites of the dimeric asymmetric unit (AarCH6•CoA•acetate, PDB entry 4eu6, Tables 4.4 and 4.5; Figure 4.15). The predominant intermediate was modeled and refined in each. Electron density consistent with acetate was also observed in the proposed auxiliary binding site of the subunit with the greatest density congruent with the glutamyl-CoA thioester (Figure 4.15). Dynamic regions of the active sites and surrounding mobile secondary structural elements possessed relatively weak density consistent with the proposed equilibrium between open and closed conformations.

The proximal and distal carbonyl oxygens of the acetylglutamyl anhydride form hydrogen-bonding interactions with the side chain of Asn347 and the backbone nitrogen of Gly388/distal amide nitrogen of CoA, respectively. This arrangement prepares the mixed anhydride for nucleophilic attack at either carbonyl, forming the glutamyl-CoA thioester (proximal carbonyl) or reforming acetyl-CoA (distal carbonyl). Intervening tetrahedral oxyanion intermediates would be stabilized by the side chain of Asn347 (position 2) or the backbone nitrogen of Gly388/distal amide nitrogen of CoA (position 1), respectively (Scheme 4.2). The leaving-group potentials of acetate and Glu294 are likely increased by these same hydrogen-bonding interactions. The terminal methyl group

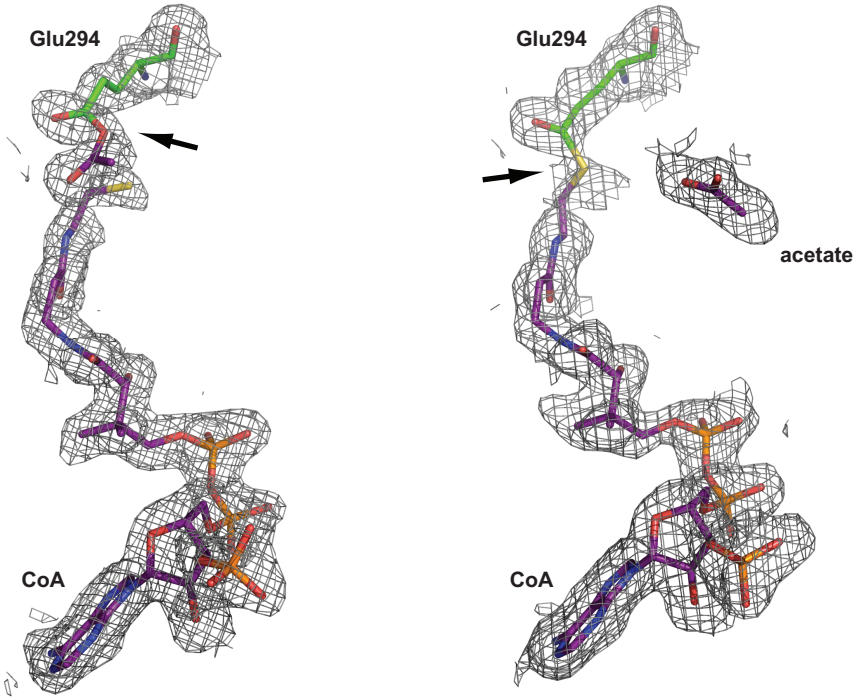

Figure 4.15. Covalent anhydride and thioester intermediates (PDB entry 4eu6). Electron density consistent with the acetylglutamyl anhydride and glutamyl-CoA thioester intermediates was observed in both active sites of the dimeric asymmetric unit following a short 2-h soak in cryoprotectant supplemented with acetyl-CoA. Only the predominant intermediate was modeled in each. **(Left)** Anhydride intermediate. **(Right)** Thioester intermediate. The points of covalent attachment are indicated (black arrows). The σ_A-weighted $2mF_o - DF_c$ map, calculated with CoA, acetate, and Glu294 omitted, is contoured at 0.9 (anhydride) and 0.6 (thioester) sigma and carved with a 2-Å radius.

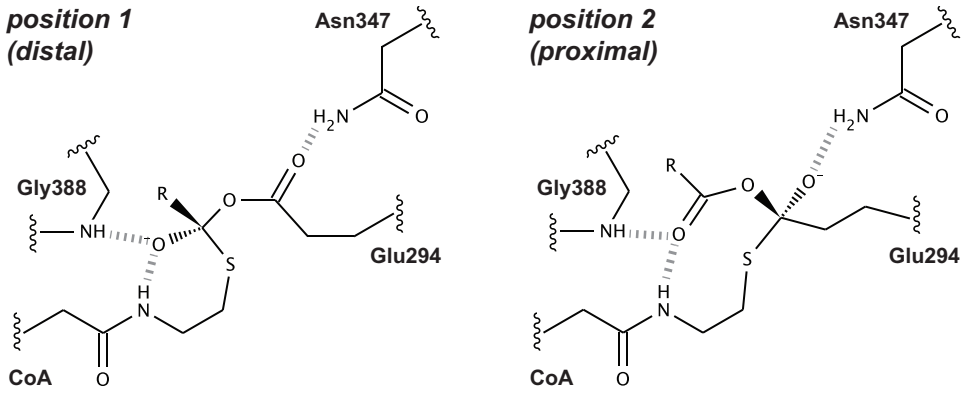

Scheme 4.2. Tetrahedral oxyanion intermediates. Four tetrahedral oxyanion intermediates [R = -CH_3 (acetyl) or -$CH_2CH_2COO^-$ (succinyl)] are formed at two unique positions during the SCACT reaction. None are formed within a traditional oxyanion hole, but all are stabilized by one or more hydrogen-bonding interactions.

of the mixed anhydride forms hydrophobic contacts with the side chains of Phe35, Thr36, Ala70, Phe92, Leu114, Val270, and Val295. The accompanying CoA thiolate is bound in the same extended conformation described above for CoA with the terminal sulfur forming hydrogen-bonding interactions with HOH517 and the backbone nitrogen of Val270.

The carbonyl oxygen of the glutamyl-CoA thioester retains the hydrogen-bonding interaction of the proximal carbonyl of the acetylglutamyl anhydride with the side chain of Asn347. This conformation prepares the intermediate for nucleophilic attack by the carboxylate substrate (or product), forming the second mixed anhydride (or reforming the first mixed anhydride) and the CoA thiolate. The transient tetrahedral oxyanion intermediate would be stabilized by hydrogen-bonding interactions with Asn347 (Scheme 4.2). As the tetrahedral oxyanion intermediate decomposes, the leaving-group potential of the CoA thiolate is likely increased by hydrogen-bonding interactions with HOH517 and the backbone nitrogen of Val270. The accompanying acetate occupies the auxiliary

binding site, forming hydrogen-bonding and/or electrostatic interactions with the side chains of Ser71, Thr94, and Arg228.

Proposed roles of Asn347. Asn347 is appropriately located to prearrange Glu294 in the reactive conformation, stabilize two of four tetrahedral oxyanion intermediates (position 2, Scheme 4.2), and augment the leaving-group potential of the glutamyl carboxylate. AarCH6-N347A exhibited significantly and globally reduced catalytic activity but largely unaffected apparent substrate affinity. Both findings correlate with the proposed roles of Asn347. Loss of catalytic activity by the mutant enzyme could conceivably be attenuated by an advantageously positioned water between Glu294 and Asp391.

Molecular modeling of Michaelis complexes and glutamylsuccinyl anhydride. Molecular modeling and molecular mechanics calculations were employed to construct the crystallographically unobserved Michaelis complexes and the single unobserved covalent intermediate glutamylsuccinyl anhydride. When combined with crystallographic results these techniques provide a complete structural description of the ground-state complexes and intermediates in the SCACT reaction (Figure 4.16 and Scheme 4.3).

Modeled glutamylsuccinyl anhydride was restrained to be in much the same conformation as the crystallographically observed acetylglutamyl anhydride, but the position of the distal carboxylate and adjacent methylene group were optimized using molecular mechanics calculations. Hydrogen-bonding interactions were formed with the side chain of Ser71 and the backbone nitrogens of Ser71 and Thr36, while appropriate hydrophobic contacts were created with the side chains of Phe35, Thr36, Ala70, Phe92,

Leu114, Val270, and Val295. In this conformation the succinyl moiety possesses a nearly trans geometry.

The Michaelis complex involving acetyl-CoA was modeled in the curled conformation of dethiaacetyl-CoA. Hydrogen-bonding interactions were formed with the backbone nitrogen of Gly388 and the distal amide nitrogen of the CoA moiety, while the terminal methyl group was placed in contact with the side chains of Phe35, Thr36, Ala70, Phe92, Leu114, Val270, and Val295. Energy minimization introduced small conformational deviations relative to dethiaacetyl-CoA can be attributed to inherent differences in bond lengths and bond angles involving carbon (dethiaacetyl-CoA) and sulfur (acetyl-CoA) atoms.

The Michaelis complex involving succinyl-CoA was also modeled in the curled conformation of acetyl-CoA, while the succinyl moiety was arranged in the extended trans geometry of glutamylsuccinyl anhydride. Energy minimization retained all hydrogen-bonding interactions and hydrophobic contacts observed for dethiaacetyl-CoA and modeled for (acetyl-CoA and) glutamylsuccinyl anhydride.

Acetate and succinate were placed adjacent to the crystallographically observed glutamyl-CoA thioester intermediate in modeled Michaelis complexes. Both carboxylates were positioned according to the conformations of the corresponding mixed anhydrides and then optimized using molecular mechanics calculations. All hydrogen-bonding interactions and hydrophobic contacts from the initial complexes were retained after energy minimization.

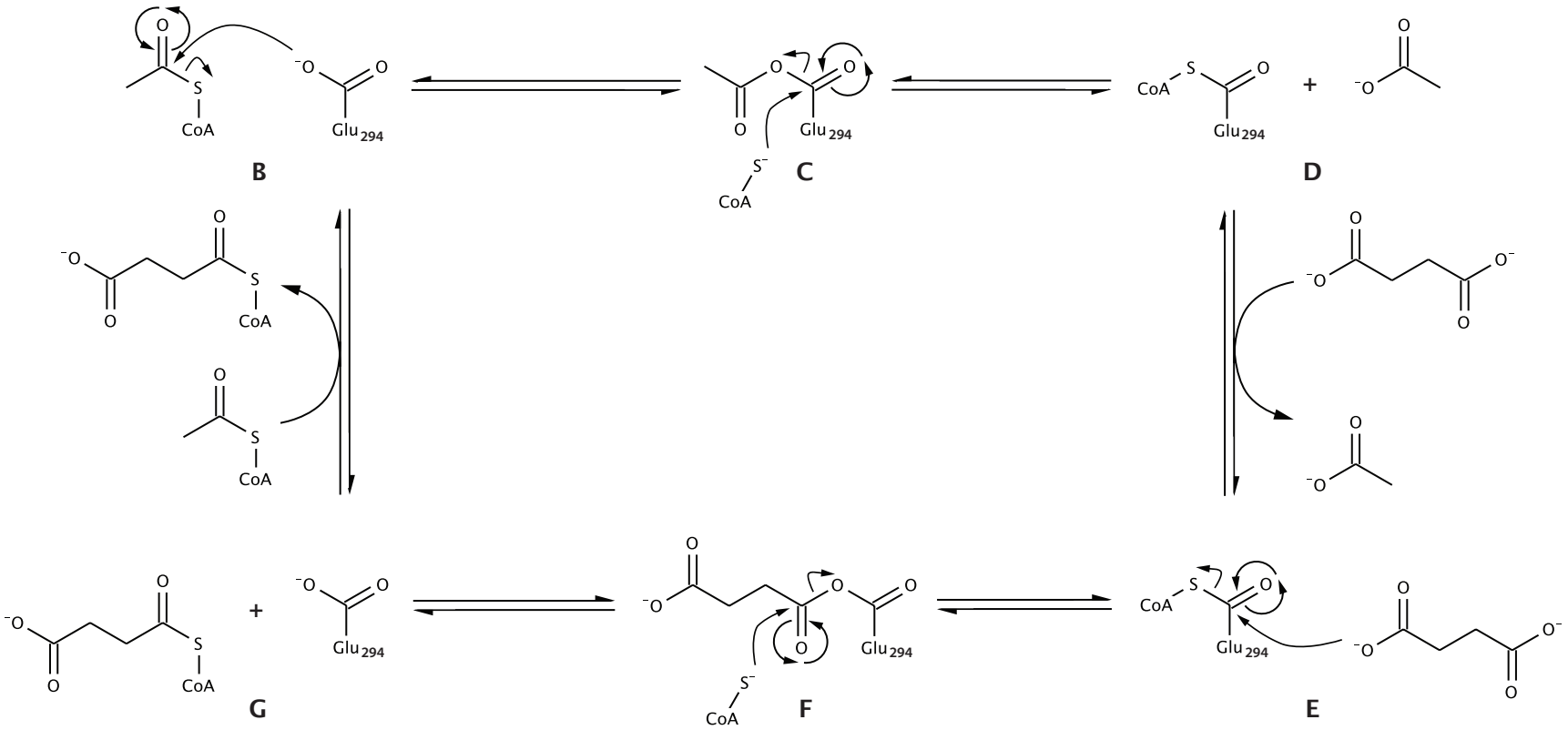

Scheme 4.3. Abbreviated SCACT mechanism (reverse biosynthetic direction). The SCACT reaction proceeds through a series of anhydride, tetrahedral oxyanion (not shown), and thioester intermediates. All individual steps and the overall reaction are fully reversible. B: acetyl-CoA, C: acetylglutamyl anhydride and CoA thiolate, D: glutamyl-CoA thioester and acetate, E: glutamyl-CoA thioester and succinate, F: glutamylsuccinyl anhydride and CoA thiolate, and G: succinyl-CoA. Labels correspond to panels in Figure 4.16.

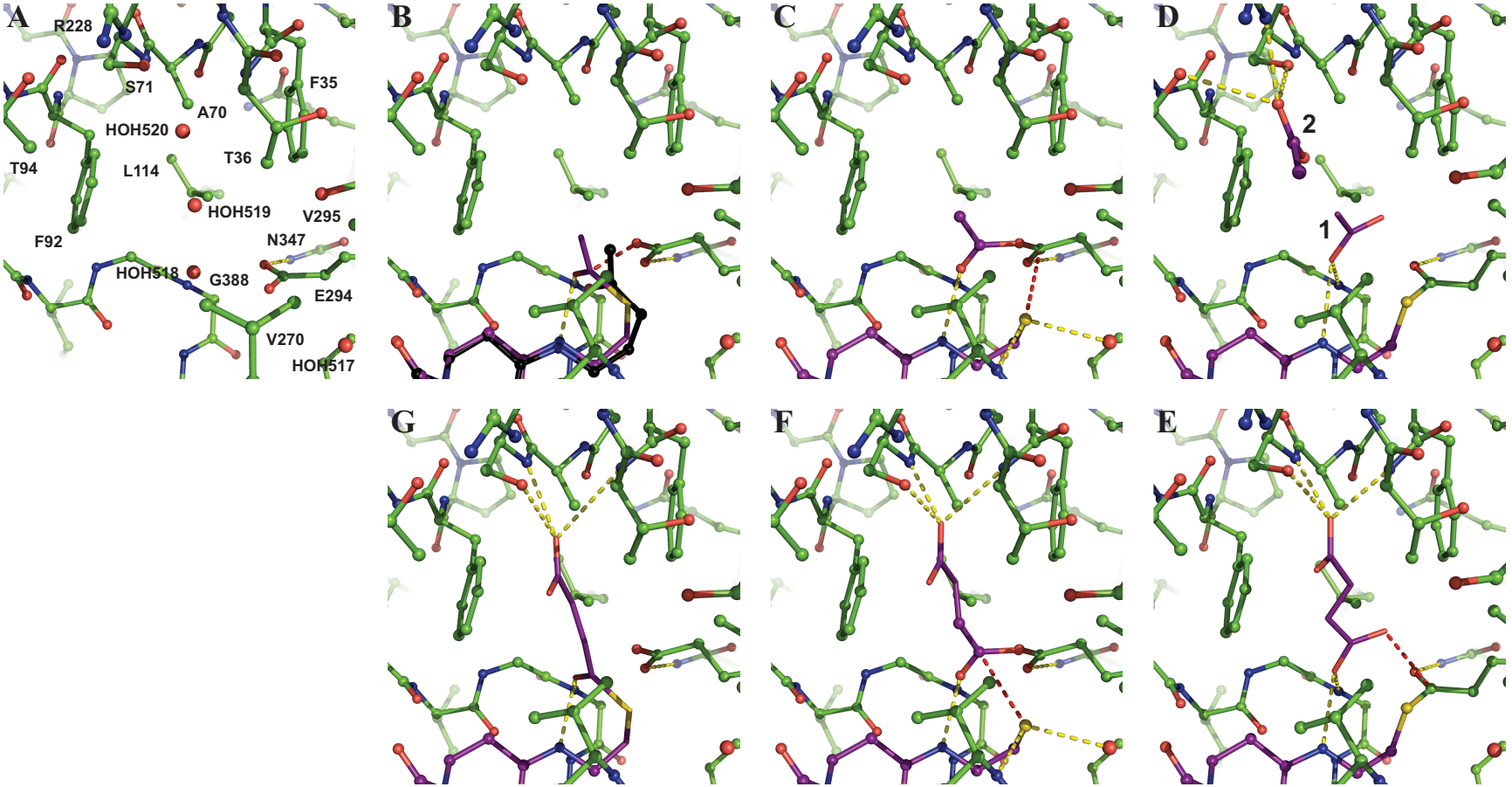

Figure 4.16. Structural characterization of the SCACT reaction (reverse biosynthetic direction). Crystallographically observed intermediates (ball-and-stick representation) and modeled intermediates (stick representation) were combined to produce a complete structural description of the SCACT reaction. **(A)** Unliganded. **(B)** Acetyl-CoA [and dethiaacetyl-CoA (black)]. **(C)** Acetylglutamyl anhydride and CoA thiolate. **(D)** Glutamyl-CoA thioester and acetate. [Acetate is depicted in two positions. Position "2" was crystallographically observed (Figure 4.15). Position "1" was modeled.] **(E)** Glutamyl-CoA thioester and succinate. **(F)** Glutamylsuccinyl anhydride and CoA thiolate. **(G)** Succinyl-CoA. Modeled intermediates were manually positioned within the active site and equilibrium conformations were determined using molecular mechanics calculations. Atoms shown in ball-and-stick representation were "frozen" or omitted during optimization. Yellow and red dotted lines indicate hydrogen bonds and possible paths of nucleophilic attack, respectively.

Proposed roles of Ser71. Ser71 forms hydrogen-bonding interactions with acetate and succinate in the auxiliary binding site and succinate, succinyl-CoA, and glutamylsuccinyl anhydride in the primary binding site. AarCH6-S71A displayed moderately reduced apparent binding affinity and greatly reduced catalytic activity, much greater than that expected from the loss of a single noncatalytic hydrogen-bonding interaction. Catalytic activity and apparent binding affinity were also reduced in reactions containing (acetyl-CoA and) propionate [$k_{cat} = 8 \pm 1\ s^{-1}$, $K_m = 900 \pm 200$ mM, and $k_{cat}/K_m = (8 \pm 2) \times 10^0\ M^{-1}\ s^{-1}$], which should not directly interact with Ser(Ala)71 in the Michaelis complex, the product complex, or any intervening covalent intermediate.

The specific activity of AarCH6-S71A oddly decreased in a nonlinear manner at low enzyme concentrations. [Reaction times were shortened to allow for higher enzyme concentrations in LCF/LCR assays.] Neither the wild-type enzyme nor any of the other mutant enzymes exhibited this phenomenon. Deoligomerization of the dimeric biological unit would be consistent with this observation; however, Ser71 is far-removed from the subunit interface.

Introduction of the Ser71→Ala mutation allowed the primary succinate binding pocket to collapse (AarCH6-S71A•CoA, PDB entry 4eu8, Tables 4.6 and 4.7; Figure 4.17). Without the two hydrogen bonds between the side chain of Ser71 and the backbone nitrogens of Thr36 and Gly37, the loop connecting β1 and α2 shifted toward Ala71. In the resulting conformation, the side chain of Thr36 blocks a large portion of the reaction pocket. While acetate and propionate are significantly smaller than succinate, the relocated side chain of Thr36 may nonetheless interfere with binding of propionate and

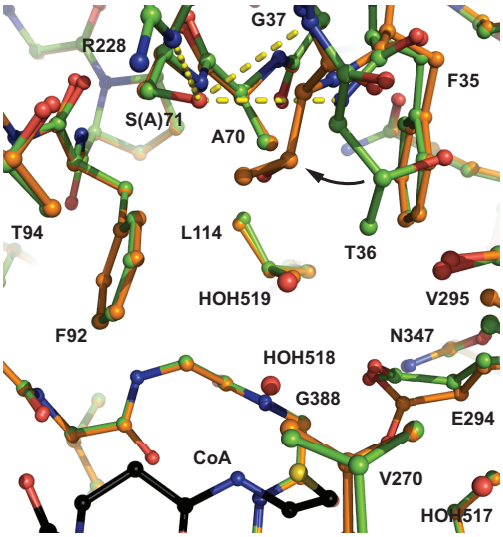

Figure 4.17. Collapse of the succinate binding pocket of AarCH6-S71A. Without the three structural hydrogen-bonding interactions (yellow dotted lines) formed between the side chain of Ser71, the side chain of Arg228, and the backbone nitrogens of Thr36 and Gly37, the loop connecting β1 and α2 shifts. In the resulting conformation, the side chain of Thr36 blocks a large portion of the succinate binding pocket. CoA and all waters are omitted from the AarCH6 model (green, PDB entry 4eu5). CoA (black), the catalytic water, and two placeholder waters are included from the AarCH6-S71A model (orange, PDB entry 4eu8). The placeholder water HOH520 (Figure 4.16) was displaced by Thr36.

inhibit ingress and egress into and from the reaction pocket of both propionate and acetate.

Introduction of the Ser71→Ala mutation also removed a hydrogen bond between the side chains of Ser71 and Arg228. Without this interaction, Arg228 was pulled from the active site in both the closed and the open conformations (Figure 4.17). In the closed conformation, repositioning of the domain linker (including Arg228) was accompanied by a significant coordinated shift in the surface-exposed secondary structural elements in the N-terminal domain (Figure 4.18). This previously unobserved motion may correlate with the apparent deoligomerization of the AarCH6-S71A dimer.

Acid tolerance. Circular dichroism was used to monitor temperature-induced changes in the secondary structures of AarC and AarCH6 as a function of pH (Figure 4.19). Both proteins possessed maximal stability under slightly acidic conditions, decreasing

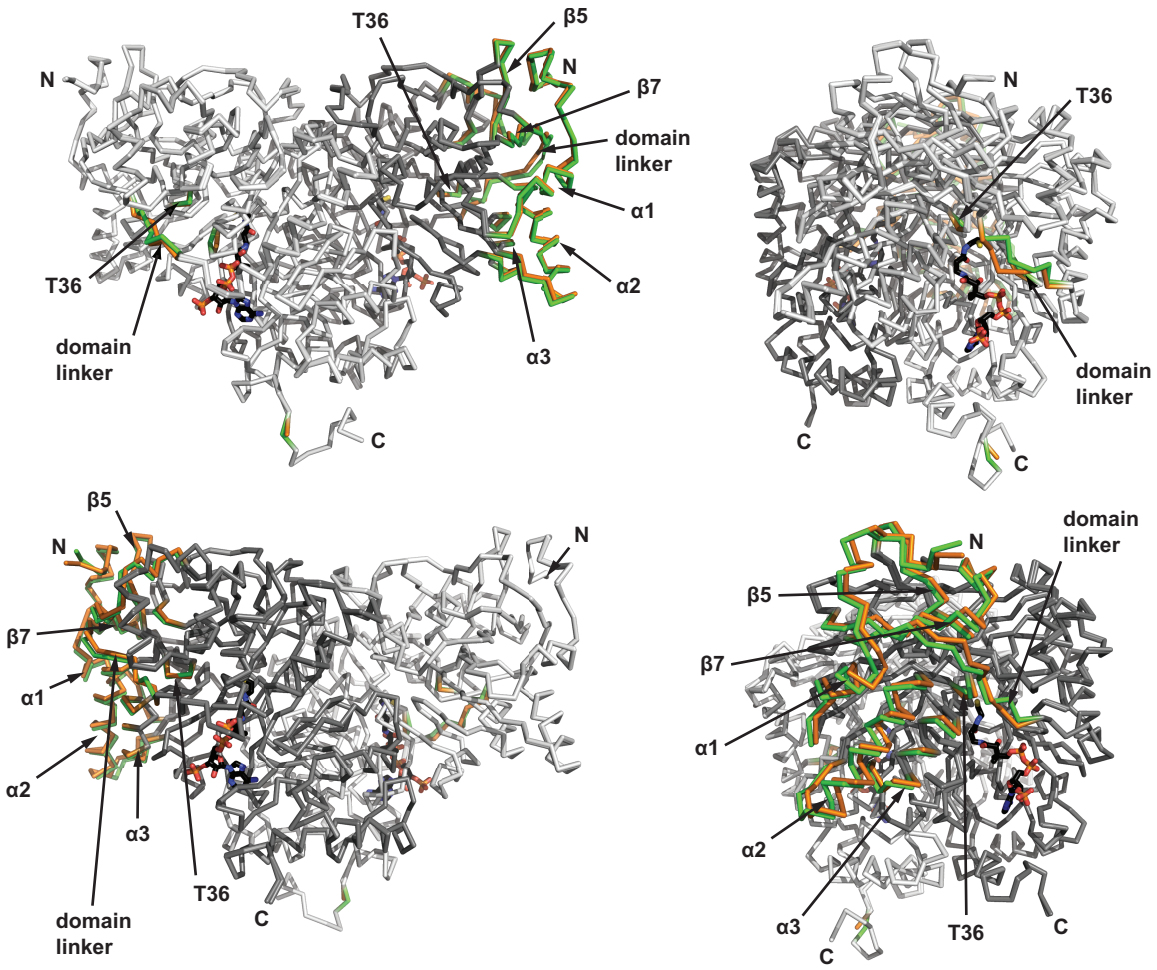

Figure 4.18. Conformational motions in AarCH6-S71A. In the open conformation (light gray), AarCH6-S71A (PDB entry 4eu8) displays only minor, local structural rearrangements relative to AarCH6 (PDB entry 4eu5). In the closed conformation (dark gray), however, AarCH6-S71A exhibits widespread, coordinated conformational shifts in the N-terminal domain. In both conformations, the loss of the hydrogen-bonding interaction between Ser71 and Arg228 allows the side chain of Arg228 to be pulled from the active-site cleft. Dynamic regions (Rmsd ≥ 0.75 Å for Cα atoms) are differentially colored (AarCH6, green; AarCH6-S71A, orange). CoA from the AarCH6-S71A model is colored black.

gradually under alkaline conditions and relatively sharply under increasingly acidic conditions (Figure 4.20). Under low pH conditions that would likely result in protonation of histidine, the hexahistidine fusion protein was marginally less stable than the untagged enzyme. Despite reduced stability at moderately acidic pH, AarC remained folded under all conditions encountered in the *A. aceti* cytoplasm (pH 3.8 – 6.8 and ≤ 35 °C).

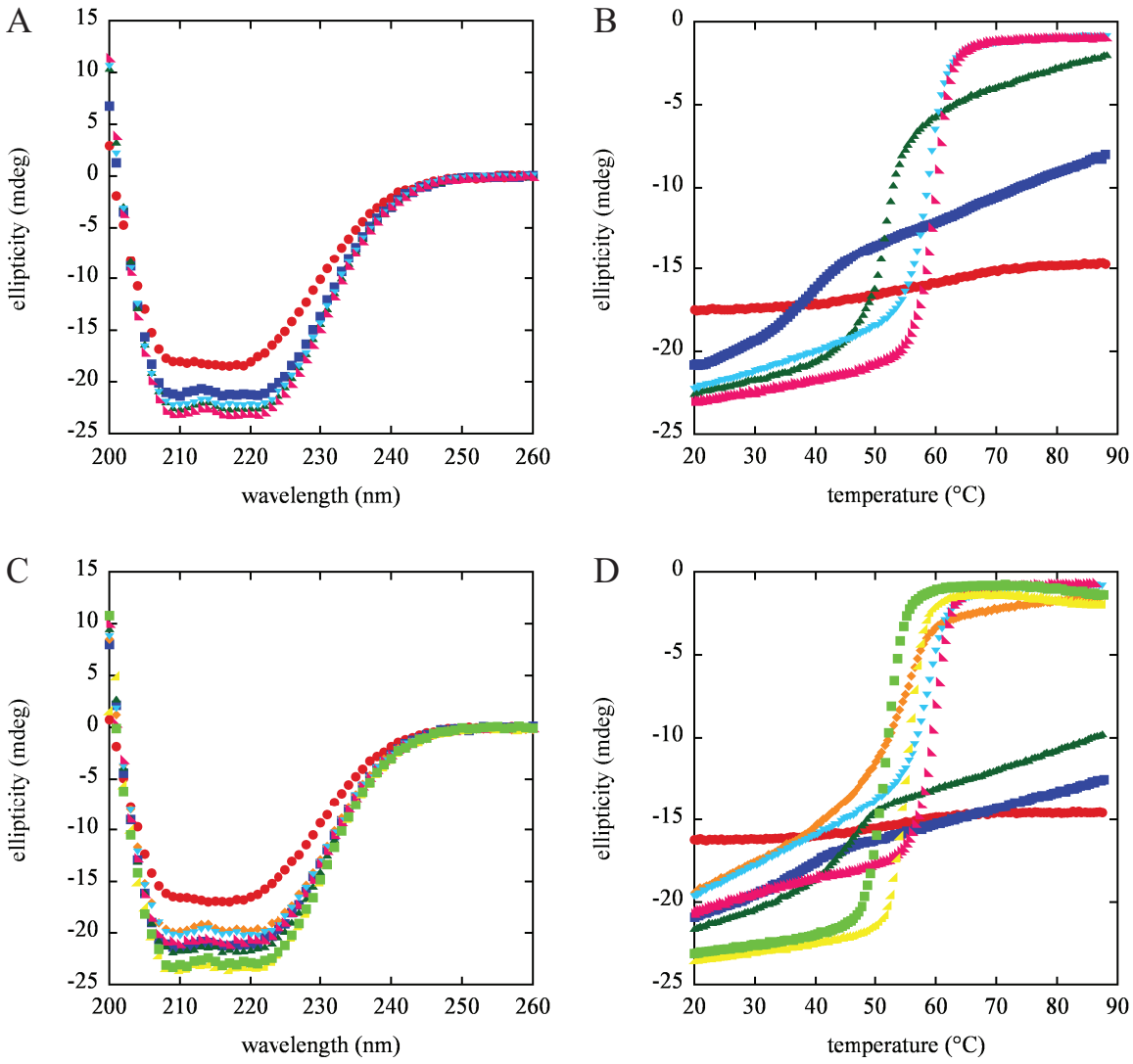

Figure 4.19. Thermal denaturation of AarC and AarCH6 as a function of pH. Temperature-induced changes in secondary structure were assessed by monitoring ellipticity at 222 nm. Melting experiments were performed across a range of pH conditions: 3.5 (red), 4.0 (blue), 4.5 (green), 5.0 (orange), 5.5 (cyan), 6.5 (magenta), 7.5 (yellow), and 8.5 (lime). **(A)** AarC far-UV CD spectra. **(B)** AarC melting profiles. **(C)** AarCH6 far-UV CD spectra. **(D)** AarCH6 melting profiles.

The acid stability of *A. aceti* proteins has been linked to an unusual but characteristic charge decoration (*10, 20, 21*) shared by AarC (Figure 4.21). With the exception of the positively charged active site and surrounding electrostatic gradient, the surface of AarC appears largely neutral with only punctuate clusters of significant homogeneous charge. The charge pattern in and around the active-site cleft may have evolved to funnel negatively charged acyl-CoA and carboxylate substrates toward Glu294.

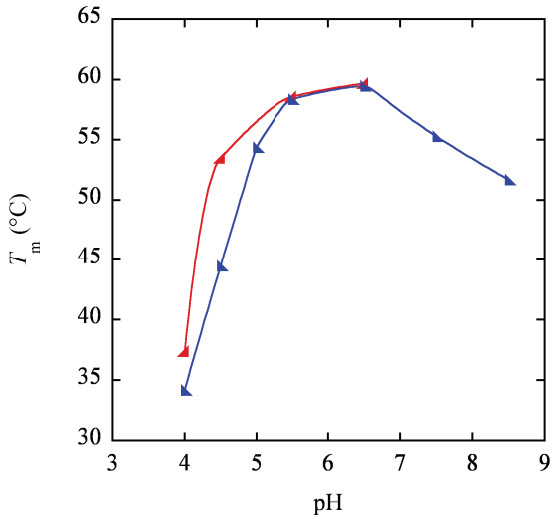

Figure 4.20. Thermal denaturation of AarC and AarCH6 as a function of pH [2]. Melting temperatures (T_m) were determined from changes in ellipticity at 222 nm. AarC (red triangles) and AarCH6 (blue triangles) are maximally stable at slightly acidic pH. At low pH, the hexahistidine tag appears to destabilize AarCH6.

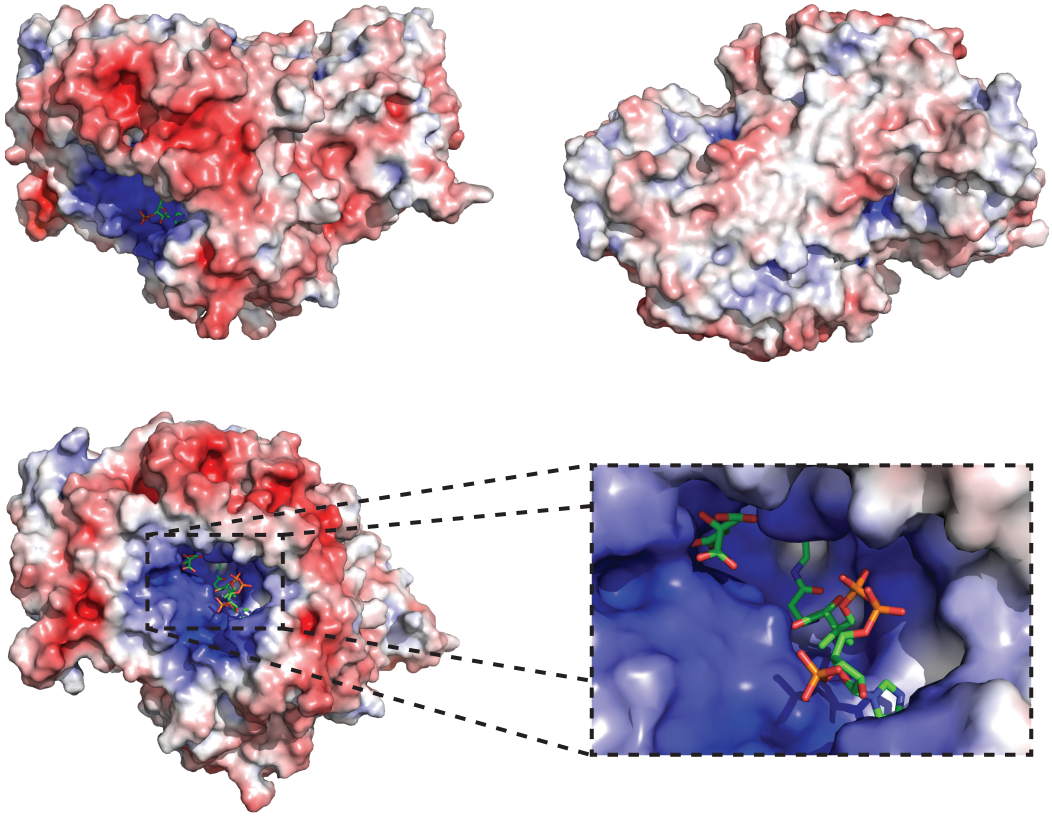

Figure 4.21. Electrostatic surface of AarC (PDB entry 4eud). The protein surface is colored red for negatively charged areas and blue for positively charged areas. The saturation of the colors is proportional to the degree of electrostatic charge from −7 *kT/e* to +7 *kT/e.* The charge surface was computed at pH 7 using the PDB2PQR web server and the APBS plugin for PyMOL. CoA and citrate are depicted in stick representation.

DISCUSSION

The identities of the covalent intermediates formed during the class I CoA-transferase reaction were established over 35 years ago by William P. Jencks and colleagues (*3*-*7*). Those same studies also predicted a protein conformational change upon formation of the initial Michaelis complex (*4*) and a common binding pocket for the acyl moiety of the acyl-CoA substrate, the first acylglutamyl anhydride intermediate, and the carboxylate product (*5*). Subsequent efforts have unfortunately provided little additional insight. This study continues the work of W. P. Jencks and provides the first complete structural description of the ground-state complexes and intermediates in the class I CoA-transferase reaction.

Catalytic implications of the novel oxyanion hole. AarC employs a previously unidentified oxyanion hole configuration composed of the backbone nitrogen of Gly388 and the distal amide nitrogen of CoA (position 1, Scheme 4.2). Unlike traditional oxyanion holes in which the amide dipoles are prearranged (*22*), this novel oxyanion hole synchronizes alignment of the amide dipoles and formation of the Michaelis complex. This process inevitably decreases the affinity of the ground-state complex but should not affect subsequent stabilization of the negatively charged transition state and tetrahedral oxyanion intermediate. Furthermore, the reduced energetic gap between the Michaelis complex and the Arrhenius complex should increase the rate of catalysis.

A mechanistic archetype for the class I CoA-transferase reaction. The reaction mechanism proposed for AarC appears to be conserved across phylogenetically diverse class I CoA-transferases. A structural alignment of distantly related enzymes with varied

substrate preferences and backbone topologies revealed conservation or functional replacement of all catalytic residues and the single catalytic water identified in AarC (Val270, Glu294, Asn347, Gly388, and HOH517; Figure 4.22 and Table A.2). The more dissimilar class I structures lack a catalytic asparagine but possess an apparent catalytic glutamine in a different but functionally equivalent position. This common arrangement of catalytic residues suggests that the novel oxyanion hole found in AarC is a general feature of class I enzymes.

Many aspects of the class I mechanism may be shared by the phylogenetically and structurally related class II CoA-transferases.

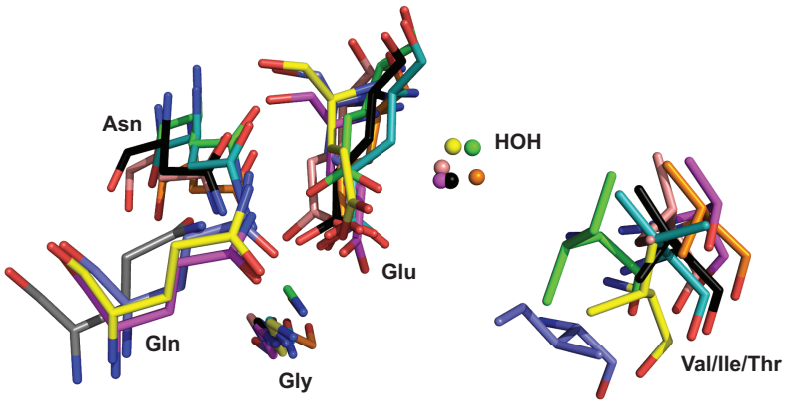

Figure 4.22. Structural alignment of phylogenetically diverse class I CoA-transferases. CoA-transferase structures were aligned to AarC (PDB entry 4eud, chain A, black) using the Dali web server (http://ekhidna.biocenter.helsinki.fi/dali_server) (*42*). Only proposed catalytic residues and a single catalytic water are shown. Putative succinyl-CoA:acetate CoA-transferase from *Pseudomonas aeruginosa* (PDB entry 2g39, chain A, green), putative succinyl-CoA:acetate CoA-transferase from *Porphyromonas gingivalis* (PDB entry 2nvv, chain A, teal), 4-hydroxybutyrate CoA-transferse from *Clostridium aminobutyricum* (4-HB-CoAT, PDB entry 3gk7, chain A, salmon), butyryl-CoA transferase from *Yersinia pestis* (RipA, PDB entry 3qli, chain A, orange), succinyl-CoA:acetoacetate CoA-transferase from pig heart (SCOT, PDB entry 3oxo, chain F, slate), short-chain-fatty-acid CoA-transferase from *Escherichia coli* (YdiF, PDB entry 2ahv, chain D, yellow), acetate CoA-transferase from *E. coli* (ACT, PDB entry 1k6d, chain A, α-subunit only, gray), and glutaconate CoA-transferase from *Acidaminococcus fermentans* (GCT, PDB entry 1poi, chain B, α- and β-subunits, magenta). The biological units of most structures are homodimers with a single subunit comprising each active site. The biological units of ACT and GCT, however, are heterotetramers with two subunits comprising each active site: the catalytic glutamine is located in the α-subunit while all other catalytic residues are located in the β-subunit. Conserved or functionally equivalent catalytic residues (Table A.2) are provided in Appendix A.

Roles of conformational dynamics in CoA transfer. Large rigid-body motions are a common feature of transferase enzymes (*23*). The class I CoA-transferases RipA (*24*), YdiF (*8*), 4-HB-CoAT (*25*), and SCOT (*26-28*) have been previously observed to undergo significant rearrangements upon binding CoA. Four such motions have been proposed to occur during CoA transfer, permitting substrate and product association and dissociation, respectively, in the open form and protecting the labile anhydride intermediates from bulk solvent and preventing dissociation of the CoA thiolate in the closed form (*25*). Using truncated substrate analogues, W. P. Jencks further predicted that favorable binding interactions between the protein and the unreactive portions of the acyl-CoA substrate (e.g. the diphosphate moiety) are utilized to not only induce a conformational change in the enzyme but also to accelerate CoA transfer (*4, 29*).

AarC seems to undergo a similar series of large rigid-body conformational changes during transfer of CoA. Upon initially binding the acyl-CoA substrate, the active site closes, sequestering Glu294 and the reactive thioester in the reaction pocket. This motion, driven by electrostatic and hydrogen-bonding interactions with the diphosphate moiety and pantetheine arm, "clamps" the reactive thioester against the nucleophilic glutamate carboxylate. This restrictive conformation may increase the rate of catalysis by decreasing the entropy that must be lost to form a new covalent bond and by creating steric strain that would be relieved in the tetrahedral oxyanion intermediate and the transition state (*5*). Additionally, closure of the active site appropriately positions the backbone nitrogen and side chain of Val270 to increase the leaving-group potential of the CoA thiolate and shield the transient mixed anhydride, respectively. The hydrogen-

bonding interaction may also retain the active site in the closed conformation until the glutamyl-CoA thioester is formed. Exchange of the resulting carboxylate product and carboxylate substrate requires that the active site open. Opening may be aided by binding of the carboxylate substrate in the auxiliary site as the side chain of Arg228 samples positions both in and out of the active-site cleft. After the carboxylate substrate reaches the reaction pocket, the active site closes, isolating the glutamyl-CoA thioester and the carboxylate substrate. Again, closure may provide catalytic acceleration by inducing steric strain that would be relieved in the transition state and decreasing the loss of entropy required to form a new covalent bond. The hydrogen-bonding interaction with the backbone nitrogen of Val270 may once more increase the leaving-group potential of the CoA thiolate while the side chain shields the intermediary mixed anhydride. Before the acyl-CoA product can dissociate, the active site must reopen. Opening of the active site in both product complexes may be driven by the same reduced entropy and steric strain that increases the rate of catalysis.

Rapid catalytic turnover appears largely dependent on conformational dynamics. While Arg228 is inherently linked to the protein conformational equilibrium in AarC, corresponding residues are not obvious in other class I CoA-transferases. This may in part explain the comparatively low specific activity of most class I enzymes. [The specific activity of AarC(H6) is among the highest of any characterized CoA-transferase.] Furthermore, auxiliary carboxylate binding sites of any type are not obvious in other class I CoA-transferases. Nonetheless, highly positively charged active-site clefts are conserved across phylogenetically diverse class I enzymes (not shown) and may facilitate

complexation of structurally varied but consistently negatively charged carboxylate substrates.

Primary and secondary determinants of substrate specificity. Class I CoA-transferases are notoriously promiscuous (*5, 8, 30-33*). AarCH6, however, appears to be unusually stringent. Only nine of twenty-four arguably structurally similar potential alternate carboxylate substrates supported detectable CoA-transferase activity. None supported activity greater than 10% of that produced by acetate or succinate. Separate binding sites for the physiological carboxylate substrate and carboxylate product have been considered previously (*9*). While two carboxylate binding sites were identified in AarC (Figure 4.23), each seems able to accommodate either acetate or succinate and only one site appears capable of involvement in the formation of Michaelis complexes.

Phe35, Thr36, Ala70, Ser71, Phe92, Leu114, Val270, Val295, Gly388, and the distal amide nitrogen of CoA compose the primary binding site and form the periphery of the

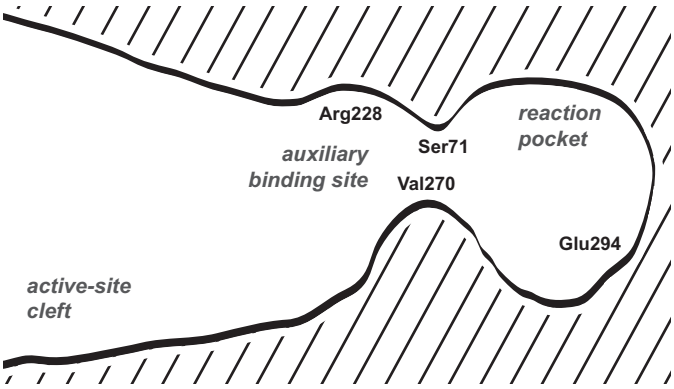

Figure 4.23. Cartoon representation of the AarC active site. Two carboxylate binding sites were identified in the funnel-shaped active-site cleft of AarC. The primary binding site (or reaction pocket) contains the catalytic glutamate Glu294 and binds all Michaelis complexes and both covalent mixed anhydride intermediates. In the closed conformation, the side chain of Val270 isolates the reaction pocket from bulk solvent. The secondary binding site (or auxiliary binding site) binds only the carboxylate substrate and product. Unlike the primary site, the secondary site remains accessible in the closed conformation. Complex formation involving Arg228 may influence the protein conformational equilibrium and facilitate opening of the active site. The side chain of Ser71 forms hydrogen-bonding interactions with substrates in both binding sites.

reaction pocket (Figure 4.23). Acetate and succinate, acetylglutamyl anhydride and glutamylsuccinyl anhydride, and the acyl moieties of acetyl-CoA and succinyl-CoA all bind in the primary site. Succinate, glutamylsuccinyl anhydride, and the succinyl moiety of succinyl-CoA form a common set of hydrogen-bonding interactions and hydrophobic contacts. The same is true of acetate, acetylglutamyl anhydride, and the acetyl moiety of acetyl-CoA. The latter group of hydrogen-bonding interactions and hydrophobic contacts are a subset of the former. AarC accommodates both the succinyl and acetyl groups in the same binding pocket.

Ser71, Thr94, and Arg228 compose the secondary (or auxiliary) binding site. This accessory binding position is situated outside the reaction pocket and adjacent to the gating residue Val270 (Figure 4.23). Both the physiological substrate acetate and the failed alternate substrate citrate were crystallographically observed in this position, suggesting the auxiliary site is relatively accessible and accommodating, providing little additional stringency. The secondary binding site may nonetheless preconcentrate acetate (or succinate) and influence the conformational equilibrium inherently linked to CoA transfer. [Introduction of an Arg228→Glu mutation drastically altered the apparent binding affinities of acetate and succinate (Table 4.10).]

Citrate is sterically precluded from entering the primary binding site and did not support CoA-transferase activity. Citrate did, however, competitively inhibit SCACT activity. By binding in the auxiliary site, many of the failed alternate substrates may be able to do the same. Several of the previously performed alternate substrate screens employed for class I CoA-transferases were based not upon the CoA-transferase activity

supported by the alternate substrates but upon inhibition of the CoA-transferase activity supported by the physiological substrates (*24, 34*). The results obtained with citrate suggest that this method of screening alternate substrates could indicate falsely high levels of promiscuity.

The stringency of AarCH6 seems to result primarily from interactions in the reaction pocket. Hydrophobic residues create a largely rigid environment. Only the motion of Val270 would seem to provide the flexibility required for extended, branched, or substituted carboxylates to form Michaelis complexes. This accommodation, however, would presumably be accompanied by reduced catalytic activity. In fact, while the apparent binding affinities of all alternate dicarboxylate substrates, with the exception of glutarate, surpassed that of acetate, the catalytic turnover supported by acetate was 20-fold greater than that of any alternate dicarboxylate substrate.

Conclusion. AarC evolved to play a primary metabolic role under the selective pressure induced by high concentrations of membrane-permeant acetic acid, producing a CoA-transferase with relatively high substrate specificity and catalytic rapidity. A previously uncharacterized oxyanion hole configuration is utilized to stabilize tetrahedral oxyanion intermediates in what appears to be the archetypal mechanism for class I enzymes. The protein conformational motions inherently linked to CoA transfer are influenced by a previously unidentified auxiliary binding site that preconcentrates carboxylate substrates.

FUTURE DIRECTIONS

Molecular modeling and molecular mechanics calculations were used to generate the glutamylsuccinyl anhydride intermediate, but the short-soak method used to produce the crystallographically observed acetylglutamyl anhydride from acetyl-CoA should allow the corresponding mixed anhydride to be formed from succinyl-CoA. Crystallographic characterization could confirm the proposed hydrogen-bonding interactions with Thr36 and Ser71 and provide direct evidence for succinate complexation in the auxiliary binding site.

AarCH6-N347A preserves modest SCACT activity despite lacking the hydrogen-bond donor that stabilizes two of four tetrahedral oxyanion intermediates and increases the leaving-group potential of the glutamyl carboxylate. Crystallographic characterization would reveal if a water is present in the catalytically appropriate position between Glu294 and Asp391, facilitating CoA transfer in the absence of Asn347.

Further study of the auxiliary binding site (Ser71, Thr94, and Arg228) would benefit from the creation of more conservative mutants (e.g. AarCH6-T94V and AarCH6-R228K). AarCH6-R228E is biased by an altered charge pattern in the active site, while AarCH6-S71A is hindered by a collapsed succinate binding pocket. Kinetic characterization of AarCH6-T94V and AarCH6-E228K would allow auxiliary binding interactions to be examined without substantially altering electrostatic properties or protein conformation.

AarCH6-E435D retained full solubility while both AarCH6-E435A and AarCH6-E435Q were completely insoluble even when co-overproduced with GroEL/ES.

Crystallographic characterization could reveal how AarCH6-E435D maintained stability: if one or more waters played supporting structural roles, if a local and stabilizing conformational change occurred, and if the latter, why this stable, variant conformation was not adopted by AarCH6-E435A and AarCH6-E435Q.

REFERENCES

1. Heider, J. (2001) A new family of CoA-transferases, *FEBS Lett. 509*, 345-349.

2. Hersh, L. B., and Jencks, W. P. (1967) Coenzyme A transferase. Kinetics and exchange reactions, *J. Biol. Chem. 242*, 3468-3480.

3. Hersh, L. B., and Jencks, W. P. (1967) Coenzyme A transferase. Isolation and properties of an enzyme-coenzyme A intermediate, *J. Biol. Chem. 242*, 3481-3486.

4. White, H., Solomon, F., and Jencks, W. P. (1976) Utilization of the inactivation rate of coenzyme A transferase by thiol reagents to determine properties of the enzyme-CoA intermediate, *J. Biol. Chem. 251*, 1700-1707.

5. White, H., and Jencks, W. P. (1976) Mechanism and specificity of succinyl-CoA:3-ketoacid coenzyme A transferase, *J. Biol. Chem. 251*, 1688-1699.

6. Pickart, C. M., and Jencks, W. P. (1979) Formation of stable anhydrides from CoA transferases and hydroxamic acids, *J. Biol. Chem. 254*, 9120-9129.

7. Solomon, F., and Jencks, W. P. (1969) Identification of an enzyme-γ-glutamyl coenzyme A intermediate from coenzyme A transferase, *J. Biol. Chem. 244*, 1079-1081.

8. Rangarajan, E. S., Li, Y., Ajamian, E., Iannuzzi, P., Kernaghan, S. D., Fraser, M. E., Cygler, M., and Matte, A. (2005) Crystallographic trapping of the glutamyl-CoA thioester intermediate of family I CoA transferases, *J. Biol. Chem. 280*, 42919-42928.

9. Macieira, S., Zhang, J., Velarde, M., Buckel, W., and Messerschmidt, A. (2009) Crystal structure of 4-hydroxybutyrate CoA-transferase from *Clostridium aminobutyricum*, *Biol. Chem. 390*, 1251-1263.

10. Francois, J. A., Starks, C. M., Sivanuntakorn, S., Jiang, H., Ransome, A. E., Nam, J. W., Constantine, C. Z., and Kappock, T. J. (2006) Structure of a NADH-insensitive

hexameric citrate synthase that resists acid inactivation, *Biochemistry 45*, 13487-13499.

11. Francois, J. A., and Kappock, T. J. (2007) Alanine racemase from the acidophile *Acetobacter aceti*, *Protein Expr. Purif. 51*, 39-48.

12. Otwinowski, Z., and Minor, W. (1997) Processing of X-ray diffraction data collected in oscillation mode, *Methods Enzymol. 276*, 307-326.

13. Guex, N., and Peitsch, M. C. (1997) SWISS-MODEL and the Swiss-PdbViewer: an environment for comparative protein modeling, *Electrophoresis 18*, 2714-2723.

14. Adams, P. D., Afonine, P. V., Bunkoczi, G., Chen, V. B., Davis, I. W., Echols, N., Headd, J. J., Hung, L. W., Kapral, G. J., Grosse-Kunstleve, R. W., McCoy, A. J., Moriarty, N. W., Oeffner, R., Read, R. J., Richardson, D. C., Richardson, J. S., Terwilliger, T. C., and Zwart, P. H. (2010) PHENIX: a comprehensive Python-based system for macromolecular structure solution, *Acta Crystallogr. D Biol. Crystallogr. 66*, 213-221.

15. Emsley, P., Lohkamp, B., Scott, W. G., and Cowtan, K. (2010) Features and development of Coot, *Acta Crystallogr. D Biol. Crystallogr. 66*, 486-501.

16. Kleywegt, G. J. (2007) Crystallographic refinement of ligand complexes, *Acta Crystallogr. D Biol. Crystallogr. 63*, 94-100.

17. DeLano, W. L. (2002) The PyMOL molecular graphics system, DeLano Scientific, San Carlos, CA, USA.

18. Carson, M., Johnson, D. H., McDonald, H., Brouillette, C., and DeLucas, L. J. (2007) His-tag impact on structure, *Acta Crystallogr. D Biol. Crystallogr. 63*, 295-301.

19. Mack, M., and Buckel, W. (1997) Conversion of glutaconate CoA-transferase from *Acidaminococcus fermentans* into an acyl-CoA hydrolase by site-directed mutagenesis, *FEBS Lett. 405*, 209-212.

20. Settembre, E. C., Chittuluru, J. R., Mill, C. P., Kappock, T. J., and Ealick, S. E. (2004) Acidophilic adaptations in the structure of *Acetobacter aceti* N^5-carboxyaminoimidazole ribonucleotide mutase (PurE), *Acta Crystallogr. D Biol. Crystallogr. 60*, 1753-1760.

21. Mullins, E. A., Starks, C. M., Francois, J. A., Sael, L., Kihara, D., and Kappock, T. J. (2012) Formyl-coenzyme A (CoA):oxalate CoA-transferase from the acidophile *Acetobacter aceti* has a distinctive electrostatic surface and inherent acid stability, *Protein Sci. 21*, 686-696.

22. Kamerlin, S. C. L., Chu, Z. T., and Warshel, A. (2010) On catalytic preorganization in oxyanion holes: highlighting the problems with gas-phase modeling of oxyanion holes and illustrating the need for complete enzyme models, *J. Org. Chem. 75*, 6391-6401.

23. Koike, R., Amemiya, T., Ota, M., and Kidera, A. (2008) Protein structural change upon ligand binding correlates with enzymatic reaction mechanism, *J. Mol. Biol. 379*, 397-401.

24. Torres, R., Swift, R. V., Chim, N., Wheatley, N., Lan, B., Atwood, B. R., Pujol, C., Sankaran, B., Bliska, J. B., Amaro, R. E., and Goulding, C. W. (2011) Biochemical, structural, and molecular dynamics analyses of the potential virulence factor RipA from *Yersenia pestis*, *PLoS One 6*, 1-14.

25. Macieira, S., Zhang, J., Buckel, W., and Messerschmidt, A. (2012) Crystal structure of the complex between 4-hydroxybutyrate CoA-transferase from *Clostridium aminobutyricum* and CoA, *Arch. Microbiol. 194*, 157-166.

26. Tammam, S. D., Rochet, J., and Fraser, M. E. (2007) Identification of the cysteine residue exposed by the conformational change in pig heart succinyl-CoA:3-ketoacid coenzyme A transferase on binding coenzyme A, *Biochemistry 46*, 10852-10863.

27. Fraser, M. E., Hayakawa, K., and Brown, W. D. (2010) Catalytic role of the conformational change in succinyl-CoA:3-oxoacid CoA transferase on binding CoA, *Biochemistry 49*, 10319-10328.

28. Coker, S., Lloyd, A. J., Mitchell, E., Lewis, G. R., Coker, A. R., and Shoolingin-Jordan, P. M. (2010) The high-resolution structure of pig heart succinyl-CoA:3-oxoacid coenzyme A transferase, *Acta Crystallogr. D Biol. Crystallogr. D66*, 797-805.

29. Whitty, A., Fierke, C. A., and Jencks, W. P. (1995) Role of binding energy with coenzyme A in catalysis by 3-oxoacid coenzyme A transferase, *Biochemistry 34*, 11678-11689.

30. Selmer, T., Willanzheimer, A., and Hetzel, M. (2002) Propionate CoA-transferase from *Clostridium propionicum*. Cloning of the gene and identification of glutamate 324 at the active site, *Eur. J. Biochem. 269*, 372-380.

31. Haller, T., Buckel, T., Rétey, J., and Gerlt, J. A. (2000) Discovering new enzymes and metabolic pathways: conversion of succinate to propionate by *Escherichia coli*, *Biochemistry 39*, 4622-4629.

32. Fleck, C. B., and Brock, M. (2008) Characterization of an acyl-CoA:carboxylate CoA-transferase from *Aspergillus nidulans* involved in propionyl-CoA detoxification, *Mol. Microbiol. 68*, 642-656.

33. Buckel, W., Dorn, U., and Semmler, R. (1981) Glutaconate CoA-transferase from *Acidaminococcus fermentans*, *Eur. J. Biochem. 118*, 315-321.

34. Schweiger, G., and Buckel, W. (1984) On the dehydration of (R)-lactate in the fermentation of alanine to propionate by *Clostridium propionicum*, *FEBS 171*, 79-84.

35. Miroux, B., and Walker, J. E. (1996) Over-production of proteins in *Escherichia coli*: mutant hosts that allow synthesis of some membrane proteins and globular proteins at high levels, *J. Mol. Biol. 260*, 289-298.

36. Laboratories, B. R. (1986) BRL pUC host: *E. coli* DH5α competent cells, *Focus 8*, 9.

37. Cole, P. A. (1996) Chaperone-assisted protein expression, *Structure 4*, 239-242.

38. Matthews, B. W. (1968) Solvent content of protein crystals, *J. Mol. Biol. 33*, 491-497.

39. Kantardjieff, K. A., and Rupp, B. (2003) Matthews coefficient probabilities: improved estimates for unit cell contents of proteins, DNA, and protein-nucleic acid complex crystals, *Protein Sci. 12*, 1865-1871.

40. Dolinsky, T. J., Czodrowski, P., Li, H., Nielsen, J. E., Jensen, J. H., Klebe, G., and Baker, N. A. (2007) PDB2PQR: expanding and upgrading automated preparation of biomolecular structures for molecular simulations, *Nucleic Acids Res. 35*, W522-W525.

41. Baker, N. A., Sept, D., Joseph, S., Holst, M. J., and McCammon, J. A. (2001) Electrostatics of nanosystems: application to microtubules and the ribosome, *Proc. Natl. Acad. Sci. USA 98*, 10037-10041.

42. Holm, L., and Rosenström, P. (2010) Dali server: conservation mapping in 3D, *Nucleic Acids Res. 38*, W545-W549.

Appendix A.

Supplemental material

ADDITIONAL FIGURES AND TABLES

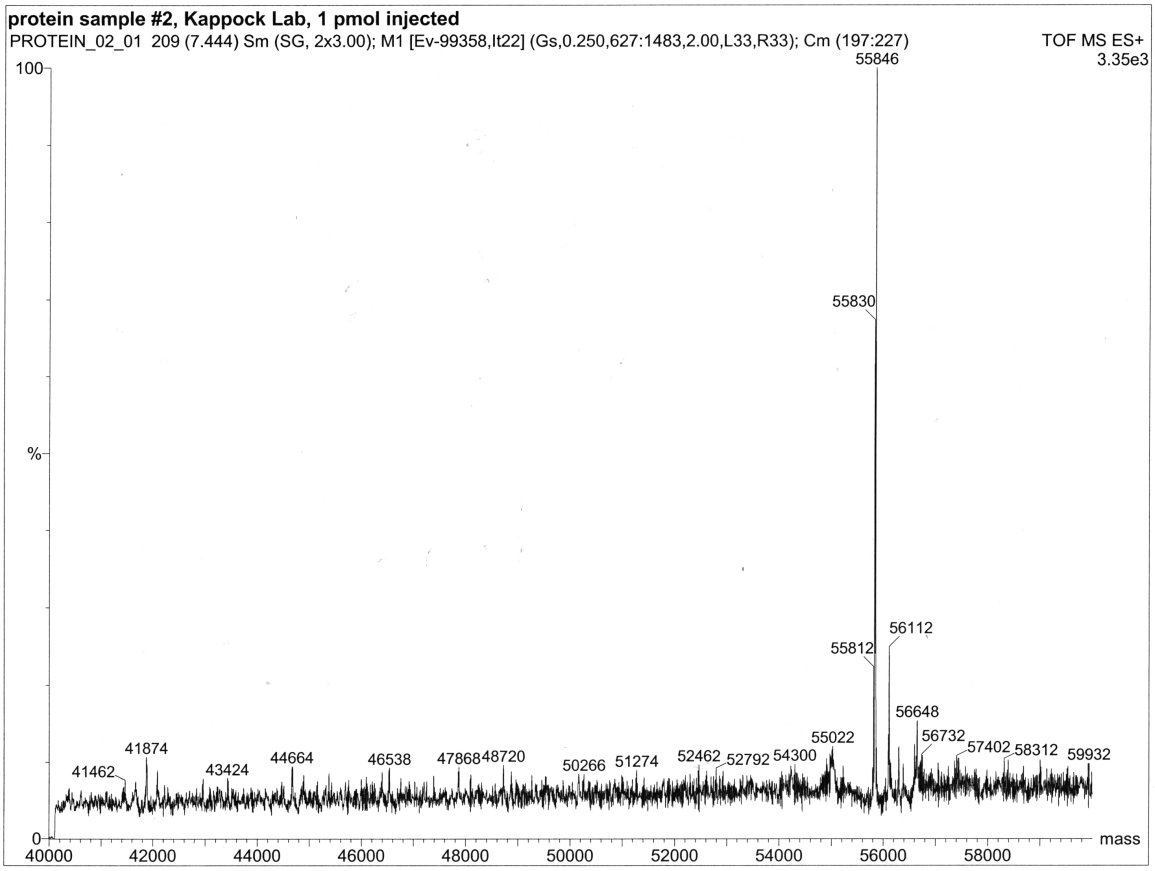

Figure A.1. ESI-TOF-MS analysis of AarCH6 (55,846 ± 2 Da observed; 55,847 Da expected [−Met1]).

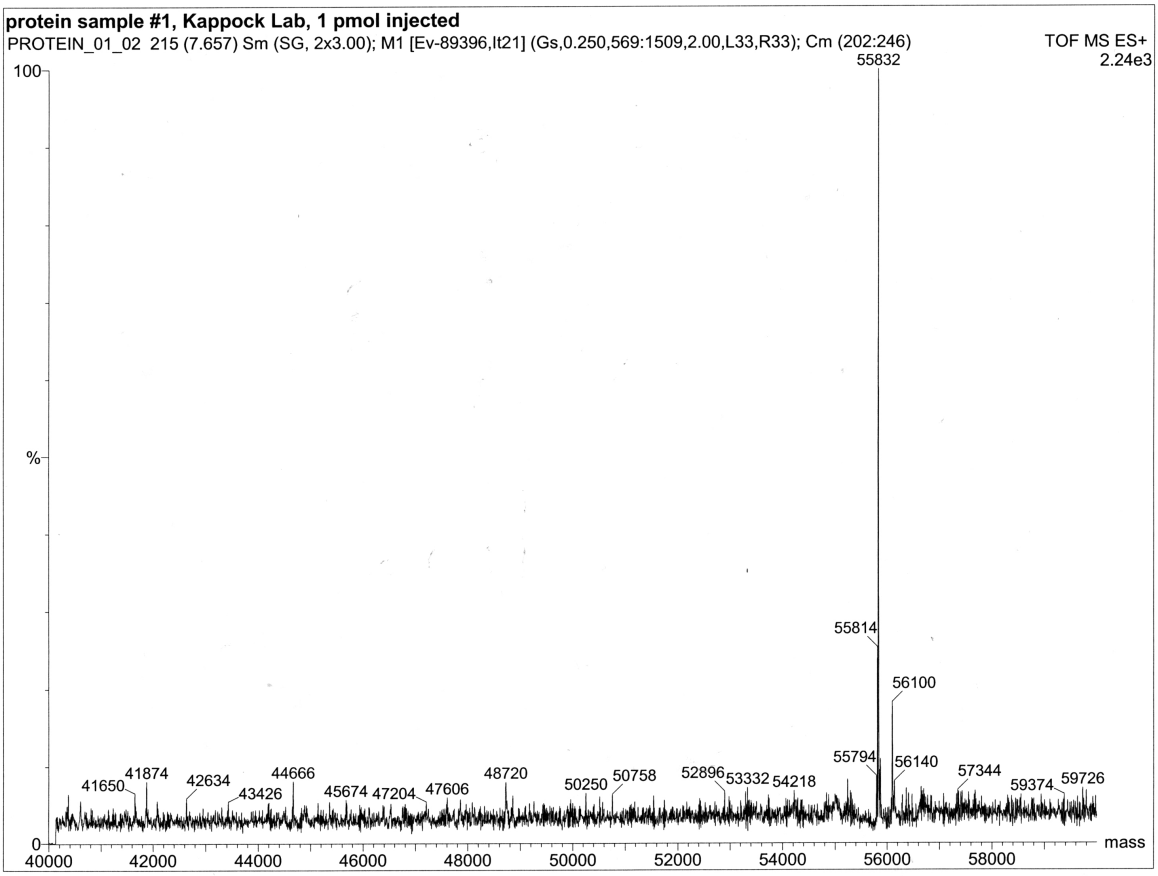

Figure A.2. ESI-TOF-MS analysis of AarCH6 following incubation with acetyl-CoA and treatment with sodium borohydride (55,832 ± 2 Da observed; 55,833 Da expected [−Met1]).

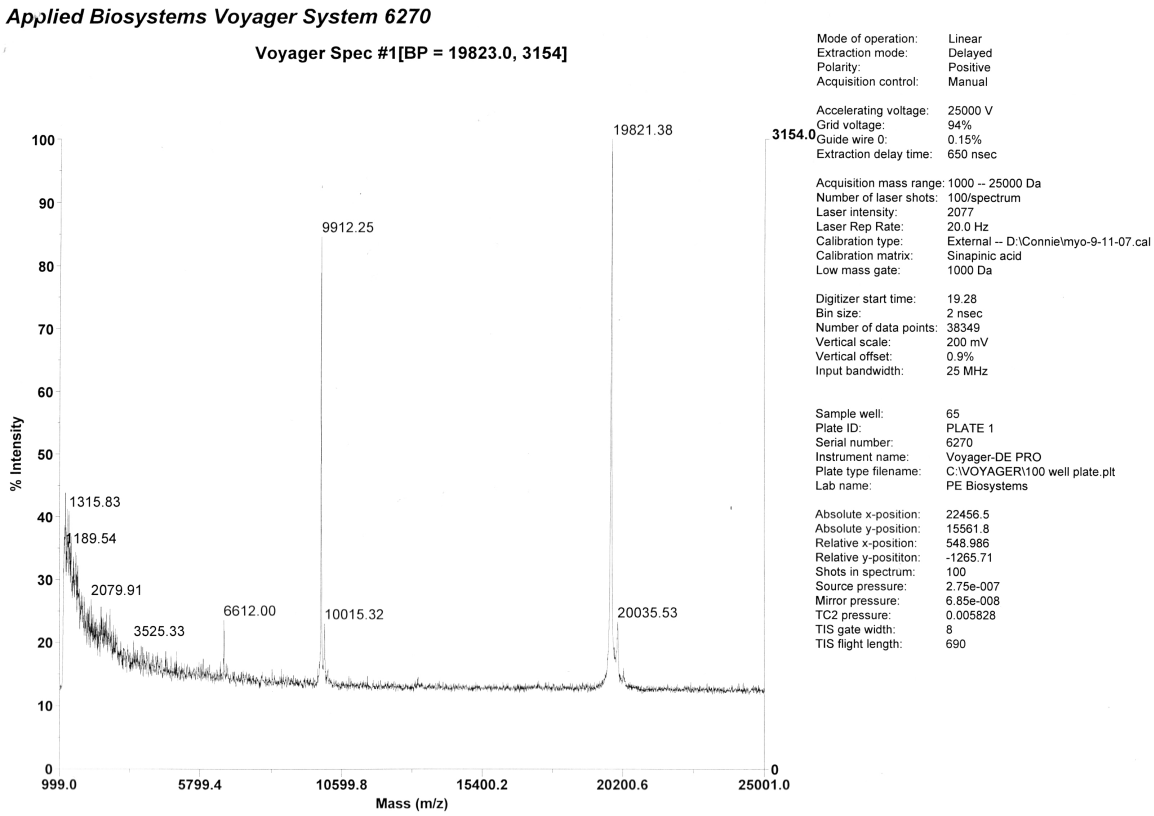

Figure A.3. MALDI-TOF-MS analysis of SixAH6 (19,821 ± 2 Da observed; 19,822 Da expected [+Met1]). N-terminally processed SixAH6 lacking Met1 was not detected, consistent with the extremely short *in vivo* half-life (~2 min) expected for a protein with an N-terminal arginine (Arg2).

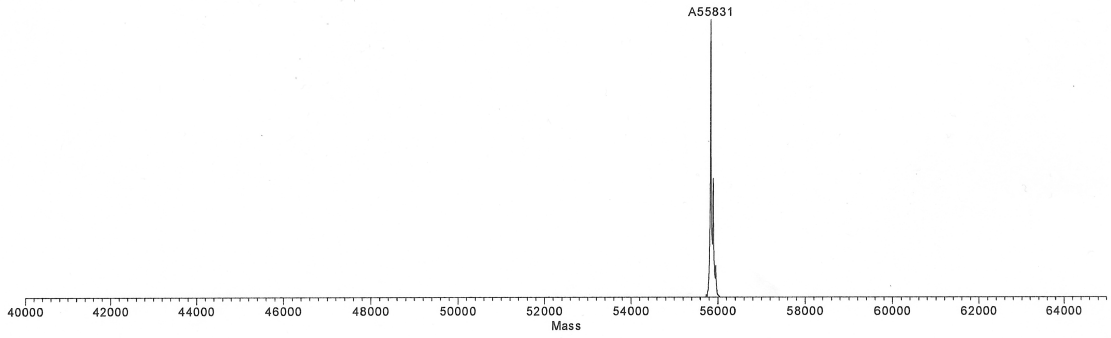

Deconvoluted spectrum

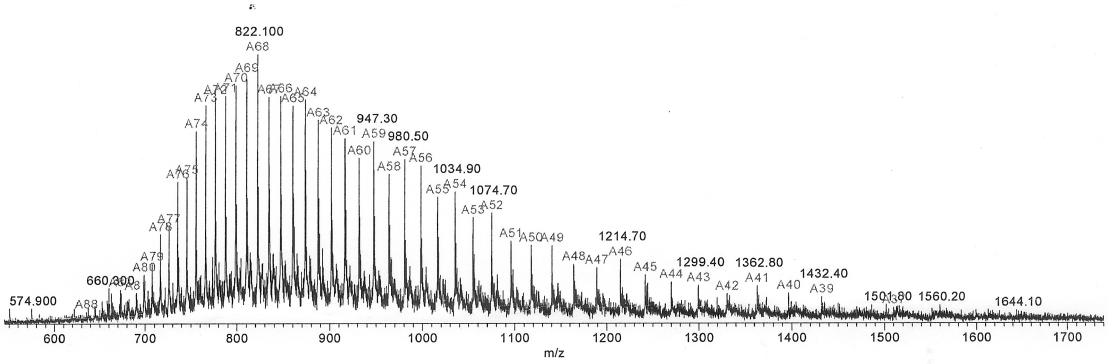

Protein spectrum

Figure A.4. ESI-TOF-MS analysis of AarCH6-S71A (55,831 Da observed; 55,831 Da expected [−Met1]).

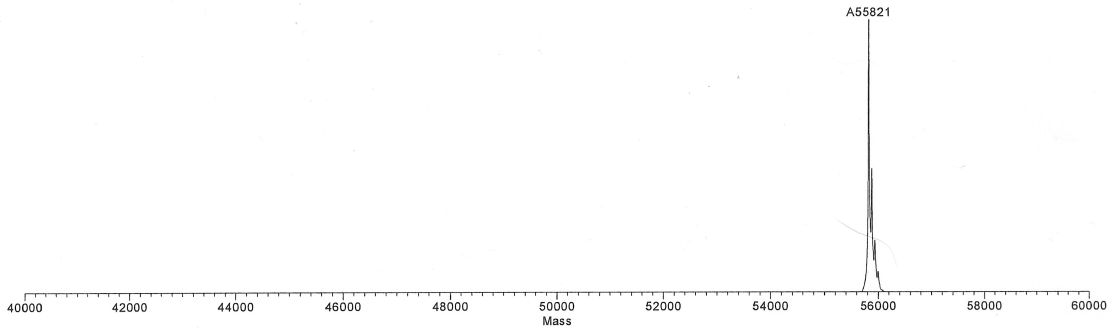

Deconvoluted spectrum

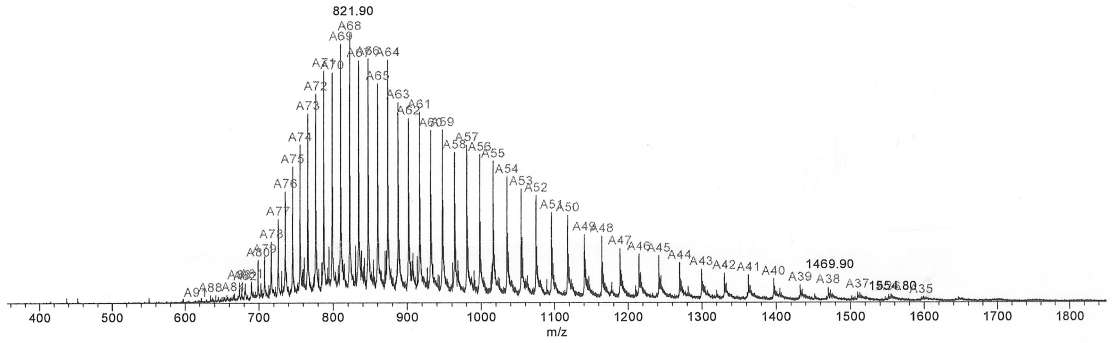

Protein spectrum

Figure A.5. ESI-TOF-MS analysis of AarCH6-R228E (55,821 Da observed; 55,820 Da expected [−Met1]).

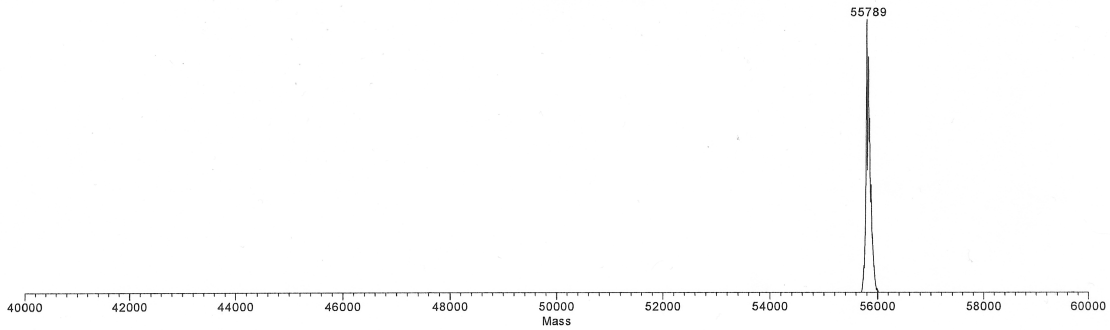

Deconvoluted spectrum

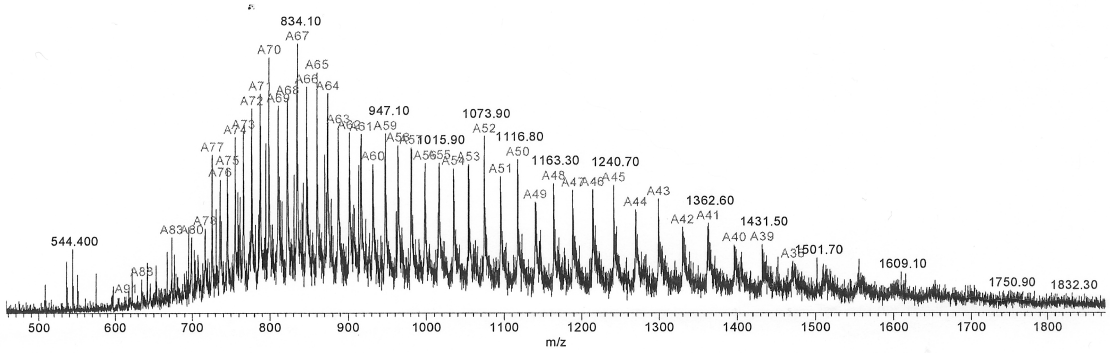

Protein spectrum

Figure A.6. ESI-TOF-MS analysis of AarCH6-E294A (55,789 Da observed; 55,789 Da expected [−Met1]).

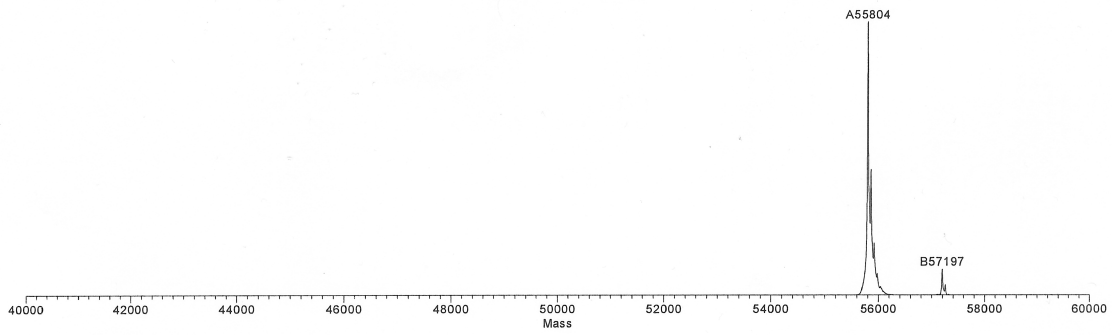

Deconvoluted spectrum

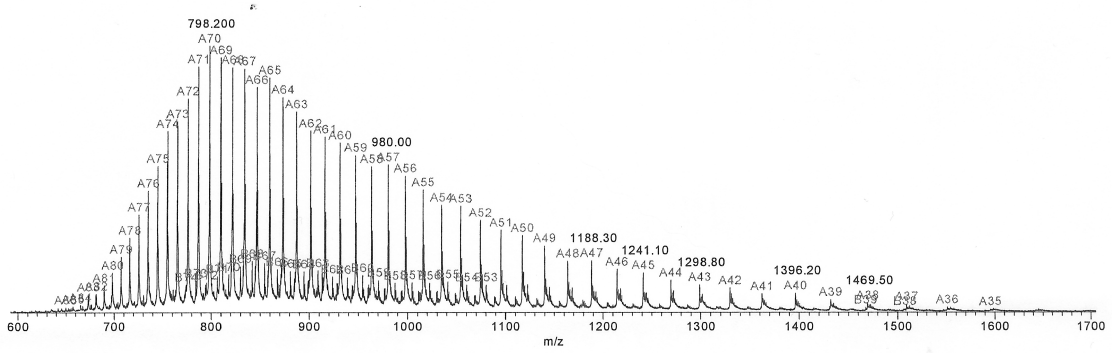

Protein spectrum

Figure A.7. ESI-TOF-MS analysis of AarCH6-N347A (55,804 Da observed; 55,804 Da expected [−Met1]). The minor peak does not correspond to the thioester intermediate (57,197 Da observed; 56,554 Da expected).

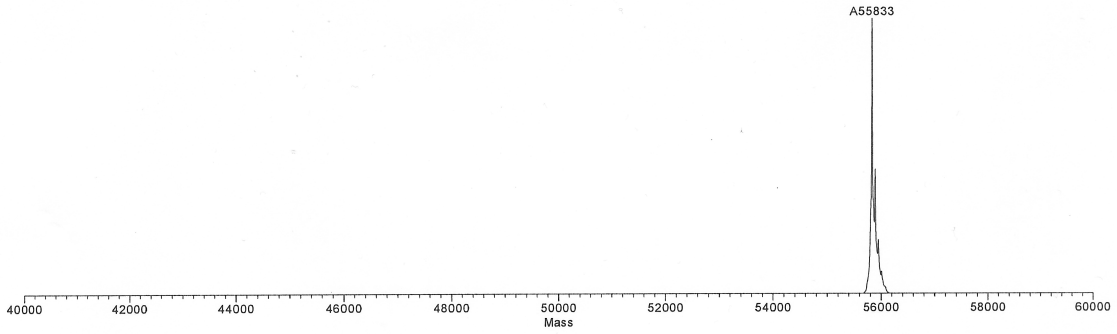

Deconvoluted spectrum

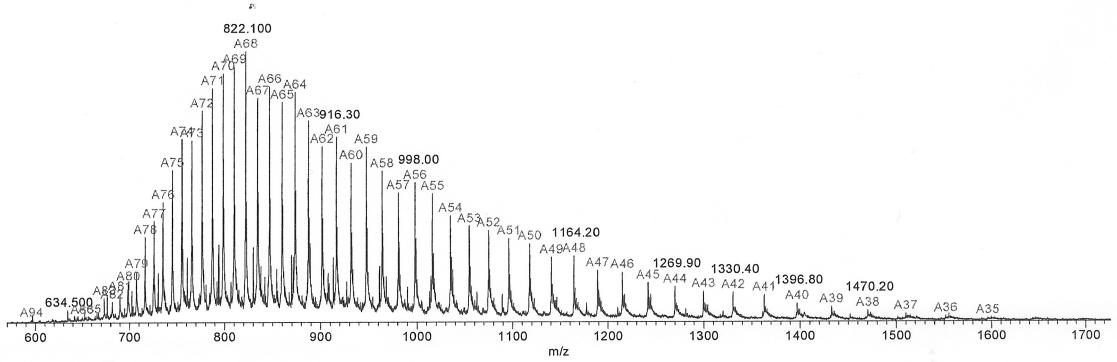

Protein spectrum

Figure A.8. ESI-TOF-MS analysis of AarCH6-E435D (55,833 Da observed; 55,833 Da expected [−Met1]).

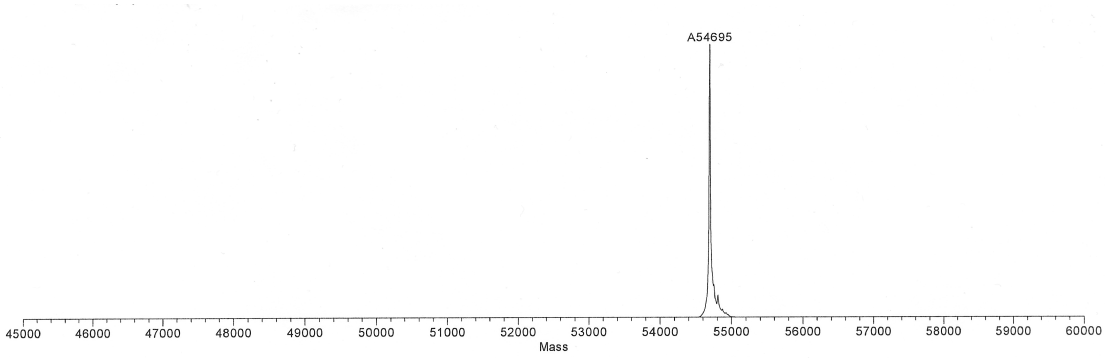

Deconvoluted spectrum

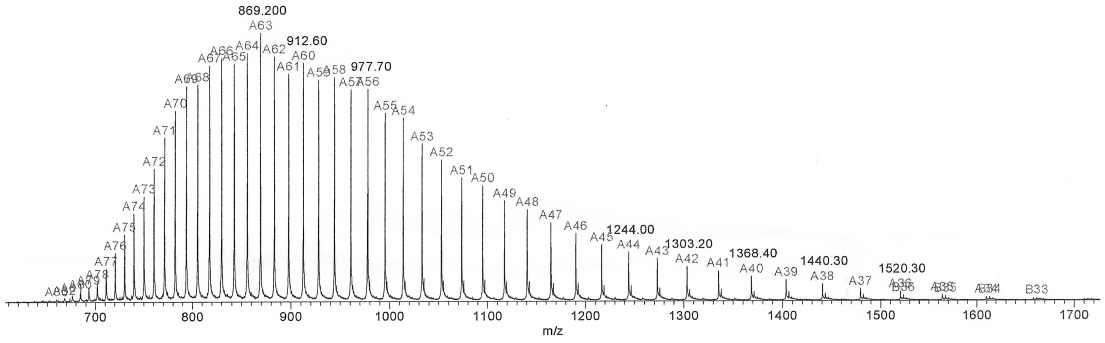

Protein mass spectrum

Figure A.9. ESI-TOF-MS analysis of AarC (54,695 Da observed; 54,695 Da expected [−Met1]).

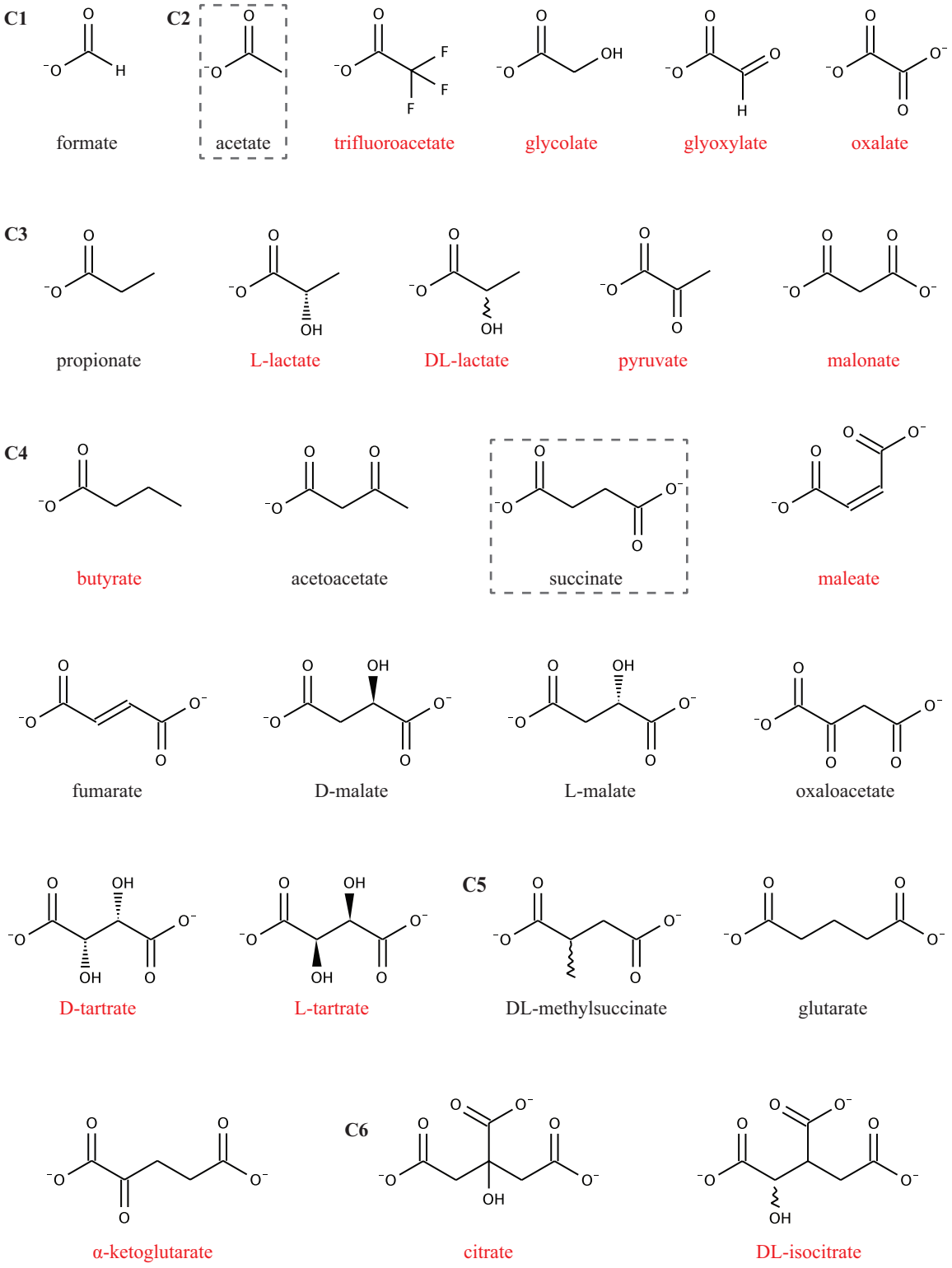

Figure A.10. Physiological and potential alternate carboxylate substrates for AarCH6. Compounds are sorted by number of carbon atoms (C1 – C6). Compounds with black labels, including acetate and succinate, supported detectable CoA-transferase activity in modified LCF/LCR assays.

Table A.1. AarCH6 kinetic constants obtained with physiological and alternate carboxylate substrates

Substrate	**Sp. activity (U/mg)**[a]	k_{cat} **(s^{-1})**[b]	K_m **(mM)**	k_{cat}/K_m **(M^{-1} s^{-1})**
formate	0.23	1.9	75	2.6×10^1
acetate[c,d]	66	280	70 (K_i = 1500)[e]	4.0×10^3
propionate	6.9	65 (65)[d]	240 (K_i = 1600)[e] (310, K_i = 1400)[d,e]	2.7×10^2 (2.1×10^2)[d]
acetoacetate[c,d]	5.7	37	130	2.8×10^2
succinate[c]	73	71	0.90	7.9×10^4
fumarate	0.75	0.89	5.4	1.6×10^2
D-malate	4.0 (0.010)[f]	12 (---)[g]	55 (---)[g]	2.2×10^2 (---)[g]
L-malate	0.44 (0.41)[f]	0.80 (0.74)[f]	20 (19)[f]	4.0×10^1 (3.9×10^1)[f]
oxaloacetate	0.060	0.083	9.4	8.8×10^0
DL-methylsuccinate	0.082	0.46	58	7.9×10^0
glutarate	0.029	0.27	290	9.3×10^{-1}

[a] Alternate CoA-acceptors were screened in modified LCR assays as described in Chapter 4. The limit of detection was ~0.01 U/mg. [b] Kinetic constants were obtained using modified LCR assays as described in Chapter 4 unless otherwise noted. Saturation experiments were performed in duplicate. [c] Kinetic constants were taken from Chapter 2. [d] Kinetic constants were obtained using modified LCF assays containing 50 mM potassium phosphate, pH 8.0, 100 mM potassium chloride, 0.2 mM succinyl-CoA, varying concentrations of carboxylate substrate, and 5 – 50 ng AarCH6. Saturation experiments were performed in duplicate. [e] Data were fit to a substrate inhibition model. [f] Two acyl-CoA/acyl-isoCoA product pairs (likely constitutional isomers) were observed. [g] Under normal substrate conversion conditions, formation of the minor product pair was too slow to be measured relative to that of the major product pair.

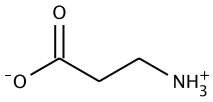

3-aminopropionate

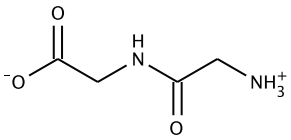

glycylglycine

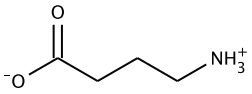

4-aminobutyrate

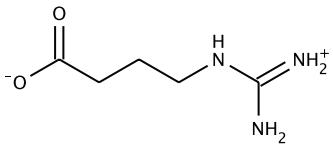

4-guanidinobutyrate

Figure A.11. Potential zwitterionic substrates for AarCH6-R228E. None of the compounds supported detectable CoA-transferase activity in modified LCR and VisR assays.

Table A.2. Conserved or functionally equivalent catalytic residues in phylogenetically diverse class I CoA-transferases[a]

PDB id (chain)	Z score (identity)	Val270	Glu294	Asn347	Gly388	HOH517
2g39 (A)[b]	56.1 (48%)	Ile264	Glu288	Asn341	Gly382	HOH947
2nvv (A)[c]	53.2 (48%)	Val259	Glu284	Asn337	Gly378	---[k]
3gk7 (A)[d]	36.3 (24%)	Ile216	Glu238	Asn295	Gly336	HOH486
3qli (A)[e]	34.8 (25%)	Val227	Glu249	Asn306	Gly347	HOH466
3oxo (F)[f]	21.6 (18%)	Ile284	Glu305	Gln99	Gly386	---[l]
2ahv (D)[g]	21.3 (16%)	Val309	Glu333	Gln118	Gly401	HOH2682
1k6d (A)[h]	15.6 (18%)	---[j]	---[j]	Gln100	---[j]	---[j]
1poi (A)[i]	14.6 (14%)	Thr31 (B)[j]	Glu54 (B)[j]	Gln103	Gly137 (B)[j]	HOH270 (B)[j]
1poi (B)[i]	9.6 (18%)	Thr31	Glu54	Gln103 (A)[j]	Gly137	HOH270

[a] Catalytic residues in AarC (bold) were determined through crystallographic, mutagenic, and kinetic analyses as described in Chapter 4. Conserved or functionally equivalent residues in structurally related class I CoA-transferases were identified by manual inspection of structures aligned to AarC (PDB id 6tba, chain A) using the Dali web server. [b] Putative succinyl-CoA:acetate CoA-transferase from *Pseudomonas aeruginosa*. [c] Putative succinyl-CoA:acetate CoA-transferase from *Porphyromonas gingivalis*. [d] 4-hydroxybutyrate CoA-transferse from *Clostridium aminobutyricum* (4-HB-CoAT). [e] Butyryl-CoA transferase from *Yersinia pestis* (RipA). [f] Succinyl-CoA:acetoacetate CoA-transferase from pig heart (SCOT). [g] Short-chain-fatty-acid CoA-transferase from *Escherichia coli* (YdiF). [h] Acetate CoA-transferase from *E. coli* (ACT, α-subunit only). [i] Glutaconate CoA-transferase from *Acidaminococcus fermentans* (GCT, α- and β-subunits). [j] Each active site in ACT and GCT is composed of two heteromeric subunits. [k] Few waters were modeled due to the low resolution of the dataset (2.7 Å). [l] Few waters were modeled (~55 per chain) despite the moderate resolution of the dataset (2.3 Å).

LICENSE AGREEMENT

Copyright Clearance Center

Confirmation Number: 10583493
Order Date: 10/14/2011

Customer Information

Customer: Elwood Mullins
Account Number: 3000457933
Organization: Elwood Mullins
Email: mullins@purdue.edu
Phone: +1 (765)4966814
Payment Method: Invoice

Order Details

Archives of microbiology

Billing Status: **N/A**

Order detail ID:	57609300
Article Title:	The internal pH of Acetobacterium wieringae and Acetobacter aceti during growth and production of acetic acid
Author(s):	Menzel, Ulrike
DOI:	10.1007/BF00414767
Date:	Oct 01, 1985
ISSN:	0302-8933
Publication Type:	Journal
Volume:	143
Issue:	1
Start page:	47
Publisher:	SPRINGER-VERLAG

Permission Status: **Granted**
Permission type: Republish or display content
Type of use: use in a thesis/dissertation
Order License Id: 2767921092287

Portion	Figures
Author of this Springer article	No
Title of your thesis / dissertation	A specialized citric acid cycle requiring succinyl-coenzyme A (CoA):acetate CoA-transferase (AarC) confers acetic acid resistance on the acidophile Acetobacter aceti
Expected completion date	Dec 2011
Estimated size(pages)	100

Note: This item was invoiced separately through our **RightsLink service.** More info **$ 0.00**

Total order items: 1 **Order Total: $0.00**